# 8. Supplement

## 8.1. Publication I: Raman excitation profiles of hybrid systems constituted by single-layer graphene and free base phthalocyanine: Manifestation of two mechanisms of graphene-enhanced Raman scattering

Tereza Uhlířová[a], Peter Mojzeš[b], Zuzana Melniková[c] Martin Kalbáč[c], Veronika Sutrová[a,d], Ivana Šloufová[a], Blanka Vlčková[a*]

[a] Charles University, Faculty of Science, Department of Physical and Macromolecular Chemistry, Hlavova 8, Prague 2, 128 40, Czech Republic, vlc@natur.cuni.cz

[b] Charles University, Faculty of Mathematics and Physics, Institute of Physics, Ke Karlovu 5, Prague 2, 121 16, Czech Republic

[c] J. Heyrovsky Institute of Physical Chemistry of the ASCR, v.v.i, Dolejškova 3, 182 21 Prague 8, Czech Republic

[d] Institute of Macromolecular Chemistry AS CR, Heyrovsky Sq. 2, 162 06 Prague 6, Czech Republic

My contribution:

Reference sample preparation, SEM imaging, participation on MS preparation.

Research article

Journal of RAMAN SPECTROSCOPY

Received: 9 March 2017 Revised: 14 June 2017 Accepted: 14 June 2017 Published online in Wiley Online Library: 26 July 2017

(wileyonlinelibrary.com) DOI 10.1002/jrs.5206

# Raman excitation profiles of hybrid systems constituted by single-layer graphene and free base phthalocyanine: Manifestations of two mechanisms of graphene-enhanced Raman scattering

Tereza Uhlířová,[a] Peter Mojzeš,[b] Zuzana Melniková,[c] Martin Kalbáč,[c] Veronika Sutrová,[a,d] Ivana Šloufová[a] and Blanka Vlčková[a]*

**The ability of single-layer graphene (SLG) to enhance Raman scattering of planar aromatic molecules denoted graphene-enhanced Raman scattering (GERS) is currently the subject of focused interest. We report on manifestations of two mechanisms of GERS in Raman spectra of glass/SLG/free base phthalocyanine ($H_2Pc$) monolayer (ML) hybrid systems: (i) photoinduced charge transfer from SLG Fermi level to LUMO of $H_2Pc$ excited at onset of the near IR region, and (ii) modification of resonance Raman scattering of $H_2Pc$ in the visible region by SLG–$H_2Pc$ interaction resulting into delocalization of the electronic transition over the benzene rings of $H_2Pc$. Glass/SLG/$H_2Pc$ hybrid systems with either a bilayer or a monolayer of $H_2Pc$ molecules and a graphite/$H_2Pc$ (ML) reference system were prepared by a spectrally controlled adsorption–desorption of $H_2Pc$ from solution, followed by Raman mapping of samples at excitation wavelengths in the 532–830 nm range, construction of excitation profiles for $H_2Pc$ Raman bands of the glass/SLG/$H_2Pc$ samples and determination of GERS enhancement factors for the glass/SLG/$H_2Pc$ (ML) sample *versus* the graphite/$H_2Pc$ (ML) reference sample (3–24 at 633 nm and 3–19 at 647 nm excitations). Selectivity of the excitation profiles and of the GERS enhancement factors with respect to localization of the vibrational modes within the $H_2Pc$ molecule demonstrates involvement of a different resonant electronic transition in each of the two mechanisms of GERS. Copyright © 2017 John Wiley & Sons, Ltd.**

**Keywords:** graphene-enhanced Raman scattering; single-layer graphene; free base phthalocyanine; Raman excitation profiles; photoinduced charge transfer

## Introduction

Raman spectroscopy is currently one of the principal tools used for characterization of graphene, a planar sheet of $sp^2$-bonded carbon atoms forming a hexagonal honeycomb crystal lattice.[1,2]

The ability of graphene to enhance Raman scattering of molecules located on graphene surfaces in hybrid systems was first reported in 2010 and denoted graphene-enhanced Raman scattering (GERS).[3] Recently, the six years of activity in this research field have been reviewed.[4,5] The magnitude of the GERS enhancement has been found to depend on several factors, such as the structure and symmetry of a molecule, energy of its highest occupied molecular orbital (HOMO) and lowest unoccupied molecular orbital (LUMO), molecule–graphene distance, graphene sample thickness, graphene Fermi level energy and laser excitation wavelength. About 30 different molecules have already been probed for GERS, and the best results have been obtained for planar aromatic molecules and single-layer graphene (SLG).[4,5] The average GERS enhancement factor values were found to be in the 2–15 range (for planar molecules on SLG surface), while the largest GERS enhancement factor of 47 was achieved for CuPc (Pc = phthalocyanine) at 633-nm excitation.[4,5]

These experimental results have been rationalized by the theoretical treatment of the GERS effect reported in 2014.[6] The origin of GERS has been attributed to a charge transfer between Fermi level of graphene and HOMO or LUMO of an aromatic molecule of $D_{nh}$ symmetry, or to a mutual interaction between close lying Fermi level of graphene and HOMO or LUMO of the molecule,

* Correspondence to: Blanka Vlčková, Charles University, Faculty of Science, Department of Physical and Macromolecular Chemistry, Hlavova 8, Prague 2 128 40, Czech Republic.
E-mail: vlc@natur.cuni.cz

a Faculty of Science, Department of Physical and Macromolecular Chemistry, Charles University, Hlavova 8, Prague 2 128 40, Czech Republic

b Faculty of Mathematics and Physics, Institute of Physics, Charles University, Ke Karlovu 5, Prague 2 121 16, Czech Republic

c J. Heyrovsky Institute of Physical Chemistry of the ASCR, v.v.i, Dolejškova 3, 182 21, Prague 8, Czech Republic

d Institute of Macromolecular Chemistry AS CR, Heyrovsky Sq. 2, 162 06, Prague 6, Czech Republic

and the resonance conditions for the largest GERS enhancements have been formulated.[5,6]

Free base phthalocyanine ($H_2Pc$), a planar aromatic molecule of $D_{2h}$ symmetry (Fig. 1, inset), has been a subject of numerous spectroscopic studies motivated by its interesting electronic structure[7–11] as well as by its potential applications in molecular photonics and optoelectronics,[12,13] in gas sensor development[14] and as a sensitizer in the photodynamic therapy of cancer.[15] Owing to its $D_{2h}$ symmetry which distinguishes between the x and y directions of the electronic transition moment (Fig. 1, inset), the Q electronic absorption band of $H_2Pc$ in the visible spectral region is split into $Q_x$ and $Q_y$ branch (Fig. 1), the actual positions and maxima of which are strongly dependent on the molecular environment [7–11] Both Raman and resonance Raman (RR) spectra of $H_2Pc$ thin films (α, β and *x* phase) have been investigated,[16–20] while the RR measurements of $H_2Pc$ molecules in KBr discs and in isolation matrices have been hampered by a strong luminescence.[8,21] By contrast, quenching of the luminescence of $H_2Pc$ molecules upon their adsorption onto Ag island films allowed for obtaining both SERS and SERRS/SE(R)RS = surface-enhanced (resonance) Raman scattering/ spectra of $H_2Pc$.[7,22]

$H_2Pc$ has also been among the very first molecules probed for GERS in 2010.[3] Raman spectra of $Si/SiO_2/SLG/H_2Pc$ hybrid samples prepared by $H_2Pc$ sputtering onto the SLG surface were measured at 488.0, 514.5 and 633-nm wavelength, and quenching of the $H_2Pc$ luminescence has been demonstrated. Graphene-enhanced Raman scattering enhancement of $H_2Pc$ spectral bands by factors 5–15 has been determined in relation to the $Si/SiO_2/H_2Pc$ reference sample at 633-nm excitation. On the other hand, the actual mechanism of GERS enhancement has not been established, and the LUMO and HOMO energies considered in this paper were not appropriate, because the value of their difference corresponded with the B (Soret) electronic transition (in the UV spectral region) rather than with the $Q_x$ electronic transition corresponding with the actual HOMO − LUMO difference.

In this paper, we focus on identification of the resonance conditions for GERS and on manifestations of its mechanisms for $H_2Pc$ in hybrid systems with SLG by Raman spectral measurements in a broad range (532–830 nm) of excitation wavelengths, and by construction and analysis of Raman (GERS) excitation profiles of the Raman spectral bands of $H_2Pc$. The importance of the excitation profiles in GERS has already been demonstrated; however, up to now, this tool has been employed for investigation of the mechanism of GERS only once, and in a markedly more narrow range of excitation wavelengths.[23] On the other hand, the excitation profiles have been frequently employed in RR and SERS and SERRS spectral studies.[24–28] In our analysis of the GERS excitation profiles and GERS enhancement factors, we have focused particularly on their selectivity with respect to (i) wavenumbers of scattered photons, (ii) symmetry of vibrational modes and/or (iii) their localization within the $H_2Pc$ molecule. Preparation of both the glass/SLG/$H_2Pc$ samples and of the selected reference samples has been, in our case, based on a spontaneous adsorption of $H_2Pc$ molecules onto the particular substrate from its toluene solution (followed by the removal of excess molecules). Therefore, we have selected graphite/$H_2Pc$ as a reference sample in which the adsorption ability of the graphite substrate is similar to that of SLG, but for which no GERS enhancement has been observed.[3] We have focused particularly on achievement of a monolayer coverage of both the glass/SLG and the graphite substrate by $H_2Pc$ molecules. Concerning the assignment of vibrational modes, we found greatly helpful the recently reported DFT calculations.[8,21] Furthermore, concerning the HOMO and LUMO energies of $H_2Pc$, we rely on the results of two DFT calculations [10,29] which show a reasonable mutual agreement of their values. We also take advantage of the recently published theoretical treatment of GERS and of the formulation of the conditions for GERS.[6] In the case of $H_2Pc$, these conditions and the actual LUMO and HOMO energy values [10,28] indicate that it is worthwhile to extend Raman spectral measurements into the region of excitation wavelengths above 633 nm in which the HOMO $H_2Pc$ → Fermi level of SLG and/or Fermi level SLG → LUMO $H_2Pc$ CT transition(s) could possibly take place. As a result of this effort, we propose that two mechanisms of GERS manifest themselves in the Raman spectra of glass/SLG/$H_2Pc$ hybrid system, each in the different range of excitation wavelengths and with a different localization of the most enhanced vibrational modes within the $H_2Pc$ molecule.

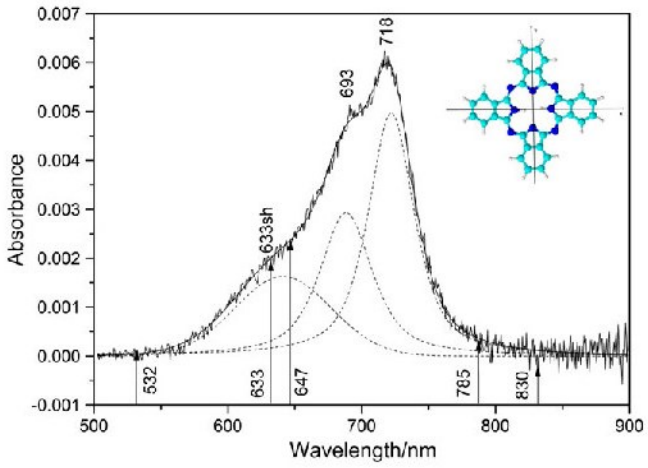


**Figure 1.** Electronic absorption spectrum of glass/SLG/$H_2Pc$ (BL)-I system: Electronic absorption bands maxima: $Q_x$ – 718 nm, $Q_y$ – 693 nm; shoulder – 633 nm. Final results of spectral bands separation: three bands presented as dashed curves (details in Fig. S3 in SI). Excitation wavelengths used for Raman measurements are marked by arrows. Inset: Schematic depiction of $H_2Pc$ molecule structure ($D_{2h}$ symmetry) with the directions of the electronic transition dipoles[39] marked by arrows. [Colour figure can be viewed at wileyonlinelibrary.com]

## Experimental

### Materials

29,31H-Phthalocyanine, $H_2Pc$ (β-form, 98%), 29,31H-phthalocyanine-C,C,C,C-tetrasulfonate hydrate, $H_2PcTS$ and cellulose nitrate were purchased from Sigma-Aldrich. Toluene for spectroscopy (Merck, Uvasol) and/or distilled deionized water were used as solvents.

### Preparation procedures

*Glass/single-layer graphene hybrid system*

Single-layer graphene was prepared by the previously reported CVD procedure.[30] The as-grown graphene was transferred to the glass substrate using cellulose nitrate (NC).[31] The majority of the NC layer was removed by methanol drops at room temperature. Then, the glass/SLG sample was annealed at 160 °C for 30 min in order to remove the NC residuals from the SLG surface.

*Glass/single-layer graphene/phthalocyanine hybrid systems*

All samples were prepared by using the same first step: The parent glass/SLG hybrid systems were overlayed by a thin layer of a saturated ($<5 \times 10^{-5}$ M) solution of $H_2Pc$ in toluene (which was filtered by the 1-μm filter prior to use). Subsequently, they were kept in the toluene-saturated atmosphere in a sealed weighting bottle for 24 h to accomplish adsorption of $H_2Pc$ onto the SLG surface. The sample was then extracted from the weighting bottle, and the solution layer was removed by soaking into a slip of filter paper. The second step aimed at the removal of excess $H_2Pc$ molecules was performed by overlaying the as-prepared glass/SLG/$H_2Pc$ sample by a thin layer of pure toluene and by keeping it in the same setup as described above for 10 min. The solvent layer was then removed by the filter paper. The particular samples mutually differed by the multiplicity of the second step applications, and this multiplicity has been employed for the sample notation throughout this paper. In particular, the samples soaked in pure toluene only once are denoted as glass/SLG/$H_2Pc$-I system, those soaked 6× as -VI system and those soaked 10× as -X system.

*Graphite/$H_2Pc$ hybrid systems* were prepared by the procedure similar to that described above for the glass/SLG/$H_2Pc$ hybrid systems. Nevertheless, the procedure was preceded by the graphite substrate preparation and followed by the specifically developed strategy of Raman spectral mapping. The detailed description of these procedures is provided in Supporting information (SI), Text S1, and documented by Figs S1 and S2 in SI.

### Instrumentation

*Raman spectra* as well as optical images of all hybrid samples and reference hybrid samples were obtained using WITec alpha300 Raman micro-spectrometer. An objective (Zeiss) with 100× magnification was used for all the above mentioned Raman spectral measurements performed at 532, 633, 647, 785 and 830-nm excitations. For measurements on WITec alpha300, two spectrographs equipped with charge-coupled device (CCD) detectors optimized for the blue–green and for the red-NIR (near infrared) spectral ranges have been used, the first one for collection of spectra at 532-nm excitation and the second one for the other four excitation wavelengths, i.e. 633, 647, 785 and 830 nm. Excitation was provided by the following lasers at the respective wavelengths and laser power values (at the sample): SHG Nd:$YVO_4$, 532 nm (2.3 mW); He–Ne, 633 nm (2.5 mW); $Kr^+$ ion, 647 nm (5.0 mW), diode, 785 nm (50.0 mW), diode, 830 nm (11.0 mW). Raman spectral mapping was performed by using the 25 μm × 25 μm area scans with 50 × 50 points. Defect-free areas of samples were selected for spectral mapping by the previously established relationship between optical images and Raman spectra of glass/SLG samples.

*UV–Vis electronic absorption spectra of glass/SLG/$H_2Pc$(BL)-I hybrid system* were measured with a home-assembled microspectrometer system consisting of a 20-W Oriel tungsten-halogen lamp coupled to a modified Nicolet Nicplan microscope which in turn passed through an Acton spectrograph (resolution of approximately 1.7 nm), and the light was finally detected by a Princeton Instruments Si diode-array detector. The measured area was 350 μm × 260 μm.[32] The very low absorbance A = 0.006 of this sample (Fig. 1) documents the impossibility to obtain meaningful absorption spectra for samples VI and X containing a monolayer of $H_2Pc$ molecules.

*Raman and UV/vis spectral measurements of solutions* are described in Text S2 in SI.

Calibrations related to Raman spectral measurements with the WITec alpha300 apparatus and spectral data processing are described in Text 2 in SI and supported by ref. [33].

### Raman excitation profiles of glass/single-layer graphene/phthalocyanine hybrid samples

Excitation profiles (EP) were constructed for each Raman spectral band of $H_2Pc$, and they represent plots of their normalized band intensity as a function of the excitation wavelength in the 532–830 nm region. The EPs were constructed from the excitation wavelength-dependent Raman spectra of glass/SLG/$H_2Pc$-I, glass/SLG/$H_2Pc$-VI and glass/SLG/$H_2Pc$-X hybrid systems collected at the 532, 633, 647, 785 and 830 nm excitations. Raman spectra of polystyrene acquired under the very same experimental conditions as those of the samples were employed as the external intensity standards. At each excitation wavelength, intensities of the $H_2Pc$ Raman bands (in terms of the band areas) in the spectrum of each of the hybrid samples were normalized to the intensity of the 1005 $cm^{-1}$ polystyrene Raman band.

### Graphene-enhanced Raman scattering enhancement factors

Graphene-enhanced Raman scattering enhancement factors were determined as the intensity ratios (in terms of the integrated band areas) of the corresponding Raman bands in the spectra of the glass/SLG/$H_2Pc$ (ML)-X sample and the graphite/$H_2Pc$ (ML) reference sample. The spectra were baseline-corrected by the third-order polynomial function which was found to be optimal for the subsequent determination of the integrated band areas. The actual values of the GERS enhancement factors of the $H_2Pc$ spectral bands are affected by an experimental error estimated to be about ±10%. The major contribution of this error stems from the fact that neither the glass/SLG nor the graphite surface of our sample and reference sample are perfectly flat, and their surface area/projected area ratio has been only roughly estimated to 1.1–1.3.[34] On the other hand, we suppose that this uncertainty does not affect the vibrational mode selectivity of the GERS enhancement factors with respect to their localization within the $H_2Pc$ molecule.

## Results and discussion

### A. Characterization of glass/single-layer graphene/phthalocyanine samples I, VI and X and determination of single-layer graphene surface coverage by phthalocyanine

Electronic absorption spectrum of glass/SLG/$H_2Pc$-I system (baseline corrected) is shown in Fig. 1. The two distinct maxima at 718 and 693 nm are attributed to the $Q_x$ (0–0) and $Q_y$ (0–0) bands, respectively. The shoulder at 633 nm is attributed to the vibronic sideband of the $Q_y$ band, i.e. to $Q_y$ (0–1) vibronic transition. The presence of three spectral bands is confirmed by the peak fitting procedure the results of which are shown in Fig. 1 (details in Fig. S3 in SI). The maxima of both Q (0–0) bands (Fig. 1) are markedly red-shifted in comparison to those of $H_2Pc$ in chloronaphtalene[13] and toluene (Fig. S4 in SI) solutions, in isolation matrices[8] and in polysiloxane films.[13] In particular, the $Q_x$ bands are located in the 670–702 nm range and the $Q_y$ bands in the 627–666 nm range in the systems reported previously[8,13] and/or shown in Fig. S4 in SI. In addition to that, SERRS excitation profiles of $H_2Pc$ molecules adsorbed on Ag island films show maxima at 692 ($Q_x$) and

Journal of RAMAN SPECTROSCOPY

674 nm ($Q_y$), respectively.[7] The red shift of both Q-bands in the electronic absorption spectrum of the glass/SLG/$H_2$Pc-I system thus indicates the presence of J-type dimers (or very small aggregates) of $H_2$Pc molecules on SLG.[10,35,36]

For further characterization of the glass/SLG/$H_2$Pc hybrid system I as well as of the hybrid systems VI and X, we compared the number of scattering molecules in all these three systems. For this purpose, we performed Raman spectral mapping of the same areas (25 × 25 μm) of the three samples under the same measurement conditions, namely at 532-nm excitation, which appears to be out-of-resonance for both isolated $H_2$Pc molecules (Fig. S4 in SI and refs. [8,13]) as well as for those in the glass/SLG/$H_2$Pc-I system (Fig. 1). Because at a non-resonant excitation, the intensity of Raman scattering is directly proportional to the number of scattering molecules,[37] the mutual comparison of the relative average band intensities of the same selected spectral bands (determined from the spectra shown in Fig. S5 in SI and set to 1.00 for the system I) provided us with the comparison of the relative numbers of scattering molecules in the three systems (Fig. S6 in SI). This comparison demonstrates that the additional soaking in pure toluene/performed 5 more times for the sample VI (6×) than for the sample I (1×) reduced the number of scattering molecules to less than a half of the original value, namely to 0.41. By contrast, a further additional soaking in pure toluene performed 4 more times for the sample X (10×) than for the sample (6×) has not further reduced the number of scattering molecules, because the values of 0.41 and 0.44, respectively, can be considered as comparable regarding the precision of the experiment. We thus attribute the sample I to the glass/SLG/~ a bilayer (BL) of $H_2$Pc hybrid system, and the samples VI and X to the glass/SLG/~ a monolayer (ML) of $H_2$Pc hybrid systems.

### B. Assignment of Raman spectral bands of phthalocyanine and single-layer graphene in glass/phthalocyanine/single-layer graphene hybrid systems and their comparison with those of the reference systems

Raman spectral bands of both SLG and $H_2$Pc were observed for all three glass/SLG/$H_2$Pc hybrid systems, i.e. (BL)-I, (ML)-VI and (ML)-X, at all five excitation wavelengths, i.e. at 532, 633, 647, 785 and 830 nm (Figs 2–4). Full range Raman spectra of these samples at 633 and 647-nm excitations are compared in Figs S7 and S8 (SI). By contrast, the Raman spectral bands of $H_2$Pc were observed only at 633 and 647-nm excitations for the graphite/$H_2$Pc (ML) reference sample. Raman spectra of the glass/SLG/$H_2$Pc (ML)-X sample and of the graphite/$H_2$Pc (ML) reference sample at 633 and 647-nm excitations are mutually compared in Figs 5 and 6. The average values of the $H_2$Pc Raman band wavenumbers of all three glass/SLG/$H_2$Pc samples and of the graphite/$H_2$Pc reference sample are listed in Table 1.

Table 1 demonstrates the large extent of similarities in the spectral band wavenumbers of $H_2$Pc for all three samples as well as for the reference one. On the other hand, one can notice minor, but very important differences in the $H_2$Pc Raman spectra between the glass/SLG/$H_2$Pc (BL)-I sample and the (ML) samples -VI and -X, as well as between the glass/SLG/$H_2$Pc (ML) samples and the graphite/$H_2$Pc (ML) reference sample. The former differences are represented by the appearance of a new 1533 $cm^{-1}$ band and by the shift of the 951 $cm^{-1}$ band to 958 $cm^{-1}$ upon reduction of the $H_2$Pc coverage in the glass/SLG/$H_2$Pc hybrid samples from ~a bilayer to a monolayer. The latter differences manifest themselves by the presence of new spectral bands, namely those at 1533, 1218, 958 and 750 $cm^{-1}$, for the glass/SLG/$H_2$Pc (ML) samples as

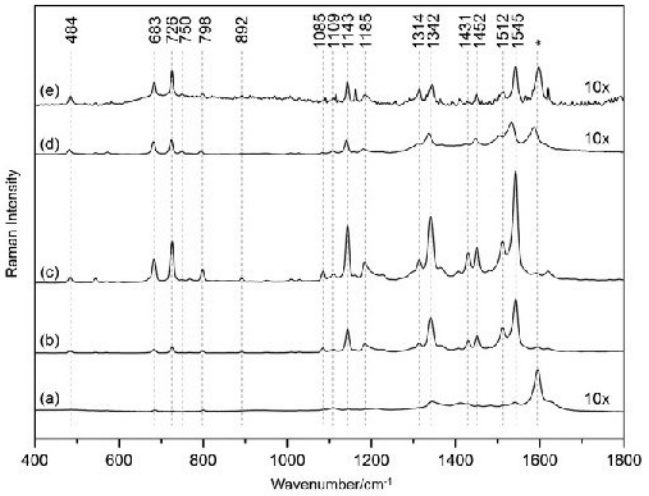


**Figure 2.** Raman spectra of glass/SLG/$H_2$Pc (BL)-I system measured at (a) 532-nm, (b) 633-nm, (c) 647-nm, (d) 785-nm and (e) 830-nm excitation wavelengths. The G band of SLG is marked by an asterisk. The bands in the 1500–1600 $cm^{-1}$ range at 785-nm excitation are slightly downshifted by a sample-specific effect.

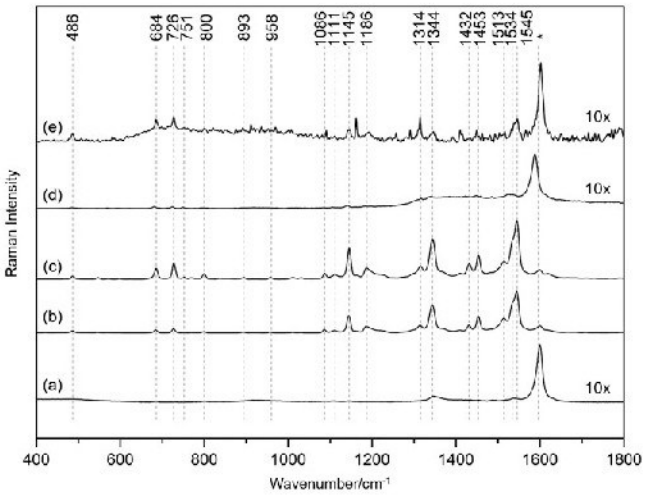


**Figure 3.** Raman spectra of glass/SLG/$H_2$Pc (ML)-VI system measured at (a) 532-nm, (b) 633-nm, (c) 647-nm, (d) 785-nm and (e) 830-nm excitation wavelengths. The G band of SLG is marked by an asterisk. The bands in the 1500–1600 $cm^{-1}$ range at 785-nm excitation are slightly downshifted by a sample-specific effect.

compared to the graphite/$H_2$Pc reference sample, and their appearance can be attributed to the differences between the strength of the SLG–$H_2$Pc (ML) and the graphite–$H_2$Pc (ML) interaction (details in Text S4 in SI).

For a proper understanding of the above mentioned spectral differences as well as for interpretation of Raman (GERS) excitation profiles and GERS enhancement factors *(vide infra)*, the assignment of $H_2$Pc spectral bands to vibrational modes of the particular symmetry species and localization within the molecule is of key importance. A detailed description of additional experiments and arguments for both types of band assignment presented in Table 1 (i.e. the symmetry and the localization of the Raman active vibrational modes) is provided in Text 3 in SI and related to refs. [38–41]. Briefly, the assignment of the spectral bands to Raman active



  

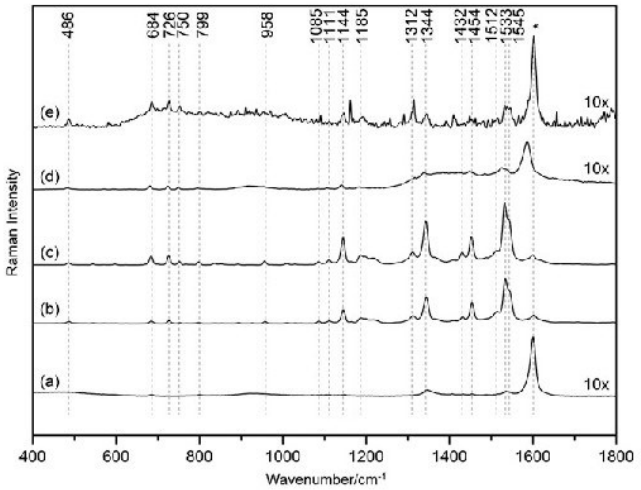


**Figure 4.** Raman spectra of glass/SLG/$H_2Pc$ (ML)- X system measured at (a) 532-nm, (b) 633-nm, (c) 647-nm, (d) 785-nm and (e) 830-nm excitation wavelengths. The G band of SLG is marked by an asterisk. The bands in the 1500–1600 $cm^{-1}$ range at 785-nm excitation are slightly downshifted by a sample-specific effect.

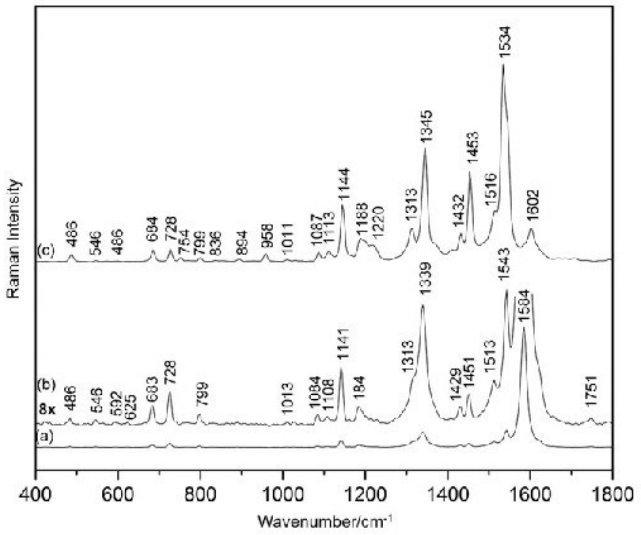


**Figure 5.** Comparison of Raman spectra of (a) graphite/$H_2Pc$ reference system, (b) the same spectrum expanded 8× and (c) glass/SLG/$H_2Pc$ (ML)-X system at 633-nm excitation. Spectra (a) and (c) are shown in scales respecting the intensity ratio of their absolute Raman signals.

modes of the isolated $H_2Pc$ molecule of a particular symmetry and localization based on DFT calculations [8,21] has been adopted for assignment of the corresponding modes of $H_2Pc$ in the hybrid systems (Table 1).

In addition to the $H_2Pc$ fundamentals (Table 1), overtone and combination bands of the totally symmetric $A_g$ fundamentals have been observed in Raman spectra of all three glass/SLG/$H_2Pc$ hybrid samples as well as in those of the graphite/$H_2Pc$ reference sample at both 633 and 647-nm excitation (Table S2, and Figs S7 and S8 in SI). Nevertheless, their number as well as relative intensities is markedly lower for the reference sample than for the three hybrid samples. No overtones of the SLG Raman modes[42] were observed in the spectra of the hybrid systems with SLG.

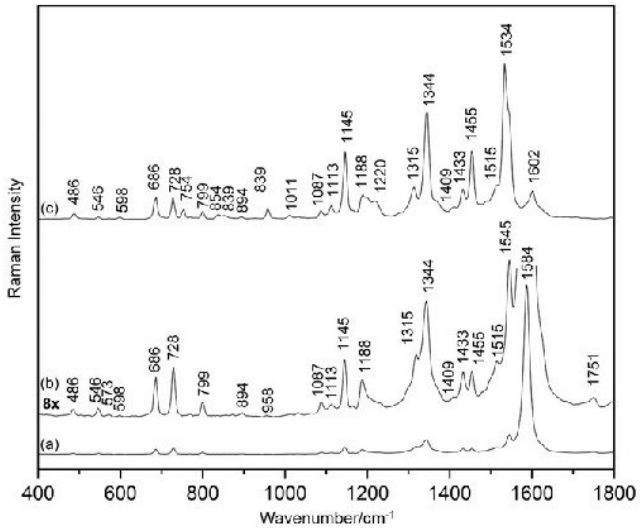


**Figure 6.** Comparison of Raman spectra of (a) graphite/$H_2Pc$ reference system, (b) the same spectrum expanded 8× and (c) glass/SLG/$H_2Pc$ (ML)-X system at 647-nm excitation. Spectra (a) and (c) are shown in scales respecting the intensity ratio of their absolute Raman signals.

Finally, we turn our attention to the assignment of SLG mode bands in the Raman spectra of the hybrid systems and to their comparison with those of the glass/SLG reference system. The bands of the SLG modes in the Raman spectra of the glass/SLG/$H_2Pc$ hybrid systems are most clearly observed at 532-nm excitation, at which the spectral bands of the $H_2Pc$ fundamentals are weak and those of overtones are absent (Fig. S7, SI). The only exception is the ~1344 $cm^{-1}$ band of the D mode which overlaps with the 1343 $cm^{-1}$ band of $H_2Pc$. The G bands of the hybrid systems are found at 1595 $cm^{-1}$ (sample BL-I) and 1600 $cm^{-1}$ (samples ML-VI and ML-X), while the same band of the parent glass/SLG system is located at 1598 $cm^{-1}$. The G-band of SLG was observed for all three hybrid samples as well as for the parent glass/SLG sample at all five excitation wavelengths, yielding the average values of 1595 $cm^{-1}$ for sample BL-I, 1599 $cm^{-1}$ for samples ML-VI and ML-X, and 1598 $cm^{-1}$ for the parent glass/SLG system. The position of the G band is, for all these systems, higher than that of the pristine SLG which is found at 1585 $cm^{-1}$.[1,2] This discrepancy can most probably be explained by n-doping of SLG by the Na-containing glass substrate, as described in the recently published paper.[43] On the basis of the above mentioned wavenumber difference of the G mode position, the level of n-doping of SLG on glass samples was estimated to induce a ca 0.3-eV upshift of the Fermi level of pristine SLG (from −4.6 $eV^3$ to −4.3 eV) on the basis of the graph in Fig. 8.5, ref. [2]. Furthermore, the wavenumbers of the spectral bands of the dispersive 2D mode (Table S3 in SI) of samples BL-I, ML-VI, ML-X and of the parent glass/SLG samples show a reasonably good mutual agreement (analogously to the case of the G band). These observations indicate that deposition of $H_2Pc$ onto the glass/SLG system has not induced any detectable effect of an additional doping or strain in SLG.

### C. Excitation profiles of selected Raman bands of glass/single-layer graphene/phthalocyanine hybrid systems

Excitation profiles (EPs) of $H_2Pc$ Raman spectral bands were constructed from Raman spectra of glass/SLG/$H_2Pc$ (BL)-I, glass/SLG/$H_2Pc$ (ML)-VI and glass/SLG/$H_2Pc$ (ML)-X hybrid systems collected

Journal of RAMAN SPECTROSCOPY

**Table 1.** Average wavenumbers (in $cm^{-1}$) of $H_2Pc$ spectral bands in Raman spectra of the hybrid systems investigated and their assignment to vibrational modes of $H_2Pc$

| SLG/$H_2$Pc-I BL | SLG/$H_2$PcVI ML | SLG/$H_2$PcX ML | Graphite/$H_2$Pc ML | Mode symmetry | Mode description |
|---|---|---|---|---|---|
| 484 | 486 | 486 | 485 | $B_{1g}$ | Benzene ring rocking and central ring deformation |
| 545 | 546 | 545 | 546 | $A_g$ | — |
| 571 | 571 | 571 | 573 | $A_g$ | Benzene ring deformation/central ring breathing |
| 683 | 684 | 684 | 685 | $A_g$ | Bridging C—N—C sym. def. and benzene ring deformation |
| 726 | 726 | 726 | 728 | $A_g$ | Pyrrole deformation and C—N—C rocking |
| 750 | 751 | 750 | — | IR act. | N—H out-of-plane deformation |
| 768 | 771 | 770 | 768 | $A_g$ | — |
| 798 | 800 | 799 | 799 | $A_g$ | Pyrrole and benzene ring C—C str. |
| 892 | 893 | 893 | 894 | $B_{1g}$ | — |
| 951 | 958 | 958 | — | IR act. | C—H out-of-plane deformation |
| 1009 | 1010 | 1010 | 1013 | $A_g$ | Sym. benzene ring C—H def |
| 1028 | 1030 | 1030 | 1030 | $B_{1g}$ | — |
| 1085 | 1086 | 1085 | 1086 | $B_{1g}$ | N—H in-plane deformation |
| 1109 | 1111 | 1111 | 1111 | $A_g$ | — |
| 1143 | 1145 | 1144 | 1144 | $A_g$ | Benzene ring C—C str. and C—H deformation |
| 1162 | 1163 | 1163 | 1163 | $A_g$ | — |
| 1184 | 1186 | 1185 | 1186 | $A_g$ | C—H def. on benzene ring |
| 1220 | 1222 | 1218 | — | $B_{1g}$ | C—H def, benzene ring def. and N—H in-plane deformation |
| 1314 | 1314 | 1312 | 1316 | $B_{1g}$ | — |
| 1342 | 1344 | 1344 | 1343 | $A_g$ | Benzene ring C—C str. and pyrrole C—C stretch |
| 1408 | 1408 | 1409 | 1409 | $A_g$ | — |
| 1431 | 1432 | 1432 | 1431 | $B_{1g}$ | — |
| 1452 | 1453 | 1454 | 1453 | $A_g$ | C—H def. |
| 1512 | 1513 | 1512 | 1514 | $A_g$ | — |
| — | 1534 | 1533 | — | $A_g$ | Bridging $C_\alpha$–$N_m$–$C_\alpha$ asym. str. and $C_\alpha$–$N_H$–$C_\alpha$ sym. str. |
| 1543 | 1545 | 1545 | 1544 | $A_g$ | Bridging $C_\alpha$–$N_m$–$C_\alpha$ asym. str. and $C_\alpha$–$N_H$–$C_\alpha$ sym. str. |
| 1620 | 1621 | 1619 | Not observable | $B_{1g}$ | Benzene ring deformation |

at the 532, 633, 647, 785 and 830-nm excitation wavelengths (Figs 2–4 and details in Experimental). The EPs are presented in Figs 7 and 8, profiles A-C. Shown in Fig. 7(A–C) are the overviews of EPs of all selected $H_2Pc$ spectral bands of all three samples, while the corresponding details of the close-lying EPs of the less enhanced bands are shown in Fig. S10, profiles A–C (SI). The details of the EPs in the high excitation wavelengths region (785 and 830 nm) of all three samples are presented in Fig. 8, profiles A–C.

In case of all three samples, the EPs of the selected spectral bands exhibit a maximum for the 647-nm excitation. Furthermore, while the EP of glass/SLG/$H_2$Pc (BL)-I sample appears to be rather flat at higher excitation wavelengths (with some of the bands slightly declining and some slightly increasing, Figs 7 and 8, profiles A), the EPs of glass/SLG/$H_2$Pc (ML)-VI and glass/SLG/$H_2$Pc (ML)-X hybrid systems show a pronounced normalized intensity increase from 785 to 830 nm for at least half of the spectral bands (Figs 7 and 8, profiles B and C). Importantly, the EPs of the glass/SLG/$H_2$Pc (BL)-I Raman spectral bands (profiles A in Figs 7 and 8, and in Fig. S10 in SI) can be related to the electronic absorption spectrum of this hybrid system (Fig. 1). The particular EPs were analyzed in the following manner. The sequences of relative intensities of the individual spectral bands were determined for all three hybrid systems at 633 and 647-nm excitations, for glass/SLG/$H_2$Pc (BL)-I also at 785 nm and for glass/SLG/$H_2$Pc (ML)-VI and glass/SLG/$H_2$Pc (ML)-X systems also at 830-nm excitations. The series were analyzed in terms of the symmetries of the corresponding normal vibrations and their localizations within the $H_2$Pc molecule. For the totally symmetric vibrations, the sequence of the decreasing normalized band intensities in the resonance Raman spectra excited at a particular excitation wavelength corresponds to the decreasing magnitude of changes of their normal coordinates upon the electronic transition which is in resonance with the particular excitation wavelength. The largest changes of the normal coordinates of the totally symmetric $A_g$ modes thus determine localization of the resonant electronic transition within the $H_2$Pc molecule.[24] An analogous approach has been already successfully employed, e.g. for the SERRS EPs analysis.[27]

*Excitation profiles of Raman bands of glass/single-layer graphene/phthalocyanine (BL)-I hybrid system*

The sequence of the most intense bands of $H_2$Pc at 647-nm excitation (Figs 7, 8 and Fig. S10 in SI, profiles A) was ascertained as follows: 1543 ($A_g$) > 1341 ($A_g$) > 1143 ($A_g$) > 726 ($A_g$) > 1451 ($A_g$) > 683 ($A_g$) ~ 1184 ($A_g$) ~ 1314 ($B_{1g}$) > 1367 > 798 ($A_g$) > 1110 ($B_{1g}$) > 1085 ($B_{1g}$) > 484 ($B_{1g}$) > 544 ($A_g$) > 768 ($A_g$) > 1009 ($B_{1g}$) >1162 ($A_g$) > 1029 ($B_{1g}$) > 750. The most enhanced modes belong to $A_g$ symmetry and comprise both stretching and deformation (bending) vibrations of the macrocycle (Table 1). The $B_{1g}$ modes, the $A_g$ vibrations localized also (or preferentially) on the benzene ring, as well as C—H deformation modes are to be found among the less enhanced ones. This enhancement pattern is consistent with the expected behavior upon excitation into $Q_x$ (or $Q_y$) purely electronic (0–0) transition which was found previously to be localized predominantly on the tetrapyrrole macrocycle in the samples constituted entirely by $H_2$Pc molecules.[17]



  

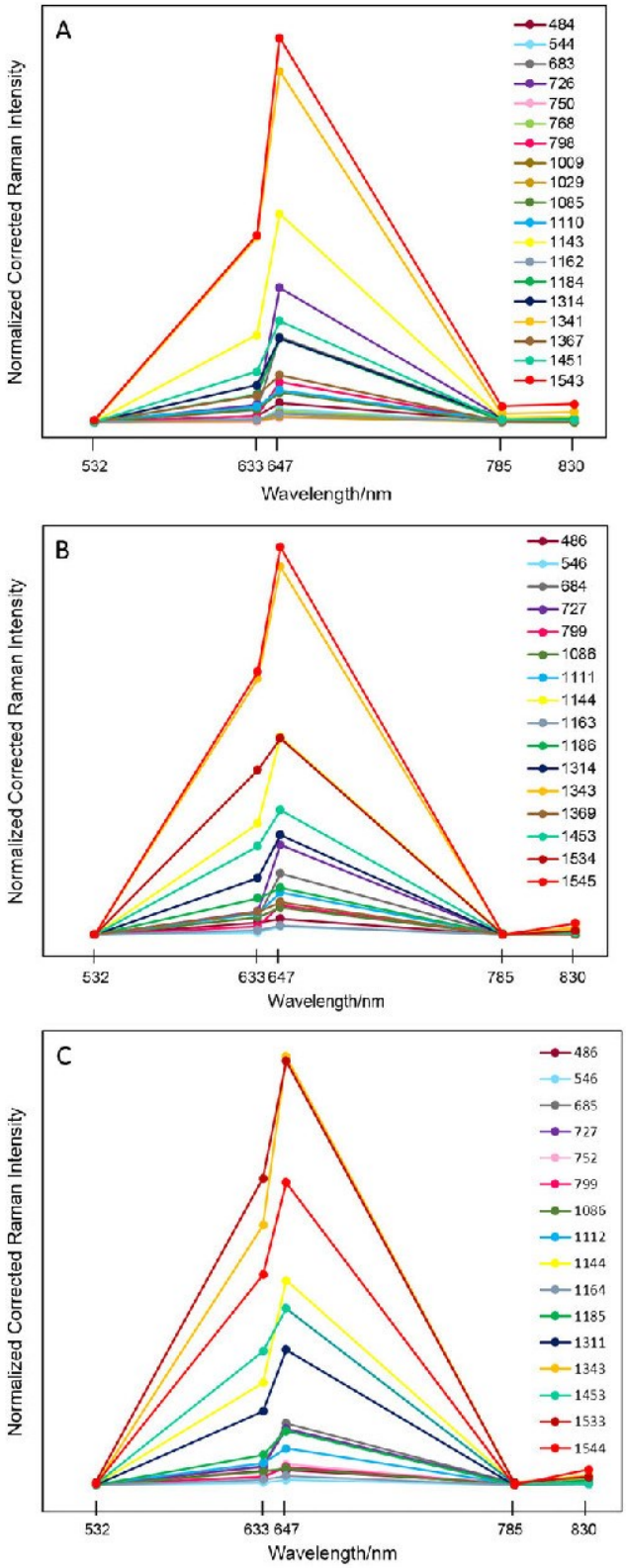


**Figure 7.** Excitation profiles of $H_2Pc$ Raman spectral bands in (A) glass/SLG/$H_2Pc$ (BL)-I system, (B) glass/SLG/$H_2Pc$ (ML)- VI system and (C) glass/SLG/$H_2Pc$ (ML)-X system in the 532–830 nm range. Details of the EPs of the less enhanced bands are provided in Fig. S10 in SI.

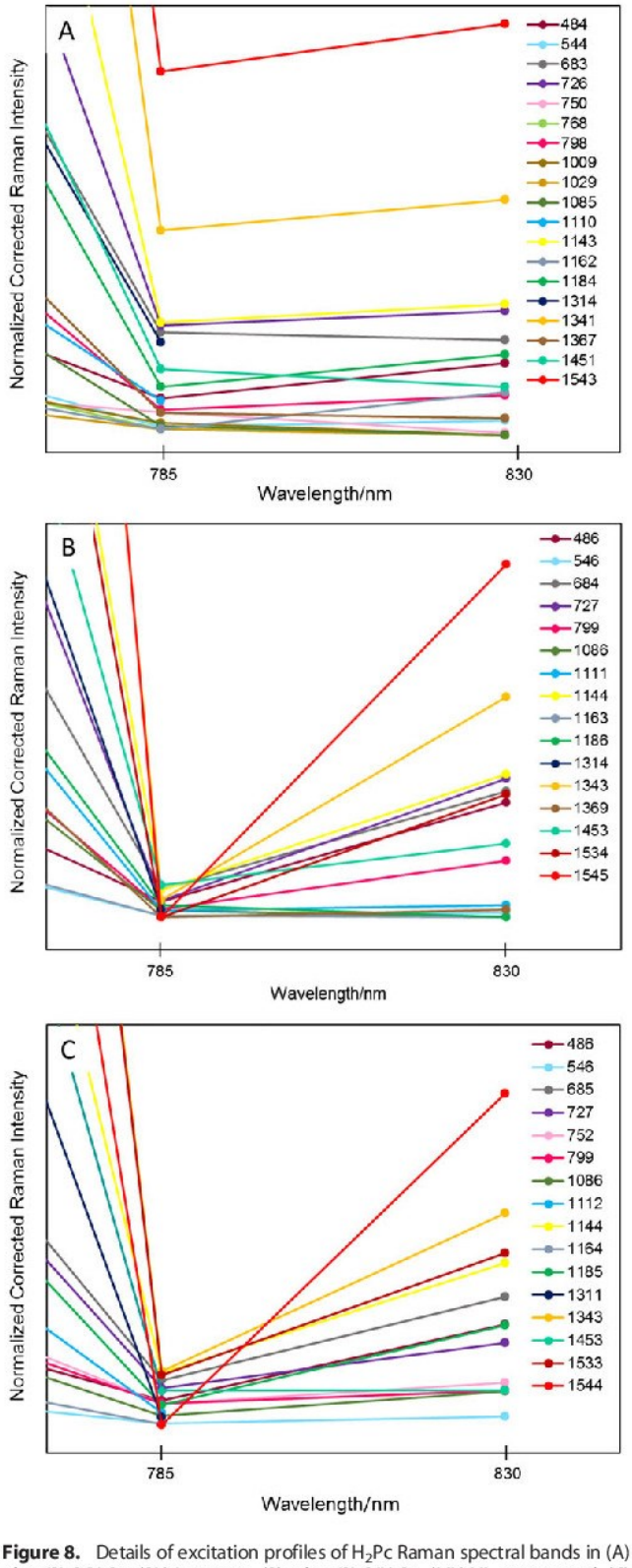


**Figure 8.** Details of excitation profiles of $H_2Pc$ Raman spectral bands in (A) glass/SLG/$H_2Pc$ (BL)-I system, (B) glass/SLG/$H_2Pc$ (ML)-VI system and (C) glass/SLG/$H_2Pc$ (ML)-X system at 785 and 830-nm excitations.

The series at 633-nm excitation (Figs 7, 8 and Fig. S10 in SI, profiles A) was found to be: 1543 ($A_g$) > 1341 ($A_g$) > 1143 ($A_g$) > 1451 ($A_g$) > 1314 ($B_{1g}$) > 1184 ($A_g$) ~ 1367 > 726 ($A_g$) > 1110 ($B_{1g}$) > 1085 ($B_{1g}$) > 683 ($A_g$) > 484 ($B_{1g}$) > 798 ($A_g$) > 1162 (Ag) ~ 1009 ($B_{1g}$) ~ 1029 ($B_{1g}$) ~ 768 ($A_g$) > 544 ($A_g$) > 750. Although the relative intensities of the three most enhanced bands (1543, 1344 and 1144 $cm^{-1}$) are comparable at the 647 and 633-nm excitations, there is a substantial difference in case of the 685 and 726 $cm^{-1}$ bands belonging to the modes localized on the $H_2Pc$ macrocycle. While they are among the more enhanced bands at 647 nm, they fall into the category of weakly enhanced ones for the 633-nm excitation.

This difference can be tentatively explained by considering the electronic absorption spectrum of the glass/SLG/$H_2Pc$-(BL)-I hybrid system (Fig. 1). While the 647-nm excitation falls within the main electronic absorption band belonging to $Q_y$ (0–0) transition, the 633-nm excitation appears to coincide with the shoulder located at about the same wavelength. This shoulder (giving rise to a separate band in peak fitting in Fig. 1) has been attributed to the vibronic $Q_y$ (0–1) side band of the $Q_y$ (0–0) electronic absorption band arising from the coupling of the $Q_x$ and $Q_y$ excited electronic states by $B_{1g}$ vibrations. [17] The difference between the position of the vibronic side band (633 nm) and the band maximum of the $Q_y$ (0–0) electronic transition is ~1368 $cm^{-1}$, i.e. it falls into the higher wavenumber region. This rationalizes the observed stronger enhancement of some of the high wavenumber $B_{1g}$ modes than that of the low wavenumber $A_g$ modes of the tetrapyrrole macrocycle at 633-nm excitation.

The coincidence of the 647-nm excitation with the $Q_y$ (0–0) electronic transition band is further corroborated by evaluation of the sequence of the most enhanced bands at 785 nm (Figs 7, 8 and Fig. S10 in SI, profiles A). Electronic absorption spectrum of the hybrid system (Fig. 1) shows that this particular excitation wavelength falls into the very onset of the $Q_x$ band with its maximum appearing at 718 nm. This implies that the enhancement of Raman spectral bands at 785-nm excitation most probably originates from resonance (or preresonance) with the $Q_x$ (0–0) electronic transition. The following sequence of normalized band intensities was determined: 1543 ($A_g$) > 1341 ($A_g$) > 1143 ($A_g$) ~ 726 ($A_g$) > 683 ($A_g$) > 1314 ($B_{1g}$) > 1451 ($A_g$) > 1184 ($A_g$) > 484 ($B_{1g}$) ~ 1110 ($B_{1g}$) > 798 ($A_g$) ~ 750 ~ 1367 > 1009 ($B_{1g}$) ~ 1085 ($B_{1g}$) ~ 544 ($A_g$) ~ 1162 ($A_g$) ~ 1029 ($B_{1g}$) ~ 768 ($A_g$). The sequence resembles to that at 647-nm excitation particularly by the appearance of the bands at 684 and 726 $cm^{-1}$ (belonging to the macrocycle modes) among the most enhanced ones.

*Excitation profiles of Raman bands of glass/single-layer graphene/phthalocyanine (ML)-VI hybrid system*

The normalized intensity sequence of the $H_2Pc$ Raman bands for the glass/SLG/$H_2Pc$ (ML)-VI system at 647-nm excitation (Figs 7, 8 and Fig. S10 in SI, profiles B) has been determined as: 1545 ($A_g$) > 1343 ($A_g$) > 1534 ~ 1144 ($A_g$) > 1453 ($A_g$) > 1314 ($B_{1g}$) > 727 ($A_g$) > 684 ($A_g$) > 1186 ($A_g$) > 1111 ($B_{1g}$) > 1369 > 799 ($A_g$) > 1086 ($B_{1g}$) > 486 ($B_{1g}$) > 1163 ($A_g$) > 546 ($A_g$). For the 633-nm excitation, the band order is the following (Figs 7, 8 and Fig. S10 in SI, profiles B): 1545 ($A_g$) > 1343 ($A_g$) > 1534 ~ 1144 ($A_g$) > 1453 (Ag) > 1314 ($B_{1g}$) > 1186 ($A_g$) > 727 ($A_g$) ~ 1369 > 1111 ($B_{1g}$) ~ 684 ($A_g$) > 1086 ($B_{1g}$) > 486 ($B_{1g}$) > 799 ($A_g$) > 1163 ($A_g$) > 546 ($A_g$). The sequences of normalized band intensities are thus quite similar at both excitations. In particular, the sequences of the first five bands are virtually the same (involving also the newly appearing 1534 $cm^{-1}$ band), while the 684 and 727 $cm^{-1}$ macrocycle bands are among the less intense ones.

*Excitation profiles of Raman bands of glass/single-layer graphene/phthalocyanine (ML)-X hybrid system*

The normalized intensity sequence for glass/SLG/$H_2Pc$ (ML)-X spectral bands at 647 nm was ascertained to be (Figs 7, 8 and Fig. S10 in SI, profiles C): 1343 ($A_g$) ~ 1533 > 1544 ($A_g$) > 1144 ($A_g$) > 1453 ($A_g$) > 1311 ($B_{1g}$) > 685 ($A_g$) > 727 ($A_g$) > 1185 ($A_g$) > 1112 ($B_{1g}$) > 752 ~ 799 ($A_g$) > 1086 ($B_{1g}$) > 486 ($B_{1g}$) > 1164 ($A_g$) > 546 ($A_g$). At 633 nm excitation, this sequence was determined as: (Figs 7, 8 and Fig. S10 in SI, profiles C): 1533 > 1343 ($A_g$) > 1544 ($A_g$) > 1453 ($A_g$) > 1144 ($A_g$) > 1311 ($B_{1g}$) > 1185 ($A_g$) > 1112 ($B_{1g}$) > 727 ($A_g$) ~685 ($A_g$) > 486 ($B_{1g}$) ~ 1086 ($B_{1g}$) ~ 799 ($A_g$) > 752 ~ 1164 ($A_g$) > 546 ($A_g$). The sequences of the normalized band intensities show a pronounced mutual analogy, and they are also quite similar to those encountered for the glass/SLG/$H_2Pc$ (ML)-VI hybrid system, particularly in observing the low wavenumber macrocycle bands among the less intense ones. The only apparent difference between the samples (ML)-VI and (ML)-X is thus a pronounced intensity gain of the 1533 $cm^{-1}$ band, which, in the latter case, becomes the most intense band at 647 nm (together with the 1343 $cm^{-1}$ band) as well as at 633 nm excitation. This difference is explained in Text S4 in SI.

*Comparison of excitation profiles of glass/single-layer graphene/phthalocyanine (BL)-I, glass/single-layer graphene/phthalocyanine (ML)-VI and glass/single-layer graphene/phthalocyanine (ML)-X hybrid systems in the visible region*

The sequences of the normalized band intensities at 633 and 647-nm excitations were found to be largely similar for both hybrid systems containing a monolayer of $H_2Pc$ molecules, i.e. (ML)-VI) and (ML)- X. By contrast, distinct differences between both systems with the $H_2Pc$ monolayer on one hand, and that with the $H_2Pc$ bilayer, i.e. (BL)-I on the other hand have been found in this respect. We propose that two factors contribute to the observed differences: (i) the electronic absorption bands of $H_2Pc$ blue-shifts upon diminishing the SLG coverage by $H_2Pc$ from a BL (formed by J-type dimers with the electronic absorption bands strongly red shifted with respect to those of the $H_2Pc$ monomers, as established in sub-Chapter A), to a ML, and (ii) the SLG–$H_2Pc$ interaction is stronger for the SLG–$H_2Pc$ (ML) hybrids than for the SLG–$H_2Pc$ (BL) one (as established in Text S4 in SI). The former factor appears to be the reason why, (i) for the glass/SLG/$H_2Pc$ (BL)-I hybrid, the 633-nm excitation falls into the vibronic $Q_y$(0–1) sideband of the $Q_y$(0–0) electronic absorption band and the 647-nm excitation into the $Q_y$ (0–0) absorption band (giving rise to the different sequences of the relative band intensities at 633 and 647-nm excitations, respectively), while, (ii) for the glass/SLG/$H_2Pc$ (ML)-VI and glass/SLG/$H_2Pc$ (ML)-X hybrids, both excitation wavelengths coincide with the $Q_y$ (0–0) electronic transition, giving rise to mutually analogous sequences of the relative band intensities at both excitations. The latter factor is proposed to be responsible for the observed differences in the sequences of relative band intensities at 647 nm, i.e. upon excitation into the $Q_y$ (0–0) electronic transition, between both systems with the $H_2Pc$ monolayer (i.e. ML-VI and ML-X) on one hand, and that with the $H_2Pc$ bilayer (i.e. BL-I) on the other hand. In particular, we propose that the above mentioned differences originate from the differences in the localization of the $Q_y$ (0–0) electronic transitions induced by the SLG–$H_2Pc$ interaction which is stronger in the SLG–$H_2Pc$ (ML) hybrids than in the SLG–

$H_2Pc$ (BL) one (as established in Text S4 in SI). This tentative explanation is consistent with the vibrational mode selectivity of GERS enhancement factors determined and presented in sub-Chapter D *(vide infra)*.

*Excitation profiles of Raman bands of glass/single-layer graphene/phthalocyanine hybrid systems in the high wavelengths region*

For the glass/SLG/$H_2Pc$ (ML)-VI and glass/SLG/$H_2Pc$ (ML)-X samples (both with a monolayer coverage of SLG by $H_2Pc$), the normalized intensities of all spectral bands strikingly drop at 785-nm excitation, while, for the majority of spectral bands, they exhibit a pronounced increase at 830-nm excitation (Fig. 8, profiles B and C). By contrast, for the glass/SLG/$H_2Pc$ (BL)-I system, the normalized band intensities show no such distinctive intensity drop and rise at 785 and 830-nm excitations, respectively (Fig. 8, profile A). Therefore, this feature appears selectively in excitation profiles of samples VI and X containing ~ a monolayer of $H_2Pc$ molecules, and it can thus be attributed to a manifestation of the SLG–$H_2Pc$ (ML) interaction.

The sequence of the normalized band intensities for glass/SLG/$H_2Pc$ (ML)-VI system at 830-nm excitation (Fig. 8(B)) was determined as: 1545 ($A_g$) > 1343 ($A_g$) > 1144 ($A_g$) ~ 727 ($A_g$) ~ 684 ($A_g$) ~ 1534 ($A_g$) ~ 486 ($B_{1g}$) > 1453 ($A_g$) > 799 ($A_g$) > 1111 ($B_{1g}$) > 1369 > 546 ($A_g$). In case of the glass/SLG/$H_2Pc$ (ML)-X sample (Fig. 8(C)), the following sequence of band intensities was found: 1544 ($A_g$) > 1343 ($A_g$) > 1533 ($A_g$) ~ 1144 ($A_g$) > 685 ($A_g$) > 486 ($B_{1g}$) ~ 1185 ($A_g$) > 727 ($A_g$) > 752 > 1453 ($A_g$) ~ 799 (Ag) ~ 1086 ($B_{1g}$) > 546 ($A_g$). Common features of the two series include the largest enhancement of the 1545 and 1343 $cm^{-1}$ bands, as well as the inclusion of the 684 and 727 $cm^{-1}$ bands of the $A_g$ modes, together with the 486 $cm^{-1}$ band of the $B_{1g}$ mode, among the strongly enhanced ones. All the latter bands belong to the modes localized on the macrocycle. On the other hand, the two above mentioned series of bands differ particularly in the relative intensity increase of the band at 1533 $cm^{-1}$ for sample (ML)-X with respect to sample (ML)-VI. This difference between the glass/SLG/$H_2Pc$-(ML)-VI and the glass/SLG/$H_2Pc$ (ML)-X hybrid systems has been encountered also at excitations in the visible spectral region, and it is attributed to reorganization of $H_2Pc$ molecules constituting a monolayer on SLG upon the repetitive soaking of the sample in toluene (explained in Text S4 in SI and supported by ref. [44]).

**D. Determination of graphene-enhanced Raman scattering enhancement factors of phthalocyanine modes in the Raman spectra of glass/single-layer graphene/phthalocyanine (ML)-X system at 633 and 647-nm excitations.**

In contrast to all three glass/SLG/$H_2Pc$ hybrid systems, the signal of $H_2Pc$ is observed only at 633 and 647-nm excitations for the graphite/$H_2Pc$ (ML) reference system. This observation indicates that the $H_2Pc$ molecules arranged in a monolayer on graphite surface experience a strong resonance enhancement of their Raman scattering only at 633 and 647-nm wavelengths. The comparison of Raman spectra of the glass/$H_2Pc$/SLG (ML)-X and of the graphite/$H_2Pc$ (ML) systems in Figs 5 and 6 shows that this resonance enhancement experiences an additional intensity increase as well as relative band intensity changes, together with the appearance of the additional spectral bands when the graphite substrate is replaced by SLG on glass. The assignment and the origin of the additional bands is addressed in the Text S4 in SI. The GERS enhancement has been quantitatively evaluated in terms of GERS enhancement factors (Table 2) which, in turn, have been determined as the intensity ratios of the corresponding $H_2Pc$ Raman spectral bands in the spectra of the glass/SLG/$H_2Pc$ (ML)-X and of the graphite/$H_2Pc$ (ML) system, respectively (details in Experimental).

The GERS enhancement factors (EFs) listed in Table 2 are in the range from 3 to 24 at 633 nm and from 3 to 19 at 647-nm excitation, and the average values of GERS enhancement factors are 9.3 and 8.4, respectively. The maximum as well as the average GERS enhancement is thus slightly higher at 633-nm than at 647-nm excitation. Furthermore, the selectivity of GERS enhancement factors at both the 633-nm and the 647-nm excitations (Table 2) with respect to the symmetry of the vibrational modes ($A_g$ or $B_{1g}$), wavenumbers of the vibrational modes (probed on the basis of their significance

**Table 2.** GERS enhancement factors calculated from the intensity ratios of the $H_2Pc$ Raman spectral bands in the spectra of glass/SLG/$H_2Pc$ (ML)-X system and of the graphite/$H_2Pc$ (ML) reference system, respectively

| Band wavenumber [$cm^{-1}$] | GERS enhancement factors at 633-nm excitation | GERS enhancement factors at 647-nm excitation | $H_2Pc$ mode symmetry | $H_2Pc$ mode assignment |
|---|---|---|---|---|
| 487 | **9** | **8** | $B_{1g}$ | b.r. rock + c.r. def |
| 685 | **5** | **5** | $A_g$ | CNC + b.r. def |
| 727 | **3** | **3** | $A_g$ | pyr + CNC def |
| 751 | On SLG only | On SLG only | IR act | oopδN—H |
| 799 | **3** | **3** | $A_g$ | νC=C (b.r. + pyr) |
| 958 | On SLG only | On SLG only | IR act | oopδC—H |
| 1087 | **8** | **5** | $B_{1g}$ | ipδN—H |
| 1114 | **12** | **16** | $A_g$ | — |
| 1144 | **8** | **10** | $A_g$ | b.r.(νCC + δCH) |
| 1220 | On SLG only | On SLG only | $B_{1g}$ | b.r. def + δCH+ ipδN—H |
| 1315 | **11** | **12** | $B_{1g}$ | — |
| 1345 | **12** | **11** | $A_g$ | νC=C (b.r. + pyr) |
| 1432 | **8** | **6** | $B_{1g}$ | — |
| 1453 | **24** | **19** | $A_g$ | b.r. δCH |
| 1516 | **7** | **5** | $A_g$ | — |
| 1534 | On SLG only | On SLG only | $A_g$ | νCNC c.r. |
| 1543 | **11** | **6** | $A_g$ | νCNC c.r. |

in the theoretical treatment of GERS[5,6]) and localization of the vibrational modes within the $H_2Pc$ molecule (assignment of bands to normal modes) has been probed. Because the ranges of GERS EFs experienced by $A_g$ and $B_{1g}$ modes (namely 3–24 for $A_g$ and 8–11 for $B_{1g}$ modes at 633-nm excitation as well as 3–19 for $A_g$ and 5–12 for $B_{1g}$ modes at 647-nm excitation) mutually overlap, and the average values of GERS EFs of $A_g$ and $B_{1g}$ modes are similar at both excitations (namely 9.4 for $A_g$ modes and 9.0 for $B_{1g}$ modes at 633-nm excitation, and 8.6 for $A_g$ and 7.8 for $B_{1g}$ modes at 647-nm excitation), no generalization concerning the dependence of the GERS EFs on the symmetry of vibrational modes can be done. In addition to that, there is no systematic dependence of GERS EFs on the wavenumbers of the vibrational modes bands, because the maximal enhancement is obtained for the 1453 $cm^{-1}$ band at both 633 and 647-nm excitations while the EF values decrease for the bands of both lower and higher wavenumbers. Localization of vibrational modes within the $H_2Pc$ molecule thus emerges as the most important factor which governs their GERS enhancement. In particular, the largest enhancement (EF values 24 and 19 at 633 and 647-nm excitation, respectively) is observed for the 1453 $cm^{-1}$ band assigned to the $A_g$ vibrational mode with a strong contribution of C—H deformation on the benzene ring. A large GERS enhancement is experienced also by the 1218 $cm^{-1}$ mode ($B_{1g}$) involving C—H and N—H in-plane deformations and benzene ring deformation (Table 2), the band of which is extremely weak in the Raman spectra of graphite–$H_2Pc$ sample, and hence its GERS enhancement factor could not be exactly determined. In fact, nearly all strongly and/or moderately enhanced bands belong to modes localized on the benzene rings of $H_2Pc$. On the other hand, the modes delocalized over the tetrapyrrole macrocycle are among the least enhanced ones (Table 2).

### E. Evidence for two mechanism of graphene-enhanced Raman scattering in glass/single-layer graphene/phthalocyanine (ML) hybrid systems

Enhancement of Raman scattering with a distinct selectivity towards localization of individual vibrational modes within the $H_2Pc$ molecule has been observed for $H_2Pc$ molecules in the glass/SLG/$H_2Pc$ (ML) hybrid systems upon excitations falling into (i) the visible (633 and 647 nm) and (ii) the onset of near IR (830 nm) spectral regions. In this sub-Chapter, we inspect the origin of each of these two enhancement effects.

**(i)** Both the 633 and 647-nm excitations fall into the electronic absorption band of a $Q_y$ (0–0) electronic transition of $H_2Pc$ molecules monolayer (more precisely, into its lower wavelengths side), as established by the analysis of EPs of the glass/SLG/$H_2Pc$ (ML) hybrids (Fig. 7(B), (C) and Fig. S10(B), (C) in SI) presented in sub-Chapter C. Both excitation wavelengths thus obey the resonance condition for GERS formulated by the first part of Eqn 15 (i) in ref. [6] which is defined as excitation into the electronic absorption band related to the HOMO–LUMO transition within a planar aromatic molecule.[5,6] Furthermore, the enhancement of Raman spectral bands of individual vibrational modes of $H_2Pc$ in glass/SLG/$H_2Pc$ (ML)-X system with respect to those of the graphite–$H_2Pc$ (ML) reference system has been quantified in terms of their mutual intensity ratios, i.e. the GERS EFs (sub-Chapter D). The fact that at least some GERS enhancement of the Raman signal has been determined for all spectral bands of $H_2Pc$ indicates a small change in the position, the intensity and/or the half-width of the electronic absorption band of the $Q_y$ (0–0) electronic transition for the $H_2Pc$ monolayer in the glass/SLG/$H_2Pc$ (ML)-X hybrid system with respect to the graphite/$H_2Pc$ reference hybrid system. Because the electronic absorption spectra of none of these two systems could be obtained (details in Experimental), we cannot precisely determine the difference between them. On the other hand, the GERS enhancement factors are slightly higher at 633-nm than at 647-nm excitation (sub-Chapter D and Table 2), while the EPs of the Raman bands of the glass/SLG/$H_2Pc$ (ML)-X hybrid system (Fig. 7 and Fig. S10 in SI) show a normalized intensity increase for all Raman bands at 647-nm excitation with respect to the 633-nm excitation. Therefore, it is the broadening of the $Q_y$ (0–0) electronic absorption band of the monolayer of $H_2Pc$ molecules in the system with SLG in comparison to that with graphite which is most consistent with the above mentioned observations. Is should also be noted that the broadening of both the $Q_y$ (0–0) and $Q_x$ (0–0) electronic absorption bands of $H_2Pc$ molecules upon their adsorption on Ag islands has been determined on the basis of detailed EPs spanning these electronic transitions, and it was attributed to bonding of $H_2Pc$ molecules to Ag by lone pairs of N atoms[7]. The nature of the relatively strong $H_2Pc$–SLG interaction (determined in Text S4 in SI) is different from the Ag–$H_2Pc$ one, because it is ascribed to $\pi - \pi$ interaction and/or van der Waals forces[3,8]. Nevertheless, its effect on the electronic absorption spectrum of $H_2Pc$ can be similar.

Furthermore, the vibrational mode selectivity of the GERS enhancement, namely the preferential GERS enhancement of the vibrational modes fully or partially localized on the benzene rings of $H_2Pc$ (established in sub-Chapter D) indicates (in accord with the theory of RRS[24]) the difference in localization of the resonant $Q_y$ (0–0) electronic transition within the $H_2Pc$ molecule between the glass/SLG/$H_2Pc$ system and the graphite–$H_2Pc$ reference system, in particular, delocalization of this electronic transition over the benzene rings of $H_2Pc$ in the former system, i.e. for $H_2Pc$ on SLG. It should be noted that both $Q_y$ (0–0) and $Q_x$ (0–0) electronic transitions were found to be localized preferentially on the $H_2Pc$ macrocycle for samples involving only the $H_2Pc$ molecules,[17] as confirmed also by the results of the ab-initio calculations of the localization of HOMO, LUMO and LUMO + 1 for the isolated $H_2Pc$ molecule.[45] The difference in the localization of the $Q_y$ (0–0) electronic transition between glass/SLG/$H_2Pc$ system and the graphite–$H_2Pc$ reference system can thus be tentatively attributed to delocalization of HOMO of $H_2Pc$ over the benzene rings $H_2Pc$ in the latter system. This situation, in turn, could originate from the relatively strong SLG–$H_2Pc$ interaction and short SLG–$H_2Pc$ distance (established in Text S4 in SI), in which the $\pi - \pi$ interaction between the benzene rings of $H_2Pc$ and the conjugated benzene rings of SLG can be expected to play an important role.

In summation, the mechanism of GERS enhancement observed for the glass/SLG/$H_2Pc$ (ML)-X hybrid system with respect to the graphite–$H_2Pc$ reference system at 633 and 647-nm excitations can be attributed to RRS of $H_2Pc$ modified by a relatively strong SLG–$H_2Pc$ (ML) interaction. The modifications manifest themselves by minor changes in the half-width of the electronic absorption band and by pronounced changes in localization of this resonant $Q_y$ (0–0) electronic transition within the $H_2Pc$ molecule (Fig. 9).

**(ii)** Upon excitations at the onset of near IR spectral region (namely those at 785 and 830 nm), the vibrational-mode specific normalized intensity increase of the majority of Raman bands of $H_2Pc$ from 785-nm to 830-nm excitation has been encountered selectively in Raman excitation profiles of the glass/SLG/$H_2Pc$ (ML)-VI and the glass/SLG/$H_2Pc$ (ML)-X hybrid systems, i.e. for samples constituted by SLG and a monolayer of $H_2Pc$ molecules (sub-Chapter C and Fig. 8(B), (C)). The absence of the Raman signal of $H_2Pc$ at both these excitations for the graphite/$H_2Pc$ (ML) reference sample

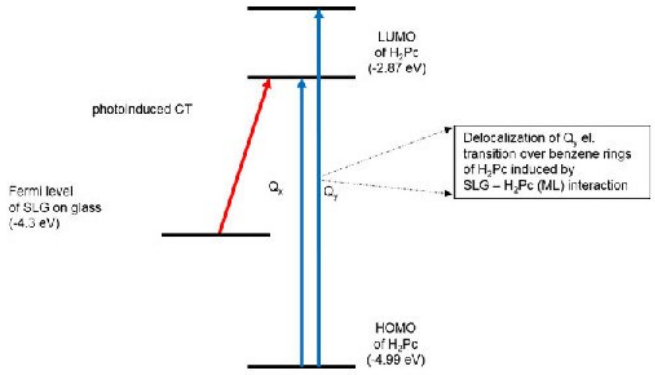


**Figure 9.** Schematic depiction of the two mechanisms of GERS operating in the glass/SLG/$H_2Pc$ (ML) system. The SLG Fermi level energy of pristine SLG (−4.6 eV)[3] has been corrected for the established n-doping of SLG by glass. HOMO and LUMO energies of $H_2Pc$ have been adopted from ref [10]. [Colour figure can be viewed at wileyonlinelibrary.com]

hampers determination of the GERS enhancement factors values. On the other hand, it indicates a substantial enhancement of Raman scattering of the above mentioned samples with respect to the reference sample at the 830-nm excitation. Furthermore, the sequence of the normalized band intensities at 830-nm excitations shows a distinct selectivity with respect to localization of the corresponding vibrational modes within the $H_2Pc$ molecule which, in turn, is largely similar for both the glass/SLG/$H_2Pc$ (ML) samples (i.e. VI and X). Importantly, for both samples, the sequence of the relative band intensities at 830 nm (sub-Chapter C and Fig. 8(B), (C)) differs from that encountered at 633-nm and 647-nm excitations which coincide with a $Q_y$ (0–0) electronic absorption band (sub-Chapter C, Fig. 7(B), (C) and Fig. S10(B), (C) in SI). For example, the 684 and 726 $cm^{-1}$ $A_g$ bands localized on the macrocycle are among the more enhanced modes in the former case, while they are among the less enhanced ones in the latter case. This difference in localization of the most enhanced bands within the $H_2Pc$ molecule indicates that at 830-nm excitation, the LUMO of $H_2Pc$ has been populated by a new electronic transition different (in its localization within the $H_2Pc$ molecule) from the two Q (0–0) electronic transitions (Fig. 9). Comparison of the SLG Fermi level energy (the position of which was corrected for doping of SLG by the glass substrate evaluated in sub-Chapter B) with the HOMO and LUMO energies of $H_2Pc$[10] demonstrated by the scheme presented in Fig. 9 indicates fulfillment of the energy condition for a photo-induced charge transfer (CT) between Fermi level of SLG and LUMO of $H_2Pc$ at 830-nm excitation. This explanation also agrees with one of the four theoretically predicted resonance conditions for the GERS enhancement observation[5,6], namely with that defined by Eqn 15 (iv) in ref. [6]:

$$h\nu_0 = E_L - E_F \quad \text{or} \quad h\nu_0 = E_L - E_F - h\nu_q,$$

where $h\nu_0$ is the energy of excitation, $E_F$ and $E_L$ are the energies of Fermi level of SLG and of LUMO of $H_2Pc$, respectively, and $h\nu_q$ is the phonon (i.e. the vibrational mode) energy. Because the sequence of the most enhanced bands does not systematically follow the phonon energy (i.e. the vibrational mode wavenumber) sequence, we reason that it is the first of the two resonance conditions in the abovementioned equation which is actually fulfilled at 867 nm, which is the wavelength equivalent of the 1.43-eV energy difference between $E_L$ and $E_F$ (Fig. 9). We can thus speculate that the 830-nm excitation falls into the lower wavelength slope of the electronic absorption band of the abovementioned photoinduced CT transition with a maximum close to 867 nm.

Furthermore, the absence of such pronounced normalized intensity increase of Raman bands in excitation profiles of the glass/SLG/$H_2Pc$ (BL)-I hybrid system indicates that observation of the photoinduced CT transition is conditioned by the stronger SLG–$H_2Pc$ interaction in the case of the monolayer coverage of SLG by $H_2Pc$ than in the case of the bilayer one (established in Text S4 in SI).

Finally, we notice some analogy between this particular mechanism of GERS and the chemical mechanism of SERS (particularly when the latter one operates in the absence of the electromagnetic mechanism of SERS on flat metal surfaces[46]). The common feature of the two mechanisms is a photoinduced CT transition from the Fermi level of the metal or SLG to LUMO of a molecule conditioned by a relatively strong surface–molecule interaction. On the other hand, it has to be noted that the chemisorption which is the necessary condition for operation of the chemical mechanism of SERS [25,26,46] is different in its nature and strength from the $\pi$–$\pi$ interaction involved in SLG-aromatic molecule (e.g. $H_2Pc$) monolayer systems; hence, different types of molecules can obey the necessary condition for this photoinduced CT mechanism in GERS and in SERS, respectively.

## Conclusions

The glass/SLG/free-base phthalocyanine ($H_2Pc$) hybrid systems with monolayer (ML) coverages of SLG by $H_2Pc$ molecules were prepared by a spectrally controlled adsorption–desorption of $H_2Pc$ molecules from solution. The graphite/$H_2Pc$ (ML) and the glass/SLG/$H_2Pc$ (BL) hybrids were prepared as well and employed as the reference systems. Raman spectra of all hybrid systems were measured as a function of excitation wavelengths in the 532–830 nm range. Assignment of the specific Raman spectral features allowed to establish the relative strength of interaction between the single carbon atom layer and $H_2Pc$ molecules: graphite–$H_2Pc$ (ML) < SLG–$H_2Pc$ (BL) < SLG–$H_2Pc$ (ML). Excitation profiles of $H_2Pc$ Raman bands of the SLG containing hybrids were constructed, and the sequences of the normalized band intensities at each wavelength were analyzed for the vibrational mode specificity.

Raman excitation profiles of glass/SLG/$H_2Pc$ (ML) hybrid systems in the 532–830 nm region have revealed two types of resonance mechanisms conditioned specifically by the relatively strong interaction between SLG and a monolayer of $H_2Pc$ molecules. Both of them manifest themselves by an additional enhancement of Raman modes of $H_2Pc$ (denoted as the GERS enhancement[3–6]); however, for each of them, a different energy as well as localization of the resonance electronic transition within the $H_2Pc$ molecule has been established. The different energies of the two resonant electronic transitions also indicate that each of them obeys a different resonance condition theoretically predicted for GERS.[6] In particular, at the 633 and 647-nm excitations falling into the low wavelength side of the $Q_y$ (0–0) electronic absorption band of $H_2Pc$, the GERS enhancement of the Raman modes of $H_2Pc$ in the glass/SLG/ $H_2Pc$ (ML) hybrid system is attributed to RRS of $H_2Pc$ modified by a relatively strong SLG–$H_2Pc$ (ML) interaction. The most pronounced modification is delocalization of the resonant $Q_y$ (0–0) electronic transition over the outer benzene rings of $H_2Pc$. Furthermore, the GERS enhancement at 830-nm excitation is ascribed to the proximity of this excitation to the energy of a photoinduced charge transfer transition from Fermi level of SLG on glass to LUMO of $H_2Pc$. The energy of this photoinduced CT transition was

calculated as the difference between the energy of the Fermi level of SLG on glass (−4.3 eV) and the previously reported energy of LUMO of $H_2Pc$[10]. To the best of our knowledge, this experimental evidence for the theoretically predicted GERS enhancement by the photoinduced CT mechanism[6] is reported here for the first time.

Finally, we propose that the approach presented in this paper for the SLG- $H_2Pc$ (ML) can be applied also to other hybrid systems constituted by SLG and a monolayer of planar aromatic molecules, provided that their specificity, namely their various $E_L$ and $E_H$ values, are taken into account. The merit of such studies is not only the observation of the GERS enhancement, but also specification of its excitation wavelength dependence and of the mechanism of its origin for a particular SLG–aromatic molecule hybrid and excitation wavelength. Another benefit is obtaining information about the Raman spectral and electronic effects of SLG–aromatic molecule interaction in such hybrid systems.

### Acknowledgments

The authors thank Prof. George R. Rossman and Prof. Antonin Vlcek for acquisition of the UV–Vis electronic absorption spectra of glass/SLG/$H_2Pc$-(BL)-I hybrid system on the special UV/Vis spectrometer assembled by Prof. G.R. Rossman at the California Institute of Technology, Division of Geological and Planetary Sciences. Financial support by the 15-01953S grant awarded by the Czech Science Foundation (Grantová Agentura České Republiky) is gratefully acknowledged.

## References

[1] A. Jorio, R. Saito, G. Dresselhaus, M. S. Dresselhaus, *Raman Spectroscopy in Graphene Related Systems*, Wiley-VCH Verlag GmbH & Co. KGaA, Weinheim, Germany, **2011**.
[2] A. C. Ferrari, D. M. Basko, *Nat. Nanotechnol.* **2013**, *8*, 235.
[3] X. Ling, L. Xie, Y. Fang, H. Xu, H. Zhang, J. Kong, M. S. Dresselhaus, J. Thang, Z. Liu, *Nano Lett.* **2010**, *10*, 553.
[4] X. Ling, S. Huang, N. Mao, J. Kong, M. S. Dresselhaus, J. Zhang, *Accounts Chem. Res.* **2015**, *48*, 1862.
[5] S. Huang, X. Ling, L. Liang, Y. Song, W. Fang, J. Zhang, J. Kong, V. Meunier, M. S. Dresselhaus, *Nano Lett.* **2015**, *15*, 2892.
[6] E. B. Barros, M. S. Dresselhaus, *Phys. Rev. B* **2014**, *90*, 90035443.
[7] A. Brotman, E. Burstein, *Phys. Scripta* **1985**, *32*, 385.
[8] C. Murray, N. Dozova, J. G. McCaffrey, N. Shafizadeh, W. Chin, M. Broquier, C. Crépin, *Phys. Chem. Chem. Phys.* **2011**, *13*, 17543.
[9] M. Cook, I. Chambrier, in *The Porphyrin Handbook, Volume 17: Phthalocyanines: Properties and Materials* (Eds: K. Kadish, R. Guilard, K. M. Smith), Academic Press, San Diego, **2003**, pp. 37–128.
[10] K. Nilson, J. Ahlund, B. Brena, E. Göthelid, J. Schiessling, N. Martensson, *J. Chem. Phys.* **2007**, *127*, 114702.
[11] B. J. C. Cabral, V. W. D. Cruzeiro, K. Coutinho, S. Canuto, *Chem. Phys. Lett.* **2014**, *595–596*, 97.
[12] M. V. Martínez-Díaz, G. de la Torre, T. Torres, *Chem. Commun.* **2010**, *46*, 7090.
[13] B. Menaa, M. Takahashi, Y. Tokuda, T. Yoko, *J. Photochem. Photobiol. A* **2007**, *194*, 362.
[14] E. N. Kaya, T. Basova, M. Polyakov, M. Durmus, B. Kadem, A. Hassan, *RCS Advances* **2015**, *5*, 91855.
[15] M. Ochsner, *J. Photochem. Photobiol. B: Biology* **1996**, *39*, 1.
[16] R. Aroca, D. P. DiLella, *J. Phys. Chem. Solid* **1982**, *43*, 707.
[17] S. Heutz, G. Salvan, S. D. Silaghi, T. S. Jones, D. R. T. Zahn, *J. Phys. Chem. B* **2003**, *107*, 3782.
[18] J. Marshell, *Mat. Sci. Res. Ind.* **2010**, *7*, 221.
[19] R. O. Loutfy, *Can. J. Chem.* **1981**, *59*, 549.
[20] S. M. Bayliss, S. Heutz, T. S. Jones, *Phys. Chem. Chem. Phys.* **1999**, *1*, 3673.
[21] C. Murray, N. Dozova, J. G. McCaffrey, S. FitzGerald, *Phys. Chem. Chem. Phys.* **2010**, *12*, 10406.
[22] R. Aroca, R. O. Loutfy, *J. Raman Spectrosc.* **1982**, *12*, 262.
[23] X. Ling, L. G. Moura, M. A. Pimenta, J. Zhang, *J. Phys. Chem. C* **2012**, *116*, 25112.
[24] R. J. H. Clark, T. J. Dines, *Angew. Chem. Int. Ed. Engl.* **1986**, *25*, 131.
[25] R. Aroca, *Surface-Enhanced Vibrational Spectroscopy*, John Wiley and Sons, Ltd., Chichester, UK, **2006**.
[26] M. Procházka, *Surface-Enhanced Raman Spectroscopy-Bioanalytical, Biomolecular and Medical Applications*, Springer International Publishing, Switzerland, **2016**.
[27] I. Srnová-Šloufová, B. Vlčková, T. L. Snoeck, D. J. Stufkens, P. Matějka, *Inorg. Chem.* **2000**, *39*, 3551.
[28] I. Šloufová, B. Vlčková, M. Procházka, J. Svoboda, J. Vohlídal, *J. Raman Spectrosc.* **2014**, *45*, 338.
[29] S. Zheng-Lin, Z. Fu-Shi, C. Xi-Qiao, Z. Fu-Qun, *Acta Phys.-Chim. Sin.* **2003**, *19*, 130.
[30] M. Kalbáč, O. Frank, L. Kavan, *L. Carbon* **2012**, *50*, 3682.
[31] T. Hallam, N. C. Berner, C. Yim, G. S. Duesberg, *Adv. Mater. Interfaces* **2014**, *1*, 1400115.
[32] M. N. Taran, G. R. Rossman, *Am. Mineral.* **2001**, *86*, 973.
[33] S. J. Choquette, E. S. Etz, W. S. Hurst, D. H. Blackburn, S. D. Leigh, *Appl. Spectrosc.* **2007**, *61*, 117.
[34] L. Henke, N. Nagy, U. Krull, *J. Biosensors and Bioelectronics* **2002**, *17*, 547.
[35] C. A. Hunter, J. K. M. Sanders, *J. Am. Chem. Soc.* **1990**, *112*, 5525.
[36] B. J. Prince, B. E. Williamson, R. J. Reeves, *JOL* **2001**, *93*, 293.
[37] K. Nakamoto, *Infrared and Raman Spectra of Inorganic and Coordination Compounds*, 4th ed., John Wiley & Sons, Inc., New York, **1986**.
[38] C. A. Melendres, V. A. Maroni, *J. Raman Spectrosc.* **1984**, *15*, 319.
[39] X. Zhang, Y. Zhang, J. Jiang, *Vib. Spectrosc.* **2003**, *33*, 153.
[40] H. F. Shurvell, L. Pinzuti, *Can. J. Chem.* **1966**, *44*, 125.
[41] D. R. Tackley, G. Dent, W. E. Smith, *Phys. Chem. Chem. Phys.* **2001**, *3*, 1419.
[42] C. Cong, T. Yu, G. F. Dresselhaus, M. S. Dresselhaus, *ACS Nano* **2011**, *5*, 1600.
[43] D. M. N. M. Dissanayake, A. Ashraf, D. Dwyer, K. Kisslinger, L. Zhang, Y. Pang, H. Efstathiadis, M. D. Eisman, *Sci. Reports* **2016**, *6*, 21070.
[44] T. Komeda, H. Isshiki, J. Liu, *Sci. Technol. Adv. Mater* **2010**, *11*, 054602.
[45] K. Toyota, J. Hasegawa, H. Takatsuji, *J. Phys. Chem. A* **1997**, *101*, 446.
[46] A. Campion, P. Kambhampati, *Chem. Soc. Rev.* **1998**, *27*, 241.

## Supporting information

Additional Supporting Information may be found online in the supporting information tab for this article.

**Supporting Information**

# Excitation wavelength dependence of Raman spectra of single layer graphene-free base phthalocyanine hybrid systems: GERS excitation profiles, mechanisms and enhancement factors

*Tereza Uhlířova*[a], *Peter Mojzeš*[b], *Zuzana Melniková*[c] *Martin Kalbáč*[c], *Veronika Sutrová*[a,d], *Ivana Šloufová*[a], *Blanka Vlčková*[a*]

[a] Charles University, Faculty of Science, Department of Physical and Macromolecular Chemistry, Hlavova 8, Prague 2, 128 40, Czech Republic

[b] Charles University, Faculty of Mathematics and Physics, Institute of Physics, Ke Karlovu 5, Prague 2, 121 16, Czech Republic

[c] J. Heyrovsky Institute of Physical Chemistry of the ASCR, v.v.i, Dolejškova 3, 182 21 Prague 8, Czech Republic

[d] Institute of Macromolecular Chemistry AS CR, Heyrovsky Sq. 2, 162 06 Prague 6, Czech Republic

* Corresponding author's e-mail: vlc@natur.cuni.cz

**Supporting Information Text 1: Preparation and Raman spectral mapping of graphite/$H_2$Pc (ML) reference sample**

A cylindrical graphite electrode for thermal evaporation of carbon was cut in half to produce a flat surface. The surface was then rubbed and polished by abrasive papers of decreasing abrasivity, and finally polished by a filter paper. The surface appeared to be flat and smooth, however, its SEM imaging revealed the presence both of the flat and smooth areas (Fig. S1, image A) and of the corrugated ones (Fig.S1, image B). Imaging with the optical microscope of the Raman microspectrometer revealed that the flat and smooth areas can be found also on the optical images (Fig. S2), and used for the subsequent Raman mapping. Moreover, the areas suitable for mapping of the graphite/$H_2$Pc reference samples could be identified also by the Raman spectra resulting from mapping of the parent graphite surface. The Raman maps of the appropriate areas showed a very low intensity of the 1344 cm-1 graphite band, in contrast to those of the corrugated ones, in which this band was very intense.

Graphite/$H_2$Pc monolayer (ML) samples were prepared by a similar strategy as those of glass/SLG/$H_2$Pc, i.e. first by soaking in $H_2$Pc solution in toluene and by a subsequent repeated soaking in pure toluene. Nevertheless, owing to stability of the graphite substrate, the preparation protocol could be simplified by its immersion into the solution and the solvent, respectively, (rather than only overlayed by each of them). Therefore, graphite was immersed into $H_2$Pc solution in toluene for 2 hours, dried by filter paper and then repeatedly immersed into pure toluene for ~24 hours. Achievement of a ~ monolayer coverage was established in a similar manner as in the case of glass/SLG/$H_2$Pc sample.

The parameters of the spectral maps acquisitions at each of the excitation wavelengths were the same as for the glass/SLG/$H_2$Pc samples. Nevertheless, owing to the above mentioned inhomogeneity of the graphite surface, it became crucial to acquire the Raman maps from exactly the same (carefully selected) flat and smooth area of the graphite surface (depicted in Fig S2) for both the graphite substrate itself, and for each of the graphite/$H_2$Pc samples at each of the excitation wavelengths. Fulfillment of this condition was accomplished by construction and application of a special sample holder, and it was repeatedly controlled by the optical imaging.

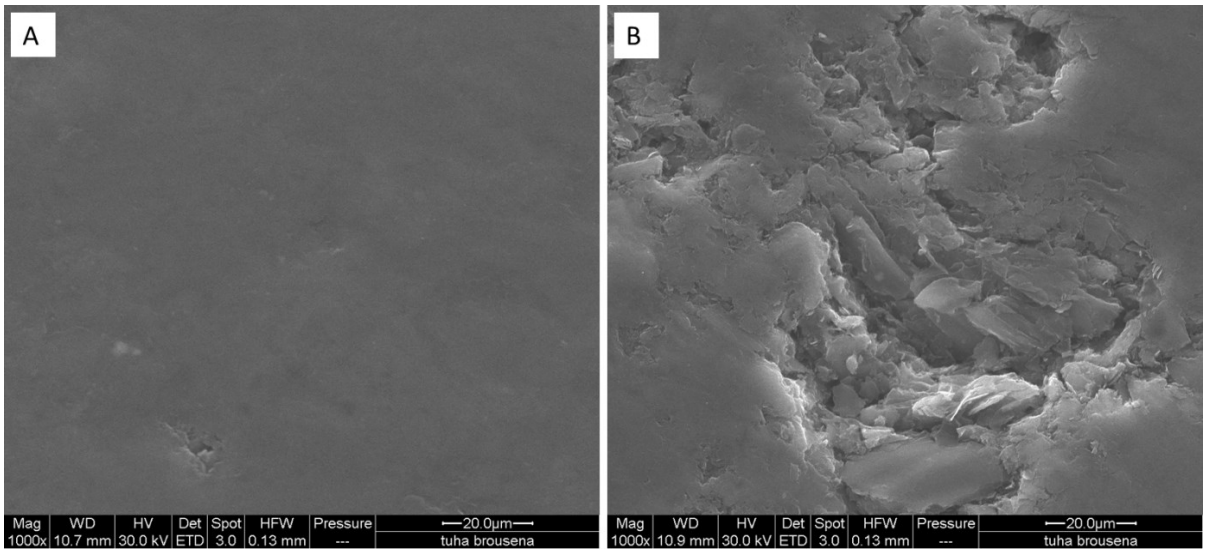


**Fig. S1** SEM images of rubbed and polished graphite surface: (A) flat area, (B) corrugated area.

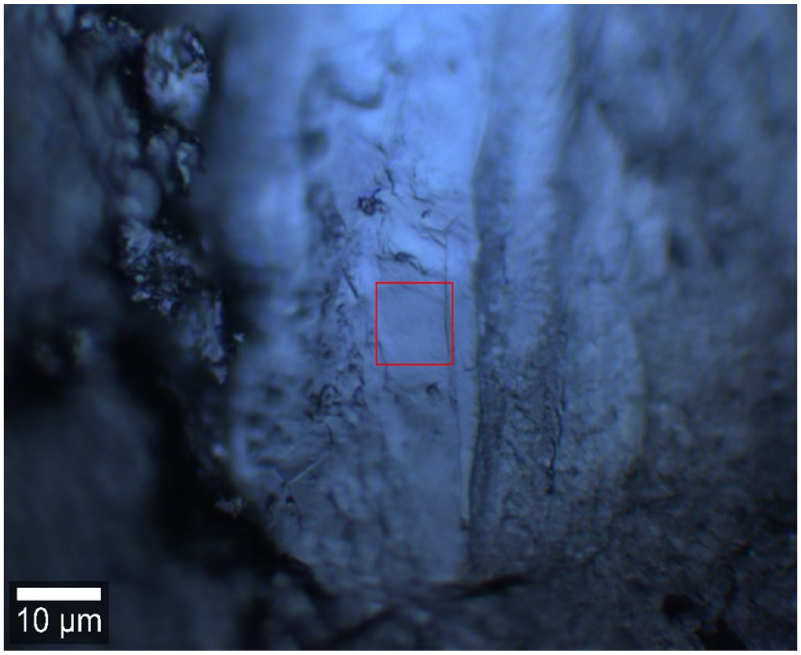


**Fig. S2** Optical image of a flat and smooth location on graphite/$H_2$Pc surface from which Raman maps were acquired.

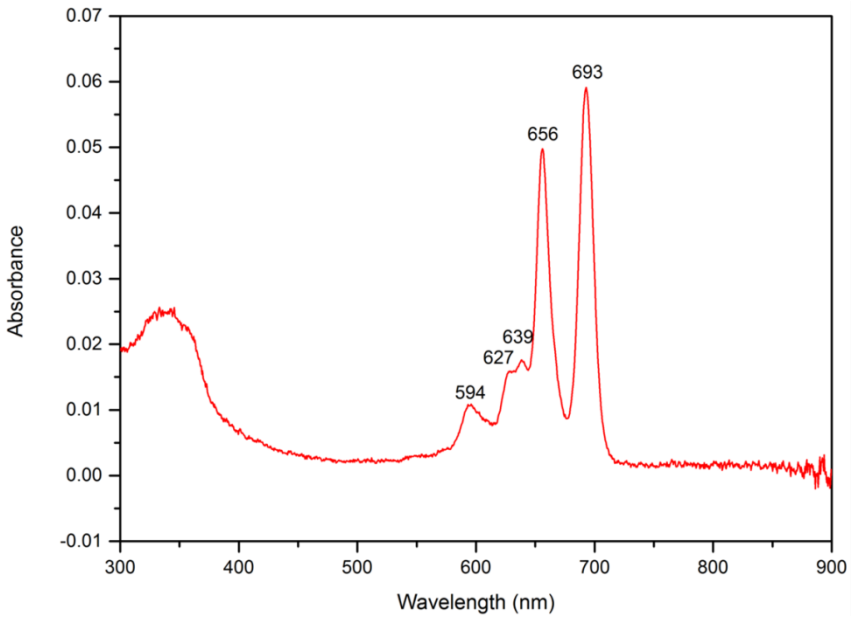


**Fig. S3** Electronic absorption spectrum of a filtered saturated (<5x10$^{-5}$ M) solution of $H_2Pc$ in toluene.

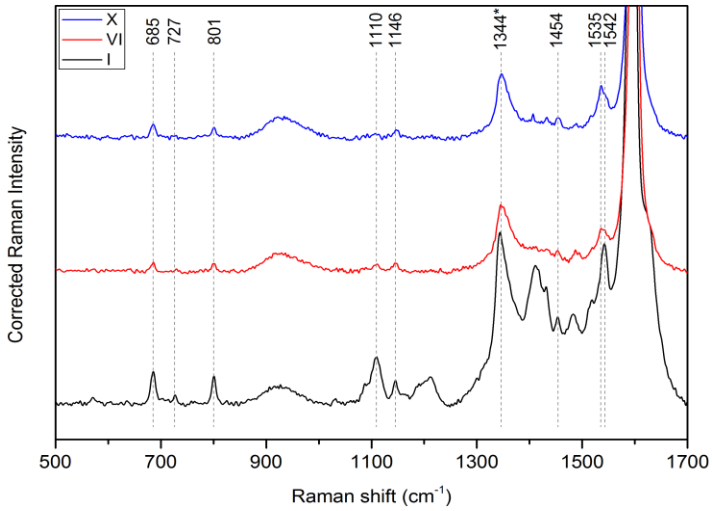


**Fig. S4** Raman spectra (500-1700 cm-1) of glass/SLG/$H_2Pc$ (BL)-I (black), glass/SLG/$H_2Pc$ (ML)-VI (red) and glass/SLG/$H_2Pc$ (ML)-X (blue) systems at 532 nm excitation.

**Supporting Information Text 2: Details of the assignment of the $H_2Pc$ Raman spectral bands in the hybrid systems.**

Since the vast majority of spectral bands observed in the spectra of all hybrid samples can be related to their analogues in the previously reported Raman spectra of $H_2Pc$ in thin films [16,17,20] and in a KBr pellet [8,21], the previously published assignments of Raman spectral bands can, in principle, be used. A normal coordinate analysis (NCA) has not been reported for $H_2Pc$. Nevertheless, the NCA performed for FePc metallophthalocyanine indicates a strong vibrational coupling of the individual (characteristic) modes and, consequently, a strong vibrational delocalization of normal modes over the Pc macrocycle.[39] Consequently, the assignment of $H_2Pc$ vibrations based on the DFT (density functional theory) calculations [8,21] appears to be more comprehensive than the previously published empirical one.[16] The former assignment has thus been adopted into Table 1.

Raman active vibrations of $H_2Pc$ molecule belong to $A_g$, $B_{1g}$, $B_{2g}$ and $B_{3g}$ symmetry species. Nevertheless, only the bands of $A_g$ and $B_{1g}$ in plane vibrations are usually observed in Raman spectra of $H_2Pc$.[8] It should be noted that both the $A_g$ and $B_{1g}$ Raman active vibrations experience a resonance enhancement upon excitations overlapping with the Q-band spectral region. Excitations at the wavelengths matching those of the purely electronic $Q_x$ (0-0) and $Q_y$(0-0) transitions lead to the resonace enhancement of totally symmetric $A_g$ modes by the Franck-Condon mechanism. In addition to that, the $B_{1g}$ modes are enhanced by the Herzberg-Teller mechanism originating from coupling of the close lying $Q_x$ and $Q_y$ excited electronic states by vibrations of $B_{1g}$ symmetry. Furthermore, excitations falling into the vibronic side-band of the $Q_y$ band (originating from coupling of the B, i.e. the Soret, and the Q electronic transitions) also lead to the resonance enhancement of both $A_g$ and $B_{1g}$ vibrations. [16,17] Assignment of the Raman spectral bands of $H_2Pc$ in the KBr pellet to $A_g$ and $B_{1g}$ symmetry species based on the DFT calculation has been performed.[8] For the experimental verification of this assignment, we attempted to determine the depolarization ratios of Raman spectral bands at an off-resonance excitation (to avoid observation of anomalously polarized bands). Since solubility of $H_2Pc$ in toluene was not sufficient for this purpose, depolarization ratios of Raman spectral bands were obtained from Raman spectral polarization measurements of an aqueous solution of the water soluble derivative of $H_2Pc$, namely $H_2Pc$-TS (TS= tetrasulphonatophenyl), at 532 nm, i.e. by the

strategy previously employed for FePc [39]. Comparison of the polarization characteristics (p-polarized, dp-depolarized) of the $H_2$PcTS Raman spectral bands with the symmetry species ($A_g$ or $B_{1g}$) assigned to the corresponding bands of the $H_2$Pc vibrations in the glass/SLG/$H_2$Pc (ML)-X system on the basis of the results of the DFT calculation for H2Pc is shown in Table S1, and the results have been incorporated into Table 1. The match between the DFT-calculated and the experimentally determined symmetry properties of vibrations derived from the depolarization ratios of their spectra bands (p-$A_{1g}$, dp-$B_{1g}$) has been obtained for all the Raman bands with a clearcut correspondence between the $H_2$Pc and $H_2$Pc-TS spectral bands. (Table S1).

The wavenumbers of Raman spectral bands observed for the glass/SLG/$H_2$Pc(BL)-I hybrid system at 633 nm (Fig. 2, spectrum b), in comparison to those in the previously reported Raman (GERS) spectra of the Si/$SiO_2$/SLG/$H_2$Pc hybrid system of about 0.2 nm thickness measured at this particular excitation wavelength,[3] show a good mutual agreement. In addition to those reported previously,[3] we report the spectral bands in the 400-600 $cm^{-1}$ region, namely those at 484, 544 and 569 $cm^{-1}$as well as two new spectral bands at 750 and 951 $cm^{-1}$. All the spectral bands in the spectra of glass/SLG/$H_2$Pc (BL)-I at 633 nm excitation have their analogues in the newly reported spectra at the 647 nm excitation (and most of them are observed also at 785, 830 and 532 nm excitations) (Fig. 2 and Table 1). At both 633 and 647 nm excitations, we observe also analogues of the 766, 1159 and 1407 $cm^{-1}$ bands (namely at 768,1162 and 1406 $cm^{-1}$) which, in ref. 3, were assigned to the SLG activated IR (infrared) modes. Nevertheless, in the meantime, analogues of these bands (765, 1155, 1407 $cm^{-1}$) have been observed in the Raman spectra of $H_2$Pc in a KBr pellet excited at 532 nm and assigned to Raman active $A_g$ modes on the basis of the DFT calculations.[21] On the other hand, the newly observed spectral bands at 750 and 951 $cm^{-1}$ do not have analogues in the previously published Raman (and/or GERS) spectra of $H_2$Pc. [3,16,21] Since these bands belong neither to Raman bands of toluene (used as solvent for $H_2$Pc deposition by adsorption) nor to those of impurities originating from the SLG deposition (they are absent in Raman spectra of the parent glass/SLG system, Fig.S7 spectrum d), their origin deserves a more thorough discussion provided below.

The 750, 958, 1218 and 1533 $cm^{-1}$ Raman bands of $H_2$Pc are the spectral features related to the SLG-$H_2$Pc interaction in glass/SLG/$H_2$Pc hybrids. Of these, the 1533 $cm^{-1}$ band occurs specifically upon SLG-$H_2$Pc (ML) interaction. We note that the 750 and 958 $cm^{-1}$ bands (which do not have any previously reported Raman analogues) do have their counterparts in the IR

spectra of $H_2Pc$, namely the 752 and 952 $cm^{-1}$ bands assigned to the out of plane N-H and out of plane C-H deformation modes, respectively.[21,40,41] Their Raman spectral activation by the SLG-$H_2Pc$ interaction could presumably be related to a decrease of the effective symmetry of $H_2Pc$ molecule ($D_{2h} \rightarrow D_{2d}$) by its axial interaction with SLG. It should also be noted that the graphite-SLG interaction is not strong enough to induce such effect, since the two above mentioned bands are virtually absent in the Raman spectra of graphite-$H_2Pc$ (ML) system. A probable reason for the graphite –$H_2Pc$ interaction being weaker that SLG-$H_2Pc$ one is the fact that in the graphite-$H_2Pc$ system, the top graphene layer of graphite interacts with both H2Pc and with the other graphene layers in graphite.

A similar argument, i.e. the relatively strong SLG-$H_2Pc$ interaction, can be used for explanation of the appearance of the 1218 $cm^{-1}$ Raman band (belonging to $B_{1g}$ symmetry mode), as well as of the 1533 $cm^{-1}$ in the spectra of glass/SLG/$H_2Pc$ hybrids. Nevertheless, the origin of the latter band requires a closer inspection for the following reasons. First, its observation is limited to the glass/SLG/$H_2Pc$/ (ML) samples VI and X, however, its actual relative intensity is different for the sample VI and X, and, for the sample X, it becomes the most intense Raman spectral band of $H_2Pc$. Secondly, in the spectra of both samples VI and X, this band is observed as the part of a doublet with a close-lying band at 1545 $cm^{-1}$ which decreases in its relative intensity for the sample X with respect to the sample VI. The latter Raman spectral band is, in turn, typical for the spectra of both glass/SLG/$H_2Pc$(BL)-I and graphite/$H_2Pc$ (ML) hybrids.

This single Raman band observed at 1543 $cm^{-1}$ for glass/SLG/$H_2Pc$(BL)-I and at 1544 $cm^{-1}$ for graphite/$H_2Pc$ (ML) corresponds with the 1540 $cm^{-1}$ band of $H_2Pc$ in the KBr pellet assigned to the C-Nm-C asymmetric stretching and C-$N_H$-C symmetric stretching, i.e. to the overall motion of 16 C-N bonds of $A_g$ symmetry. [8,21] This band has also been denoted as the cavity size marker on the basis of the spectra of various metallophthalocyanines [42]. In the case of $H_2Pc$ Raman spectra, this band has also been observed in the 1534-1539 $cm^{-1}$ range for various samples of the α -$H_2Pc$ polymorph films [16,17,20] and as a 1539 and 1525 $cm^{-1}$ doublet for the β -$H_2Pc$ polymorph films. In the latter case, observation of a doublet can be attributed to the presence of two non-equivalent $H_2Pc$ molecules in the unit cell. [9]

In search for a possible explanation of observations of the 1545, 1533 $cm^{-1}$ doublet in Raman spectra of hybrid systems constituted by SLG and a monolayer of $H_2Pc$ molecules, we speculate that there can actually be two types of adsorption sites for $H_2Pc$ on SLG, and that at one of them,

the SLG-$H_2Pc$ interaction is stronger than on the other. This, in turn, could result into observation of two C-N-C mode bands. Furthermore, the additional soaking of the sample VI in toluene could lead to reorganization of molecules within the adsorbed $H_2Pc$ monolayer resulting into a higher population of the sites with a stronger $H_2Pc$ -SLG interaction in sample X . This, in turn, can lead to the the gain of the 1533 $cm^{-1}$ band intensity on the expenses of that of the 1545 $cm^{-1}$ band. Importantly, the exchange of relative band intensities of the two above mentioned bands projects itself into the wavenumbers of the corresponding overtone bands, which are observed at 3080 $cm^{-1}$ for sample VI and at 3060 $cm^{-1}$ for sample X (Table 2 and Figs.S5 and S6). In particular, observation of the 1533 $cm^{-1}$ band overtone at 3060 $cm^{-1}$ indicates, that the corresponding fundamental is of $A_g$ symmetry and can thus be attributed the combined C-N-C vibrational mode. This assignment has been incorporated into Table 1.

Note: the references correspond to those listed in the paper.

Table S1: Wavenumbers of $H_2$PcTS Raman spectral bands (in an aqueous solution) and their polarization (p = polarized, dp = depolarized), wavenumbers of $H_2$Pc Raman spectral bands in glass/SLG/$H_2$Pc-X hybrid system and the symmetry of corresponding modes from DFT calculations by Murray et al. [21]. The 1276 $cm^{-1}$ band (marked *) belongs to sulfonate group[39]

| Band wavenumbers of $H_2$PcTS ($cm^{-1}$) | Polarization | Band wavenumbers of $H_2$Pc ($cm^{-1}$) | Symmetry |
|---|---|---|---|
| 576 | p | 545 | $A_g$ |
| 588 | p | 597 | $A_g$ |
| 688 | p | 684 | $A_g$ |
| 727 | p | 726 | $A_g$ |
| 805 | p | 798 | $A_g$ |
| | | 1010 | $A_g$ |
| 1020 | dp | | |
| 1035 | dp | 1029 | $B_{1g}$ |
| 1071 | dp | 1085 | $B_{1g}$ |
| 1103 | dp | 1111 | $B_{1g}$ |
| 1128 | dp | | |
| | | 1145 | $A_g$ |
| 1180 | p | 1185 | $A_g$ |
| 1190 | dp | 1197 | $B_{1g}$ |
| 1228 | dp | 1219 | $B_{1g}$ |
| 1276 | * | – | |
| 1312 | dp | 1311 | $B_{1g}$ |
| 1337 | p | 1343 | $A_g$ |
| 1394 | p | 1408 | $A_g$ |
| 1431 | dp | 1431 | $B_{1g}$ |
| 1463 | p | 1453 | $A_g$ |
| 1518 | p | 1512 | $A_g$ |
| 1535 | dp | 1532 | – |
| | p | 1544 | $A_g$ |
| 1578 | P | – | |
| 1614 | dp | 1620 | $B_{1g}$ |

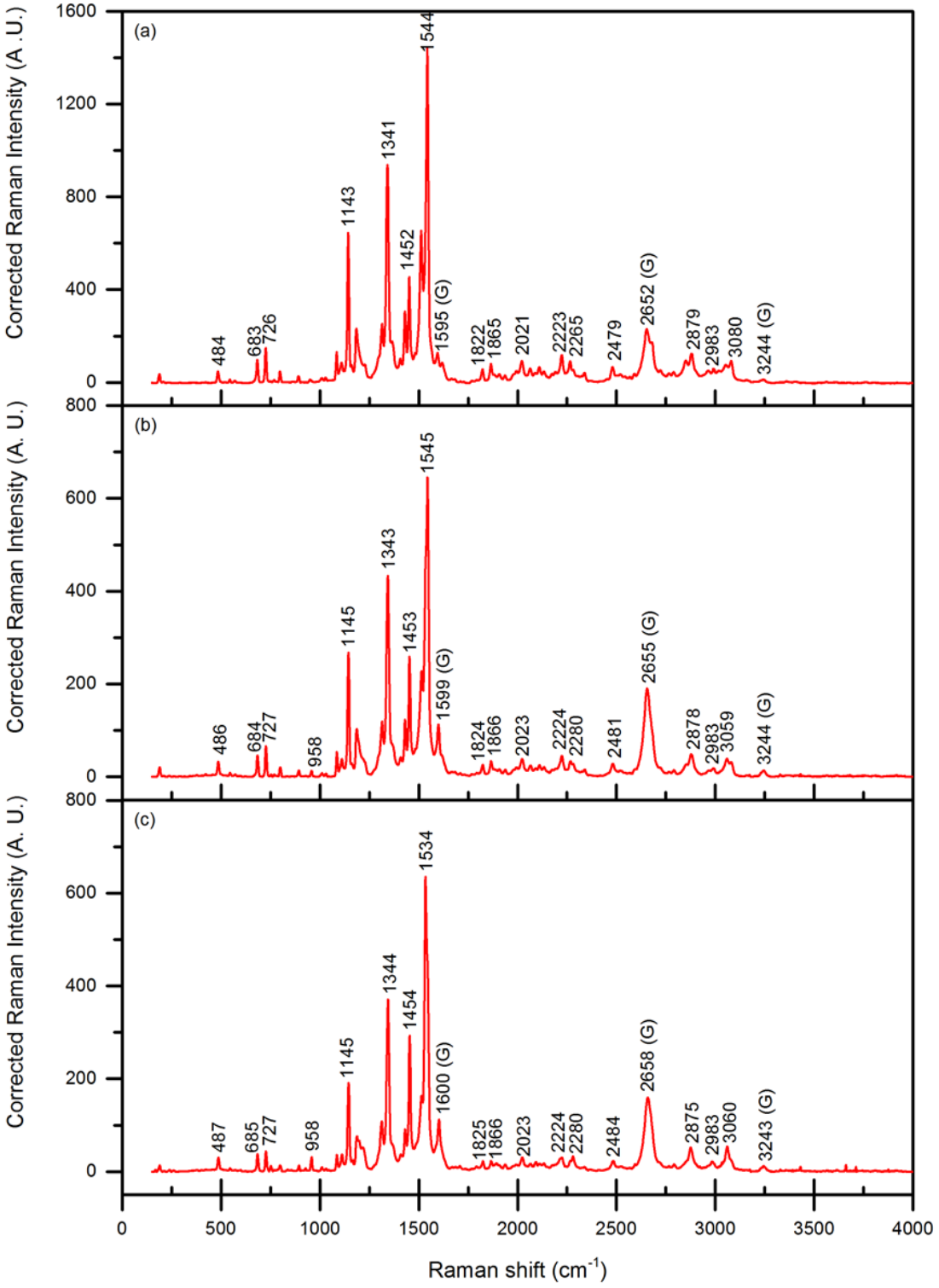


**Fig. S5** Full range (400-4000 cm-1) Raman spectra of (a) glass/SLG/$H_2$Pc (BL)-I, (b) glass/SLG/$H_2$Pc (ML)-VI and (c) glass/SLG/$H_2$Pc (ML)-X systems at 633 nm excitation.

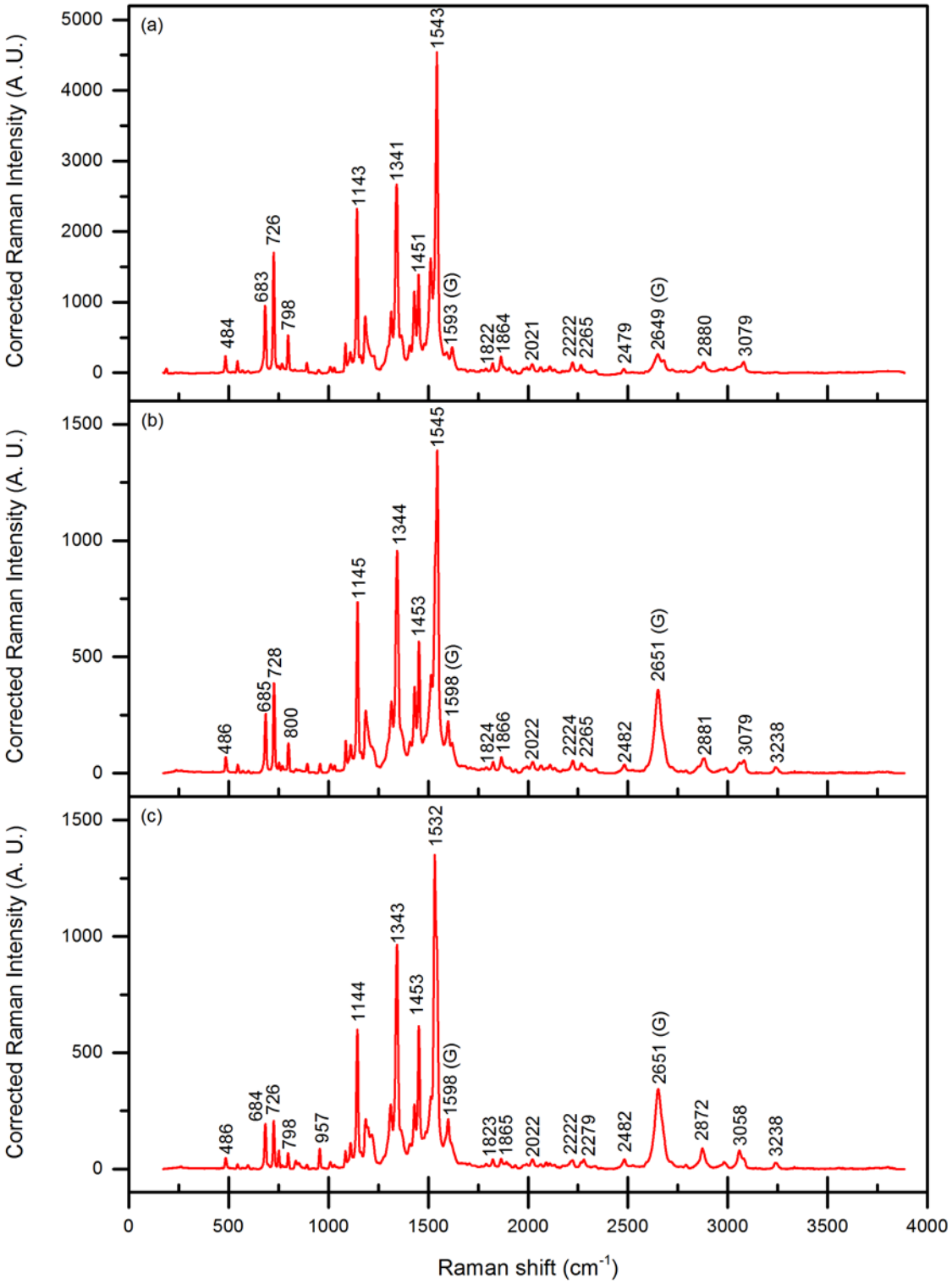


**Fig. S6** Full range (400-4000 cm-1) Raman spectra of (a) glass/SLG/$H_2$Pc (BL)-I, (b) glass/SLG/$H_2$Pc (ML)-VI and (c) glass/SLG/$H_2$Pc (ML)-X systems at 647 nm excitation.

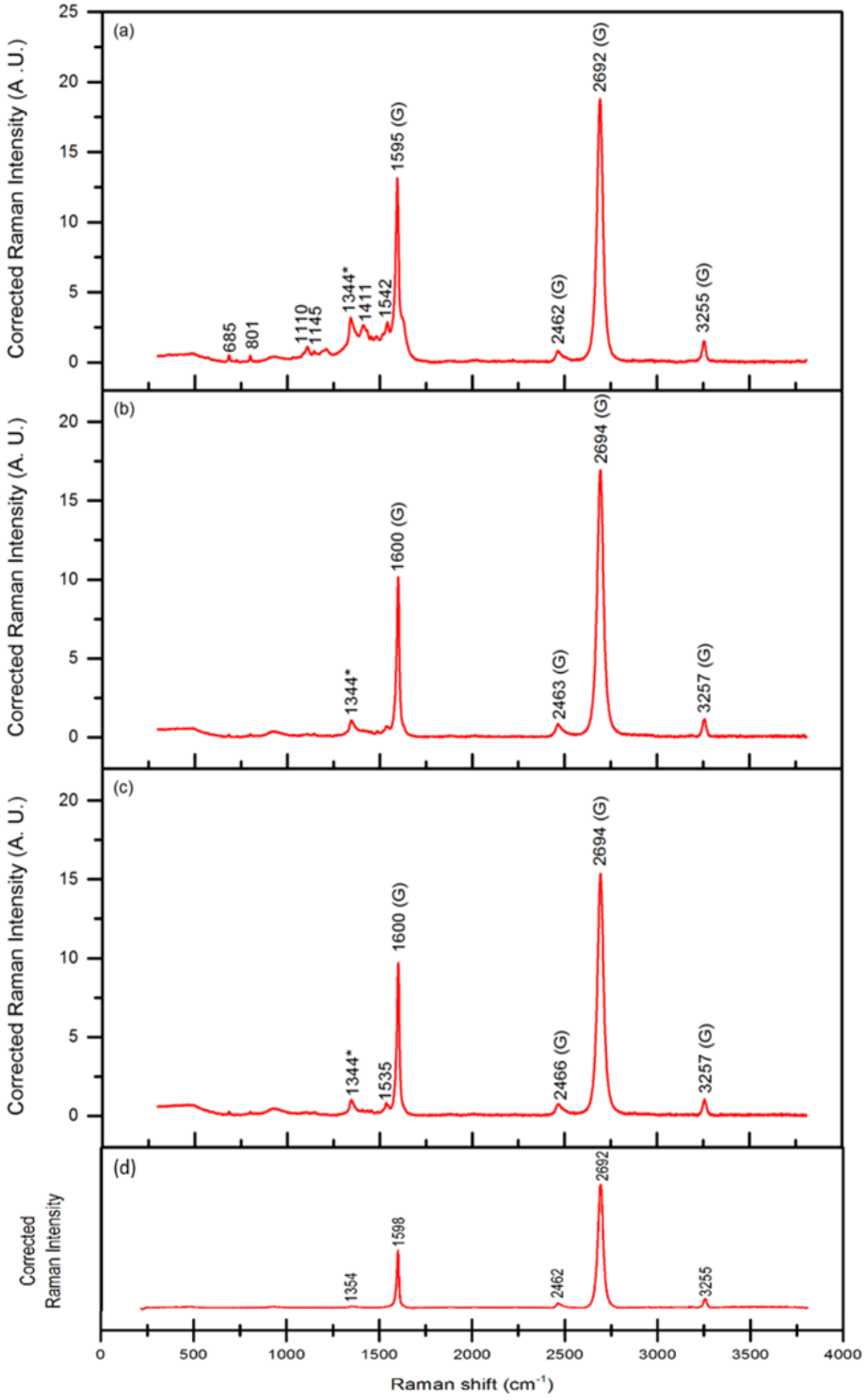


**Fig. S7** Comparison of the full range Raman spectra of glass/SLG/$H_2$Pc systems (a) (BL)-I, (b) (ML)-VI, (c) (ML)-X and of (d) glass/SLG reference system at 532 nm excitation.

Table S2: The 2D mode dispersion in the parent glass/SLG system and in the hybrid system with $H_2Pc$

| Excitation wavelength [nm] | glass/SLG/$H_2Pc$ – I | glass/SLG/$H_2Pc$ – VI | glass/SLG/$H_2Pc$ – X | glass/SLG |
|---|---|---|---|---|
| 532 | 2692 | 2694 | 2694 | 2692 |
| 633 | 2652 | 2655 | 2658 | 2655 |
| 647 | 2649 | 2651 | 2651 | 2647 |
| 785 | 2597 | 2596 | 2595 | 2600 |

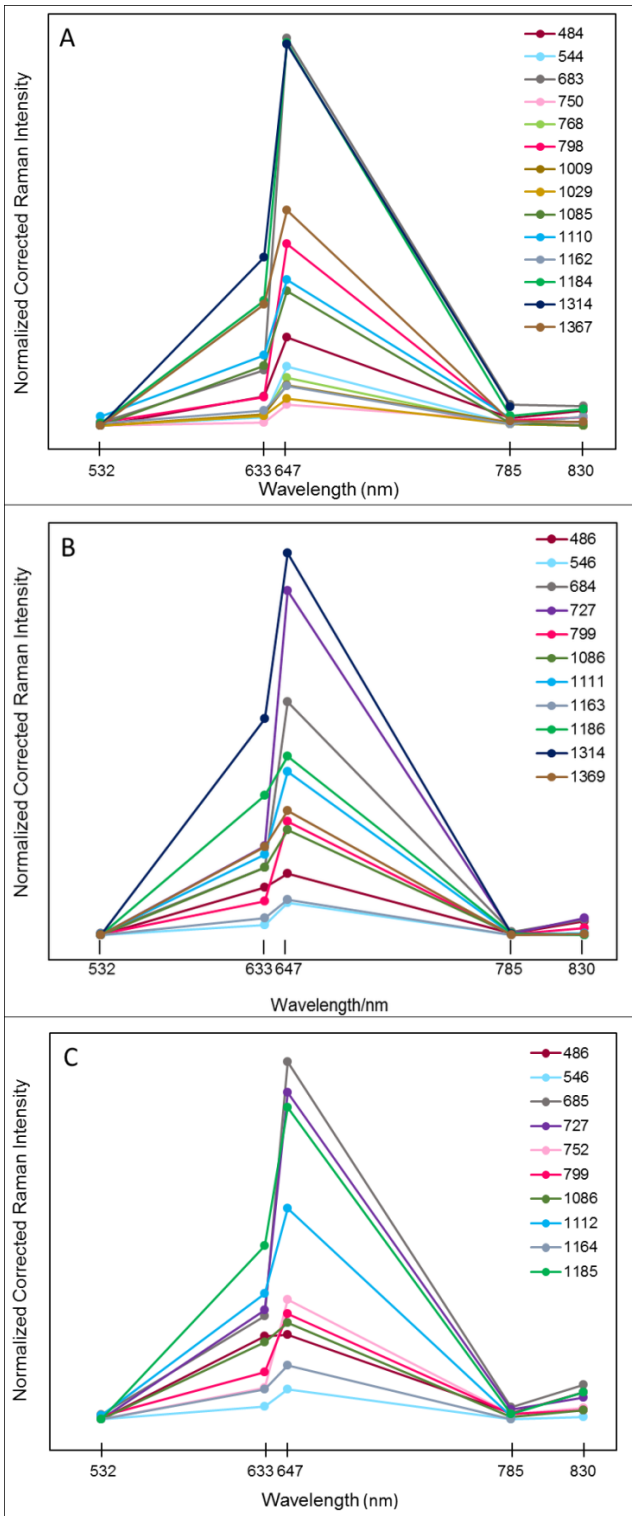


**Fig. S8** Details of Raman spectral bands excitation profiles of (A) glass/SLG/$H_2$Pc (BL)-I system, (B) glass/SLG/$H_2$Pc (ML)-VI system, (C) glass/SLG/$H_2$Pc (ML)-X system in the 532-830 nm range (with the focus on the less enhanced bands).

## 8.2. Publication II: Effect of ethanethiolate spacer presence and/or removal on morphology and optical responses of hybrid systems constituted by single layer graphene and Ag nanoparticle arrays

Veronika Sutrová[a,c], Ivana Šloufová[a], Zuzana Melniková[b], Martin Kalbáč[b], Ewa Pavlova[c], Blanka Vlčková[a]*

[a] Charles University, Faculty of Science, Department of Physical and Macromolecular Chemistry, Hlavova 8, Prague 2, 128 40, Czech Republic, vlc@natur.cuni.cz

[b] J. Heyrovsky Institute of Physical Chemistry of the ASCR, v.v.i, Dolejškova 3, 182 21 Prague 8, Czech Republic

[c] Institute of Macromolecular Chemistry AS CR, Heyrovsky Sq. 2, 162 06 Prague 6, Czech Republic

My contribution:

All experimental work: i.e. samples preparations, SERS spectral testing, TEM + SEM imaging, except of SLG sample preparation, data evaluation and principal participation in MS preparation.

LANGMUIR Article
Cite This: Langmuir 2017, 33, 14414−14424 pubs.acs.org/Langmuir

# Effect of Ethanethiolate Spacer on Morphology and Optical Responses of Ag Nanoparticle Array−Single Layer Graphene Hybrid Systems

Veronika Sutrová,[†,§] Ivana Šloufová,[†] Zuzana Melníková,[‡] Martin Kalbáč,[‡] Ewa Pavlova,[§] and Blanka Vlčková*[,†]

[†]Faculty of Science, Department of Physical and Macromolecular Chemistry, Charles University, Hlavova 8, Prague 2, 128 40, Czech Republic

[‡]J. Heyrovsky Institute of Physical Chemistry of the ASCR, v.v.i, Dolejškova 3, 182 21 Prague 8, Czech Republic

[§]Institute of Macromolecular Chemistry AS CR, Heyrovsky Square 2, 162 06 Prague 6, Czech Republic

Supporting Information

**ABSTRACT:** Single layer graphene (SLG) and two-dimensional (2-D) plasmonic Ag nanoparticle arrays assembled by chemisorption of ethanethiol (ET) molecules (AgNPs-ET) were employed as components of two types of hybrid systems designed for surface-enhanced Raman scattering (SERS) spectral probing of SLG localized in the vicinity of plasmonic NPs. Both hybrids were characterized by optical microscopy, transmission electron microscopy (TEM), surface plasmon extinction (SPE), and SERS microRaman spectral measurements at four excitation wavelengths spanning the 445−780 nm range. SERS spectral probing of the glass/SLG/AgNPs-ET hybrid prepared by overdeposition of SLG on glass by the array of ET-modified Ag NPs has shown that the chemisorbed ET acts as an efficient molecular spacer between SLG and Ag NPs surface which, in turn, enabled to obtain SERS spectra of SLG unperturbed by doping or strain. TEM imaging and SERS spectral probing of the second hybrid prepared by overdeposition of AgNPs-ET array on glass by SLG revealed removal of the adsorbed ET molecules and annealing of Ag NPs during the SLG deposition. The characteristics of the resulting glass/AgNPs/SLG hybrid system, namely (i) broad distribution of the annealed Ag NPs sizes and shapes, (ii) SPE curve covering the overall visible spectral region, (iii) absence of the ET spectral bands in SERS spectra, and (iv) fairly uniform SERS enhancement of the G and 2D mode of SLG in the 532−780 nm range in the straight sample geometry indicate that this hybrid can provide a suitable platform for investigation of the excitation wavelength dependence of combined SERS/GERS (graphene-enhanced Raman scattering) enhancement experienced by various molecular species brought into contact with SLG in this hybrid. Finally, weak optical effects attributed to increased reflectivity of SLG in the near field of Ag NPs arrays have been observed in the excitation wavelength dependence of the SERS spectra of both types of hybrid systems.

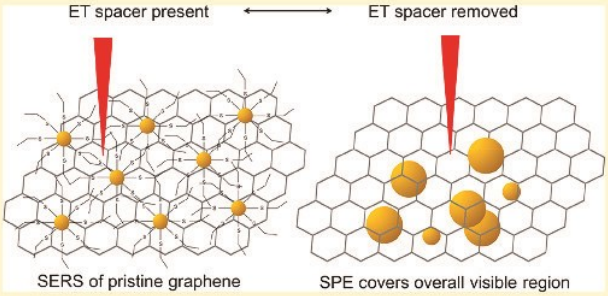


## INTRODUCTION

Hybrid systems constituted by plasmonic metal nanoparticles (NPs) and graphene are currently the subject of considerable interest stemming from the specific properties of the components as well as new effects resulting from integrating of these components. In particular, the ability of plasmonic NPs to confine visible light into subwavelength dimensions by resonance excitations of dipolar (localized) surface plasmons is widely used in plasmonics, optoelectronics, and in surface-enhanced Raman spectroscopy.[1−3] Graphene, and particularly single-layer graphene (SLG), is a highly desirable material for optoelectronics due to its unique properties, such as a ultrathin (atomic) thickness, high carrier mobility, and mechanical flexibility.[4] For example, the potential of SLG as a material for construction of fast photodetectors has been been considered, but found to be hampered by its very low quantum efficiency and an absence of the spectral selectivity. Nevertheless, these limitations have been overcome by integration of graphene with a thin layer of plasmonic nanostructures. In such systems, the plasmonic nanostructures act as nanoantennas that enhance the photoresponse selectively at their plasmon resonance wavelength(s), and thus enable construction of graphene-based photodetectors with the desired light wavelength (color) selectivity.[5] Subsequently, the wavelength-dependent absorption induced by localization of SLG into the near field optically excited in the vicinity of two-dimensional (2-D) arrays of Ag and/or Au NPs has been explored both by model calculations and experiments.[6−10]

Received: October 6, 2017
Revised: November 24, 2017
Published: November 27, 2017





DOI: 10.1021/acs.langmuir.7b03462
Langmuir 2017, 33, 14414−14424

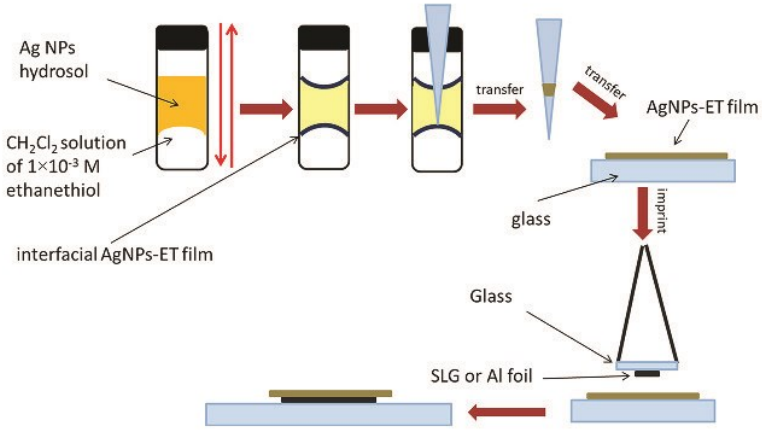


**Figure 1.** Preparation of arrays of ethanethiolate-modified Ag NPs, their deposition onto glass slides, and their transfer onto glass/SLG and/or glass/Al foil supporting surfaces.

Furthermore, the effect of coupling of SLG with plasmonic metal nanostructures, e.g., Ag or Au NPs arrays, on doping and/or strain experienced by SLG in the plasmonic metal NPs/SLG hybrid systems, has been successfully explored by surface enhanced Raman scattering (SERS) spectroscopy.[11−19] Interpretation of the SERS studies of such hybrid systems takes advantage of the previously published Raman spectral studies of SLG under various, but well-defined conditions.[20,21] Furthermore, the SERS enhancement experienced by the SLG modes has been attributed to the electromagnetic (i.e., the localized plasmon resonance) mechanism of SERS.[14] SERS spectra of SLG were obtained from hybrid systems constituted by SLG and the overdeposited plasmonic NPs as well as from the assemblies of plasmonic NPs overlaid by SLG.[11−18] A comparison of SERS of SLG from these two types of hybrid systems has been addressed,[19] however, a mutual comparison of the SERS enhancement factors experienced by the SLG modes in each of these two hybrid systems was somewhat hampered by different morphology of the Ag NPs and of their assembly in each of them. In addition to that, the hybrid systems constituted by graphene and plasmonic NPs were employed as platforms for SERS of graphene,[22] SERS spectral sensing platforms for molecules,[15,17,18,23,24] as well as for SERS spectral monitoring of plasmon-driven reactions[25] and of specific sensor−analyte interactions.[26]

In this work, we investigate the effect of ethanethiolate spacer presence and/or removal on morphology and optical responses of hybrid systems constituted by SLG and Ag nanoparticle arrays. First, we explore the effect of a thin molecular spacer separating SLG from a 2-D array of Ag NPs, on the SERS spectra of SLG. Our aim is to reveal whether the presence of the thin molecular spacer can eliminate the strain and/or doping induced by a direct interaction between SLG and Ag NPs. Our effort is targeted on (i) preservation of pristine SLG structure, and (ii) obtaining at least some SERS enhancement of Raman modes of SLG. This approach has been partially motivated by previous SERS spectral studies carried out by us and others,[3,27−30] in which SERS and/or SERRS spectra of structurally unperturbed molecular species have been obtained on substrates constituted by Ag NPs modified by molecular spacers tailored specifically for the particular types of molecular species investigated. For SERS of SLG on spacer-modified plasmonic NPs, we selected Ag NPs modified by adsorption of ethanethiol (ET) upon formation of Ag-ET surface species, as reported previously.[28] ET that is chemisorbed on Ag NPs at the interface between the aqueous and the dichloromethane phase has been shown to play a dual role: (i) a hydrophobic spacer enveloping the Ag NPs and (ii) a mediator of the 2-D assembling of ET-modified Ag NPs at the interface.[28,29]

In the first part of this paper, we report on assembling of glass/SLG/AgNPs-ET hybrid system (constituted by SLG deposited on a glass substrate and overdeposited by a 2-D array of ET-modified Ag NPs) and on the results of its SERS spectral probing at four excitation wavelengths in the 445−780 nm range. As the reference systems for evaluation of the SLG and the Ag-ET spectral bands positions and intensities, we employ the glass/SLG and the glass/AgNPs-ET system, respectively. Furthermore, we compare the morphology and surface plasmon extinction (SPE) spectra of the hybrid system and of the second reference system as a part of our effort to explain the observed additional SERS enhancement experienced by the Ag-ET surface species in the hybrid system with SLG.

In the second part of this paper, we provide SERS spectral evidence of the complete removal of the ET spacer upon deposition of SLG onto the glass-deposited 2-D array of ET-modified Ag NPs by the chemical vapor deposition (CVD) procedure,[31] namely, by the nitrocellulose (NC) method. This method of SLG transfer involves a solvent exposure as well as a moderate heating of the as prepared hybrid system.[32] We explore the effect of this procedure on the morphology and SPE of Ag NPs in the resulting glass/AgNPs/SLG hybrid system as well as on the SERS spectra of SLG. In particular, we employ a novel strategy of SERS microRaman spectral measurements of the glass/AgNPs/SLG hybrid system samples in two different orientations with respect to the incident laser excitation (further denoted as the straight and the inverted sample geometry). Comparison of the SERS enhancement experienced by the SLG spectral modes in each of the two sample geometries allows us to address the question of whether localization of the same plasmonic enhancer (i.e., a 2-D array of Ag NPs) above or underneath SLG does actually affect the experimentally determined SERS enhancement factors of the SLG spectral modes.

## ■ EXPERIMENTAL SECTION

**Materials.** Analytical-grade $AgNO_3$ and sodium borohydride as well as spectral grade dichloromethane (UVASOL) were purchased from Merck, and 1-ethanethiol (97%) from Sigma-Aldrich. Al foil was



DOI: 10.1021/acs.langmuir.7b03462
*Langmuir* 2017, 33, 14414−14424

obtained from Scienceware. Distilled deionized water was used for all sample preparations.

**Preparation of Glass/SLG Hybrid System.** SLG was prepared by the previously reported CVD procedure.[31] The as-grown graphene was transferred to the glass substrate using cellulose nitrate (NC).[32] The majority of the NC layer was removed by methanol drops at room temperature. The glass/SLG sample was then annealed at 160 °C for 30 min in order to remove the NC residuals from the SLG surface. Raman spectral mapping of the sample showed no spectral features of the NC residuals.

**Preparation of Ag NP Hydrosol.** Ag NP hydrosol was prepared by reduction of silver nitrate by sodium borohydride according to the previously published procedure.[28] A transmission electron microscopy (TEM) image of the dried drop of the hydrosol deposited on a carbon-coated grid for TEM and the distribution of the Ag NPs sizes are shown in Figure S1 in the Supporting Information (SI). The average value of Ag NPs size is 7.5 nm.

**Preparation and Deposition of Arrays of Ethanethiolate-Modified Ag NPs.** Arrays of Ag NPs modified by chemisorbed ethanethiol (further denoted as AgNPs-ET arrays) were prepared according to the procedure reported by Michl et al.[28] Briefly, a two-phase system constituted by 2 mL of Ag NPs hydrosol and 2 mL of a $1 \times 10^{-3}$ M solution of ethanethiol in dichloromethane was vigorously shaken until a lustrous nanoparticulate film appeared at the interface between the aqueous and the organic phase (photographically depicted in Figure S2). The interfacial film was then transferred by a pipet onto a glass slide (scheme in Figure 1), and it was either directly used for preparation of hybrid system I, of glass/Al foil/AgNPs-ET reference system and/or samples for TEM by imprinting on the particular supporting surface (glass/SLG, glass/Al foil, C-coated grid for TEM or SLG covered, C-coated TEM grid, respectively, Figure 1 and Figure S2 in the SI), or allowed to dry in air and employed as the reference system for SERS spectral measurements and/or as the component of the hybrid system II. By differential electronic absorption and/or SPE spectral measurements, the efficiency of the ET incorporation into interfacial films was established to be ca. 2%, and the Ag NPs assembling efficiency was found to be ca. 83%.

**Preparation of Hybrid System I.** The hybrid system constituted by SLG overdeposited by the Ag NPs-ET array was prepared by transfer of the Ag NPs-ET array from a glass slide by its imprinting onto SLG deposited on a glass slide (Figure 1 and Figure S2 in the SI).

**Preparation of Hybrid System II.** The hybrid system II was prepared by overdeposition of the glass-deposited AgNPs-ET array by SLG using the CVD procedure,[31] in particular the NC method[32] of the as prepared SLG transfer onto the Ag NPs-ET array on glass. The majority of the NC layer from the resulting glass/AgNPs-ET/SLG/NC hybrid was removed by methanol drops at room temperature. Then the glass/AgNPs-ET/SLG sample was annealed at 160 °C for 30 min in order to remove the NC residuals from the SLG surface. SERS spectral mapping of the sample (*vide infra*) showed no spectral features of the NC residuals, which, in turn, demonstrates that an advantage of this particular preparation procedure is obtaining of the spectrally pure glass/AgNPs/SLG samples.

**Preparation of Glass/Al Foil/AgNPs-ET Reference System.** This reference system was prepared by transfer of the AgNPs-ET array from a glass slide by its imprinting onto an Al foil attached to a glass slide (Figure 1).

**Instrumentation.** Raman and surface-enhanced Raman (SERS) spectra were recorded on a DXR Raman spectrometer (Thermo Scientific) interfaced to an Olympus microscope. An objective with 50× magnification was employed. The following excitation lines were used: 445 nm (diode laser), 532 nm (diode-pumped solid-state laser), 633 nm (He−Ne laser), and 780 nm (diode laser). The laser power ranged from 0.1 to 2 mW, and a full-range grating was used for all measurements. Raman and/or SERS spectra mapping was performed by measuring maps of 6 points × 6 points spanning the 60 $\mu$m × 60 $\mu$m sample area.

Surface plasmon extinction (SPE) spectra were measured on a Shimadzu UV-2401 spectrometer. Transmission electron microscopy images were obtained with a Tecnai G2 (FEI) transmission electron microscope with the acceleration voltage 120 keV. Optical microscopy images were obtained with a Leica DM6000 M (Leica Microsystems) optical microscope.

## RESULTS AND DISCUSSION

**SERS Spectra, Morphology, and Surface Plasmon Extinction of Glass/SLG/AgNPs-ET Hybrid System: The Effects of the ET Spacer Presence.** The glass/SLG/AgNPs-ET hybrid system as a sample for SERS microRaman spectral measurements is schematically depicted in Figure 2A. SERS spectra obtained from this hybrid system at 445, 532, 633, and 780 nm excitations are shown in Figure 2B, spectra a−d. All spectra in Figure 2B contain the characteristic spectral bands of the Ag-ET surface species as well as those of the G and the 2D modes of SLG, as follows from their comparison with the spectra of the glass/SLG (Figure S3) and the glass/AgNPs-ET

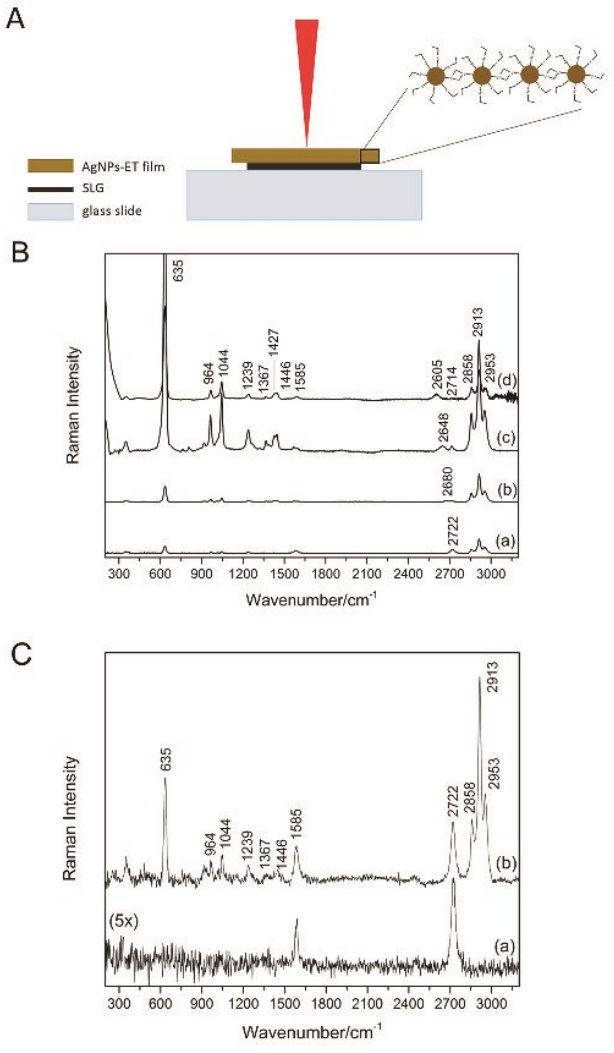


**Figure 2.** (A) Schematic depiction of glass/SLG/AgNPs-ET hybrid system as a sample for SERS microRaman measurement. (B) SERS microRaman spectra of glass/SLG/AgNPs-ET hybrid system measured at (a) 445, (b) 532, (c) 633, and (d) 780 nm excitation. (C) Comparison of SERS microRaman spectra of glass/SLG reference (a) and of glass/SLG/AgNPs-ET hybrid (b) systems at 445 nm excitation. Spectrum (a) was multiplied by a factor of 5.



DOI: 10.1021/acs.langmuir.7b03462
*Langmuir* 2017, 33, 14414−14424

(Figure S4) reference systems. The assignment of the SERS spectral bands of Ag-ET surface species as well as of Raman spectral bands of the free ET is provided in Table S1. The most pronounced differences between the spectra of ET and Ag-ET is the absence of the 2570 $cm^{-1}$ band of $\upsilon$(S−H) and the presence of the 350 $cm^{-1}$ band of $\upsilon$(Ag−S) in the latter spectrum, in contrast to the former one.

The positions of the G and 2D mode spectral bands are most clearly distinguished in the SERS spectrum of the glass/SLG/Ag NPs-ET hybrid system excited at 445 nm (Figure 2B, spectrum a), in which their relative intensities with respect to those of the Ag-ET bands are the largest. The comparison of the SERS spectra of SLG in the glass/SLG/Ag-ET hybrid and of its Raman spectra in the glass/SLG reference system obtained at the 445 nm excitation (Figure 2C, spectra a and b) show that the wavenumbers of the G mode (1585 and 1586 $cm^{-1}$) as well as of the 2D mode (2722 $cm^{-1}$) are the same (or virtually the same within the experimental error) in both systems. Moreover, the position of the G mode band at 1585 $cm^{-1}$ is close to that of the undoped SLG.[20,21] These results provide evidence of the presence of the unperturbed SLG in the glass/SLG/AgNPs-ET hybrid system. In contrast to that, a 5 $cm^{-1}$ upshift of the G mode and a slight upshift of the 2D mode attributed to n-doping and compressive strain was reported for the SLG/Ag NPs hybrid system in which SLG is in direct contact with Ag NPs.[19] Preservation of the native structure of SLG is thus ascribed to the Ag-ET molecular spacer enveloping Ag NPs and preventing the direct SLG-Ag NPs contact.

SERS enhancement factors of the G and the 2D modes of SLG in the glass/SLG/Ag-ET hybrid at each of the four excitation wavelengths were determined as the integral intensity ratios of the spectral bands of these modes in the SERS spectra of the hybrid system and in Raman spectra of the glass/SLG reference system. Their values are listed in the first two columns of Table 1. The largest SERS enhancement by a factor

**Table 1. SERS Enhancement Factors of the SLG Modes in the Glass/SLG/AgNPs-ET Hybrid System and the Average SERS Enhancement Factors of the Modes of the Ag-ET Surface Species in (I) the Glass/SLG/AgNPs-ET Hybrid System and (II) the Glass/Al Foil/AgNPs-ET Hybrid System**

| $\lambda_{exc}$ (nm) | SLG-G | SLG-2D | ET-addit (I) | ET-final (I) | ET-addit (II) | ET-final (II) |
|---|---|---|---|---|---|---|
| 445 | 2 | 2 | 1 | $5 \times 10^5$ | 4 | $2 \times 10^6$ |
| 532 | 9 | 4 | 4 | $2 \times 10^7$ | 12 | $6 \times 10^7$ |
| 633 | 9 | 6 | 4 | $8 \times 10^6$ | 15 | $8 \times 10^8$ |
| 780 | 2 | 2 | 1 | $1 \times 10^6$ | 1 | $5 \times 10^5$ |

of 9 was determined for the G mode of SLG at 532 and 633 nm excitations. This result is, in general, consistent with the shape of the SPE curve of the hybrid system (Figure 3, curve b). Nevertheless, in addition to the SPE shape, contributions of other factors have to be considered to explain the SERS enhancement at a particular excitation wavelength, namely: (i) an increase of the contribution of the light scattering to the overall extinction (sum of absorption and scattering) of a plasmonic nanoparticle array with the increasing excitation wavelength,[33] and (ii) the "second part of the electromagnetic (EM) SERS enhancement", which implies that not only the incident, but also the Raman scattered radiation is enhanced by the EM mechanism of SERS,[34] i.e., by the elastic Mie

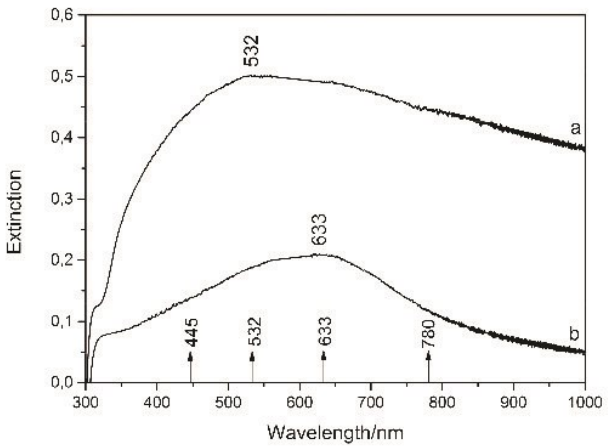


**Figure 3.** Surface plasmon extinction spectra of (a) glass/AgNPs-ET reference system, (b) glass/SLG/AgNPs-ET hybrid system, together with the projections of SERS excitation wavelengths.

scattering.[1,2] For example, the 633 nm excitation (which provides the SERS spectra with the best enhancement factors for both the G and the 2D mode, Table 1) is nearly coincident with the SPE curve maximum. The wavelength of the SPE maximum represents the wavelength at which the sum of absorption and scattering of light by the hybrid system is the largest.[1,2] On the other hand, the wavelength of the photons scattered by the G mode (at 1585 $cm^{-1}$) is 704 nm and that of the 2D mode (2648 $cm^{-1}$) photons is 760 nm, respectively, and the latter thus coincides with a lower extinction on the declining slope of the SPE band than the former (Figure S5 in the SI). Consequently, a slightly lower SERS enhancement factor (Ef) is expected and actually observed for the 2D mode (Ef = 6) than for the G mode (Ef = 9).

Importantly, the G mode enhancement (Ef = 9) at 532 and 633 nm excitation in SERS of our hybrid system with unperturbed SLG and the hydrophobic Ag-ET spacer is actually slightly higher than that experienced by the same mode in SERS of the system with SLG underneath Ag NPs (Ef = 7).[19] In the latter system, SLG is affected by compressive strain and n-doping, which, in turn, result from the direct contact between SLG and Ag NPs. This comparison indicates that the decrease of the SERS enhancement by the EM mechanism induced by a thin spacer[18] namely, in our case, by the hydrophobic Ag-ET spacer (terminated by the $CH_3$ group) of about 0.6 nm thickness has been compensated by (i) the 2-D assembling of the closely spaced, ET modified Ag NPs (*vide infra* and Figure 4B−D), i.e., by formation of a more efficient plasmonic enhancer than the assembly of mostly isolated Ag NPs[1,2] reported in ref 19, and, (ii) by the proper selection of excitation wavelength(s) with respect to the SPE of the AgNPs-ET assembly (Figure 3b).

In summation, the results of our SERS study provide evidence that employment of the thin hydrophobic spacer enables an efficient localization of SLG unperturbed by strain (affecting its mechanical properties[4,20,21]) and/or doping (affecting its electronic properties[4,20,21]) into the near field resonantly optically excited in the spacer-modified Ag NPs assembly.

In addition to that, a comparison of the optical images of the glass/AgNPs-ET reference system (Figure 4A) and of the glass/SLG/AgNPs-ET hybrid system (Figure 4B) obtained in



DOI: 10.1021/acs.langmuir.7b03462
*Langmuir* 2017, 33, 14414−14424

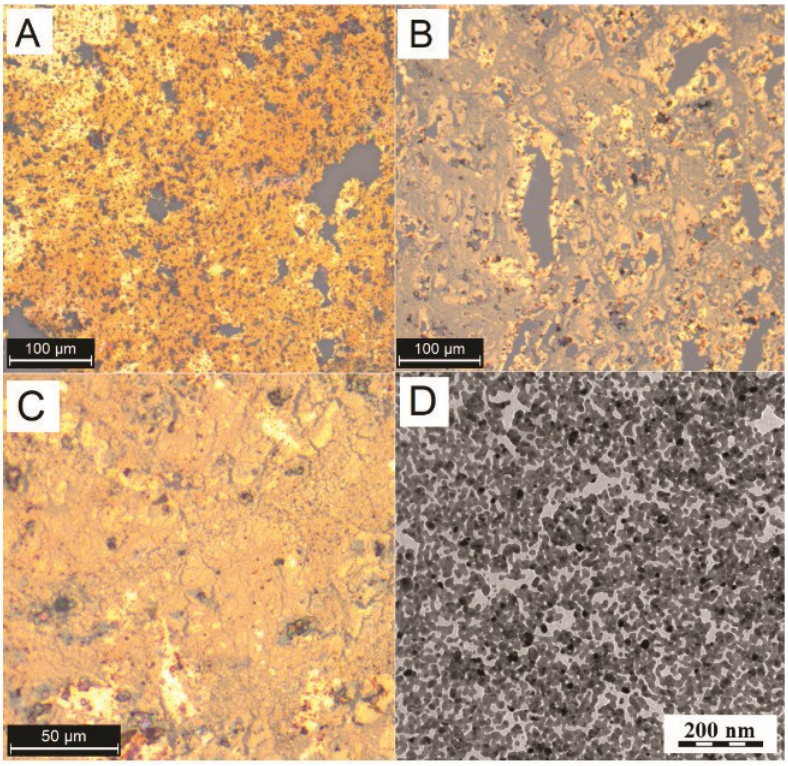


**Figure 4.** (A) Optical microscopy image of glass/AgNPs-ET reference system obtained with the 20x magnification objective. (B) Optical microscopy image of glass/SLG/AgNPs-ET hybrid system obtained with the 20x magnification objective. (C) Optical microscopy image of glass/SLG/AgNPs-ET hybrid system obtained with the 50x magnification objective. (D) TEM image of SLG/AgNPs-ET hybrid system deposited on carbon-coated Au grid.

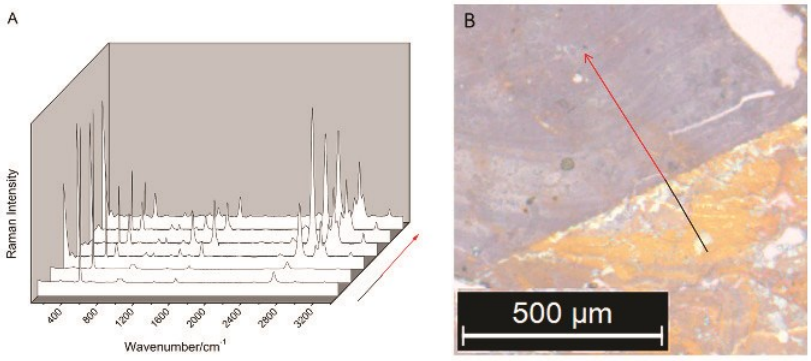


**Figure 5.** Manifestation of the additional enhancement of SERS of ET in the AgNPs-ET array induced by the presence of SLG underneath the AgNPs-ET array. (A) SERS microRaman sampling carried out at 633 nm excitation along the trajectory outlined in panel B, i.e., in the optical image of the sample; black line: the glass/AgNPs-ET part of the sample; red line: the glass/SLG/AgNPs-ET part of the sample.

the same magnification indicates that, while the hydrophobic ET-modified Ag NPs in the former system tend to form multilayers on the glass substrate (Figure 4A), the presence of SLG in the latter system has promoted the 2-D assembling of these hydrophobic Ag NPs (Figure 4B). The last mentioned observation is further corroborated by the optical images of the hybrid system in a higher magnification (Figure 4C) and by the TEM image the assembly of ET-modified Ag NPs on a SLG-covered, carbon-coated Au grid for TEM (Figure 4D).

In accord with the morphological characterization provided above, the SPE spectrum of the glass/AgNPs-ET reference system (Figure 3, curve a) shows a markedly higher extinction than that of the glass/SLG/AgNPs-ET hybrid system (Figure 3, curve b). The observed red-shift of SPE in the latter system with respect to the former one (Figure 3, curves a and b) can thus originate from the efficient SLG-Ag NPs coupling,[6] however, it can also be caused by the different morphologies of the Ag NPs assembly in each of these systems.

Furthermore, the average values of SERS enhancement factors of the spectral bands of the Ag-ET surface species have been determined for both the glass/SLG/AgNPs-ET hybrid and the glass/AgNPs-ET reference system from their SERS spectra measured at 445, 532, 633, and 780 nm excitation wavelengths (Table 1 and Table S2 in SI, respectively). Their



DOI: 10.1021/acs.langmuir.7b03462
*Langmuir* 2017, 33, 14414−14424

mutual comparison has shown that at the 532 and 633 nm excitations, the Ag-ET SERS spectral bands experience an additional enhancement by an average factor of 4 due to the presence of SLG in the hybrid system. By contrast, no such enhancement has been encountered at the 445 and 780 nm excitations (Table 1). This additional enhancement of SERS of Ag-ET has been visualized by SERS microRaman sampling experiment at 633 nm excitation in which the spectral sampling trajectory was directed over an edge of the glass-deposited SLG overdeposited by the ET-modified AgNPs array (Figure 5). The first part of the trajectory sampled ca. 1.5 $\mu m^2$ areas on the glass/Ag NPs-ET part of the sample, while the second one sampled areas of the same size on the glass/SLG/AgNPs/ET part (Figure 5B). The increase of the Ag-ET spectral bands intensity observable after the sampling trajectory crossed the SLG edge and entered the SLG-covered part of the sample is clearly visible on the SERS spectra evolution presented in Figure 5A.

On the basis of the results obtained in this paper as well as those published previously, several possibilities have been considered to explain this additional enhancement and its excitation wavelength dependence. First, (i) the graphene-enhanced Raman scattering (GERS)[35−37] and its coupling with the EM mechanism of SERS[38] has been considered. However, it has been recently concluded[36,37] that the GERS enhancement is observed only for planar aromatic molecules which is the case of neither the ET molecule, nor the Ag-ET surface species. Futhermore, (ii) the difference in the morphology (Figure 4A,B) and SPE spectra between the glass/AgNPs-ET (Figure 3A,B) and the glass/SLG/AgNPs-ET systems, i.e., measurements from a multilayer versus a monolayed of ET-modified Ag NPs can be also ruled out. The reason is that the SERS signal is collected predominantly from the first Ag NP-ET layer, as confirmed also by the same SERS enhancements of the Ag-ET vibrational modes in both systems (i.e., regardless the actual Ag NP layer thickness) observed at the 445 nm as well as at the 780 nm excitation. Furthermore, (iii) the vibrational mode selectivity of the additional enhancement has been checked by comparison of the enhancement factors of the individual Ag-ET vibrational modes (Table S3 in the SI). The enhancement factors of all these modes range from 3.3 to 4.3 at 532 nm excitation and from 3.0 to 4.4 at 633 nm excitation, i.e., there is no strong preferential enhancement of a particular vibrational mode of the Ag-ET surface species.

Finally, (iv) we consider the recently reported changes of the optical characteristics of SLG localized in the optical near field resonantly excited in 2-D Ag or Au NPs arrays.[5−10] It has been demonstrated that light absorption of SLG can be manipulated by integrating SLG with a thin layer of plasmonic nanostructures (such as the 2-D Ag or Au NPs arrays with or without a dielectric spacer between SLG and the plasmonic NPs array) upon the conditions of the resonance surface plasmon excitation.[5,7−10] In particular, the enhanced optical field thus created in the plasmonic NPs array can effectively enhance the total absorption of SLG.[5] Considering the Fresnel equations for calculation of the reflectance $R$ of a material from its "optical constants", i.e., the real (n-real refraction index) and imaginary (k-index of absorption) part of its complex refraction index ($N$),[33] the increase of the index of absorption of the material leads to increase of its reflectance $R$. Therefore, we suggest that the increased absorption of SLG coupled to AgNPs results in the increase of its reflectance, and we speculate that it is actually the increased reflectance of SLG (located underneath the ET-modified Ag NPs array) that leads to the increased SERS signal intensity of the Ag-ET surface species. This speculation is consistent with the selective observation of this additional SERS enhancement at 532 and 633 nm excitations in relation to the shape of the SPE curve of the glass/SLG/AgNPs-ET hybrid, which reaches maximal extinctions at the wavelengths corresponding to these excitations, but strongly drops both at 445 and 780 nm wavelengths (Figure 3, curve b). For testing the feasibility of the assumption that, at 532 and 633 nm excitations, SLG in the glass/SLG/AgNPs-ET hybrid system actually acts as a reflecting surface, we have carried out the following experiment: First, a new glass/Al foil/AgNPs-ET hybrid system, in which SLG was replaced by an Al foil known as a strongly reflecting mirror, was prepared. Its SERS microRaman spectra were measured at the same excitations as those of the glass/SLG/AgNPs-ET hybrid and of the glass/AgNPs-ET reference system, and the additional average SERS enhancement experienced by the vibrational modes of the Ag-ET surface species in the hybrid system with Ag foil (with respect to the reference system without the Ag foil) has been determined, yielding a factor of 12 and 15 at 532 and 633 nm excitations, respectively (Table 1). These experiments demonstrate the possibility to increase SERS signal of molecules and/or surface complexes incorporated in 2-D arrays of Ag NPs and measured by the microRaman technique by localization of the array on the strongly reflecting surface, while the 3−4 times higher enhancement produced by the Al foil than by SLG in the near field of Ag NPs indicates that SLG acts as only a weakly reflecting surface under these circumstances.

**SERS Spectra, Morphology, and Surface Plasmon Extinction of Glass/AgNPs/SLG Hybrid System Originating from the Parent Glass/AgNPs-ET System: The Effects of the ET Spacer Removal during SLG Deposition.** The second hybrid system investigated in this paper was prepared by overdeposition of the parent glass/AgNPs-ET system by SLG. SERS spectra of the resulting system measured at 445, 532, 633, and 780 nm wavelengths in the straight (i.e., as prepared) sample geometry (depicted in Figure 6A) and shown in Figure 6B contain none of the characteristic spectral bands of the Ag-ET species (assigned in Table S1 and observed in the SERS spectra of the glass/SLG/AgNPs-ET hybrid, Figure 2B).

This result indicates that ET was completely removed from the surface of the ET-modified Ag NPs during their overdeposition by SLG using the NC method of SLG transfer[31,32] (details in the Experimental Section). The hybrid system is thus denoted as glass/AgNPs/SLG (Figure 6A).

The changes in the morphology of Ag NPs caused by the moderate heating (160 °C) and the ET removal during deposition of SLG have been inspected by comparison of the TEM images of the parent AgNPs-ET array (deposited on the TEM grid prior to the SLG deposition, Figure 7A) and of the resulting AgNPs-SLG hybrid system (Figure 7B) obtained at the same magnification. The morphology changes correspond with annealing of Ag NPs (thermal and/or chemical after the ET removal from the Ag NP surface). Furthermore, the fairly uniform coverage of the glass surface by the annealed Ag NPs at a longer range 4 $\mu m \times 4$ $\mu m$ scale is depicted in Figure S6 in the SI, and the quite broad particle size distribution is quantified in Figure 7C. Monomers as well as dimers and trimers of Ag NPs can be distinguished in the TEM image of the Ag NPs-SLG system in Figure 7B. The fraction of dimers and trimers has been established to ca. 20% from of the circularity diagram in Figure 7D.



DOI: 10.1021/acs.langmuir.7b03462
*Langmuir* 2017, 33, 14414−14424

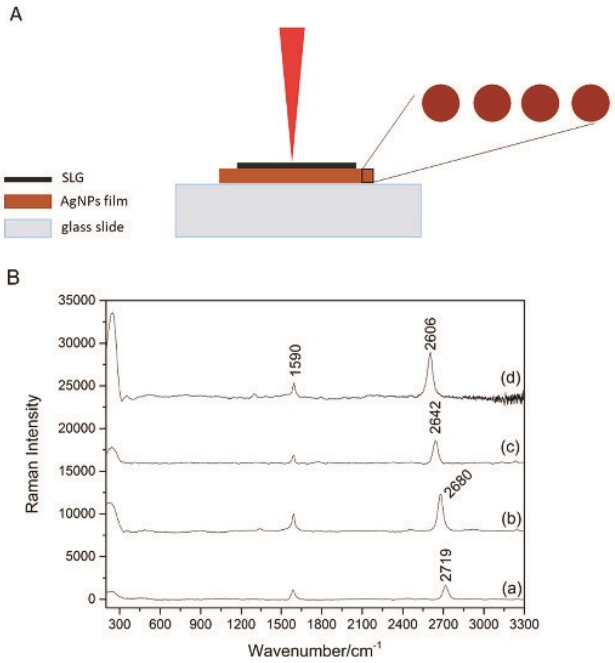


**Figure 6.** (A) Schematic depiction of glass/AgNPs/SLG hybrid system as a sample for SERS microRaman measurement in the straight geometry. (B) SERS microRaman spectra of glass/AgNPs/SLG hybrid system measured at (a) 445, (b) 532, (c) 633, (d) 780 nm excitation in the straight sample geometry.

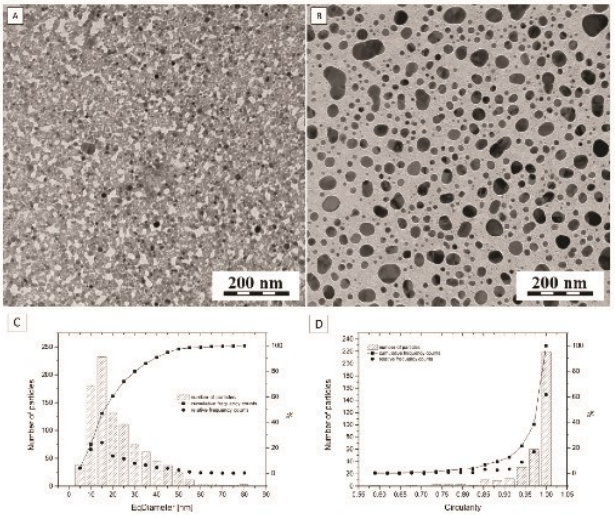


**Figure 7.** (A) TEM image of the parent Ag NPs-ET film deposited on a C-coated Au grid. (B) TEM image of AgNPs/SLG hybrid system deposited on a C-coated Au grid. (C) Particle size distribution in the AgNPs/SLG hybrid system. (D) Distribution of the particles circularity in the AgNPs/SLG hybrid system.

On the basis of the previously published studies,[39,40] we reason that both the broad particle size distribution and the presence of fused Ag NPs dimers and trimers contribute to observation of the very broad and rather flat SPE curve of the Ag NPs-SLG system, which spans the visible spectral region and extends itself into the near IR (Figure 8).

The glass/AgNPs/SLG hybrid system thus differs from the glass/SLG/AgNPs-ET hybrid addressed in the first part of this

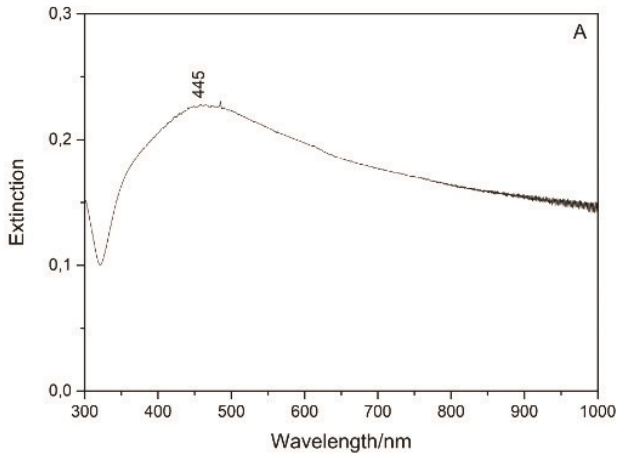


**Figure 8.** Surface plasmon extinction of the glass/AgNPs/SLG hybrid system.

paper not only by the reverse order of the components assembling, but also by the morphology and SPE of the 2-D Ag NPs array and by the Ag NPs-SLG distance (due to the ET spacer removal). Consequently, a mutual comparison of SERS enhancement factors of the G and 2D modes of SLG in these two hybrid systems is not particularly meaningful, since three different factors simultaneously contribute to their mutual difference. On the other hand, we have reasoned that SERS microRaman sample setup can offer a possibility to measure the same hybrid system in two different orientations with respect to the laser beam excitation: the straight one (Figure 6A) and the inverted one (Figure 9A). In that case, the SERS enhancement will be affected only by the different mutual positions of the same plasmonic enhancer (i.e., the Ag NPs array) and SLG (Figures 6A and 9A).

SERS spectra of the glass/AgNPs/SLG hybrid were measured at 445, 532, 633, and 780 nm excitations in both the straight (Figure 6A) and the inverted (Figure 9A) sample geometry. The SERS spectra of SLG obtained from each of them are shown in Figure 6B and Figure 9B, respectively. Since both spectra originate from the same hybrid system, the wavenumbers of the G and 2D modes have been expected, and they are actually observed to be virtually the same in both geometries at each of the four excitation wavelengths. In particular, the nondispersive G mode is located at 1590 $cm^{-1}$ in both sets of the spectra at all four excitation wavelengths. Its position is thus by 5 $cm^{-1}$ higher than that of pristine SLG[20,21] and of SLG in the glass/SLG reference sample (Figure 2C, spectrum a, and Figure S3 in the SI). At 445 nm excitation, the dispersive 2D mode is located at 2719 $cm^{-1}$ in the spectrum measured in the straight sample geometry (Figure 6B) and at 2717 $cm^{-1}$ in the spectrum obtained in the inverted geometry (Figure 9B). Its position is thus by 3 and 5 $cm^{-1}$, respectively, lower than that of SLG in the glass/SLG reference system (Figure 2C). The small upshift of the G mode wavenumber together with the small downshift of that of the 2D mode suggests a weak n-doping of SLG by Ag NPs, as reported previously.[41] SERS enhancement factors of the G and 2D modes of SLG determined as the intensity ratios of these modes in the SERS spectra of the glass/Ag NPs/SLG hybrid to those in the Raman spectra of the glass/SLG reference system (both measured in either the straight or the inverted sample geometry) are listed in Table 2 and depicted in Figure 10



DOI: 10.1021/acs.langmuir.7b03462
Langmuir 2017, 33, 14414−14424

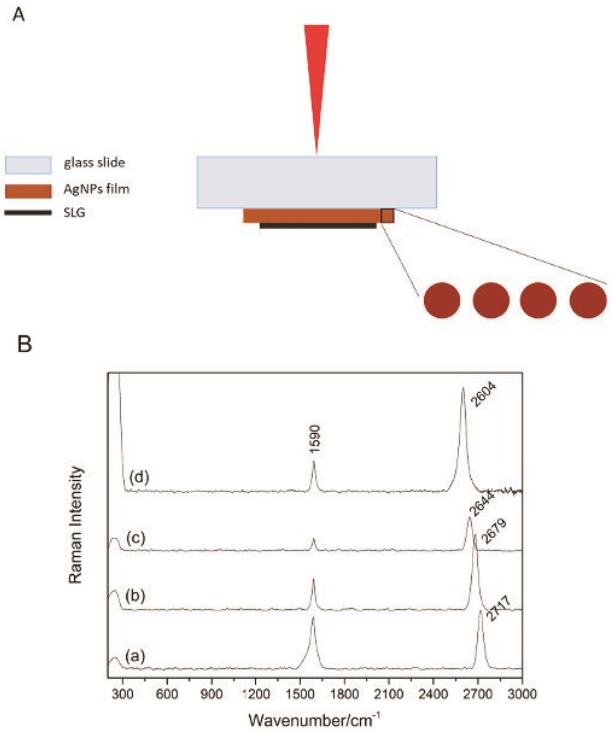


**Figure 9.** (A) Schematic depiction of glass/AgNPs/SLG hybrid system as a sample for SERS microRaman measurement in the inverted geometry. (B) SERS microRaman spectra of glass/AgNPs/SLG hybrid system measured at (a) 445, (b) 532, (c) 633, (d) 780 nm excitation in the inverted sample geometry.

(together with the error bars representing the standard deviations of band intensities resulting from evaluation of five spectral maps).

**Table 2. SERS Enhancement Factors of the SLG Modes in the Glass/AgNPs/SLG Hybrid System**

| | Ef | | | |
|---|---|---|---|---|
| | inverted geometry | | straight geometry | |
| $\lambda_{exc}$ (nm) | SLG - G | SLG − 2D | SLG - G | SLG − 2D |
| 445 | 33 | 17 | 15 | 7 |
| 532 | 14 | 9 | 11 | 7 |
| 633 | 16 | 9 | 18 | 8 |
| 780 | 19 | 10 | 8 | 5 |

The SERS Ef values (Figure 10 and Table 2) demonstrate that a significant SERS enhancement is experienced by the G and the 2D mode of SLG at all excitations (445−780 nm) and in both sample geometries. This result is attributed to the morphology of the annealed Ag NPs array in the hybrid system, namely, to the broad distribution of morphologies and sizes of Ag NPs constituting this array (Figure 7), which in turn, manifests itself by the broad SPE curve of the hybrid (Figure 8). Nevertheless, one has to keep in mind that both absorption and scattering contribute to the SPE of the Ag NPs array, while the SERS enhancement by the EM mechanism stems only from the scattering crossection. Therefore, the wavelength dependence of the scattering crosssections of Ag NPs monomers and dimers[42] is even more appropriate for correlation with the excitation wavelength dependence of the SERS Efs of the SLG modes in the two sample geometries than the SPE curve itself.

For both the G and the 2D mode of SLG, the differences between their SERS Ef's in the two samples geometries (Figures 6A and 9A) show the same excitation wavelength dependence (Figure 10 and Table 2). In particular, no significant differences in the Efs are observed at 532 and 633 nm excitations, while at 445 and 780 nm excitations, the enhancement factors are approximately 2 times larger in the inverted (Figure 9A) than in the straight (Figure 6A) sample geometry. The former observation is consistent with the presence of the same plasmonic enhancer in the hybrid system in the straight as well as inverted sample geometry (Figures 6A and 9A), while the latter one indicates that some other, excitation wavelength-dependent factor(s), affect the final SERS Efs determined in each of the two sample geometries. We propose that the most important factors are (i) absorption of both the incident and the scattered light by the Ag NPs, and (ii) increased absorption and reflectance of SLG in the optical near field resonantly excited in Ag NPs. Their mutual interplay at each excitation wavelength and in each sample geometry (in which SERS spectra of SLG from the particular hybrid system have been measured) can then positively and/or negatively affect the actual values of the experimetally determined SERS Efs of the SLG modes.

In the particular case of our hybrid system constituted by SLG on the top of the Ag NPs array, the former effect (i) is expected to affect negatively the SERS spectral intensities preferentially in the inverted sample geometry (favoring thus the straight sample geometry), while the latter effect (ii) favors the inverted geometry (in which scattered light is partially reflected back into the sample) over the straight one (in which a small fraction of the incident light is reflected from the sample surface). Since the magnitude of both effects is excitation wavelength dependent, it is understandable that the result of their interplay depends on the excitation wavelength as well.

Nevertheless, the exact values of the absorption and scattering crosssections of our particular Ag NPs array at each excitation wavelength are not available, and other factors, such as the fraction of the SLG surface located in the near field of Ag NPs at each of the excitation wavelengths, also play their role. Therefore, we can only qualitatively and tentatively address the experimentally observed excitation wavelength-dependent differences between the Efs experienced by the SLG in the straight (Figure 6A) and in the inverted (Figure 9A) sample geometry (Figure 10 and Table 2). Apparently, the two additional effects (i) and (ii) compensate each other at 532 and 633 nm excitations. By contrast, at 445 and 780 nm excitation, the measurement in the inverted geometry is favored by the 2-fold increase of the SERS Efs of both the G and 2D mode of SLG, hence the contribution of the effect (ii) is larger that that of the effect (i) at these wavelengths. We propose that this observation can be related to the efficient localization of SLG in the near field of Ag NPs resonantly excited at these excitation wavelengths (resulting into the increased reflectivity of SLG), in combination with the particular morphology of the annealed Ag NPs array. In particular, at 445 nm, the optical fields are resonantly excited preferentially in single Ag NPs: the optical fields in the vicinity of the single NPs are relatively weak,[39,40,42] but the NPs are fairly abundant (Figure 7B,C,D), hence a relatively large fraction of SLG area is localized in these optical fields. At 780 nm excitation, stronger optical fields are excited in large Ag NPs dimers and trimers, including the very strong



DOI: 10.1021/acs.langmuir.7b03462
Langmuir 2017, 33, 14414−14424

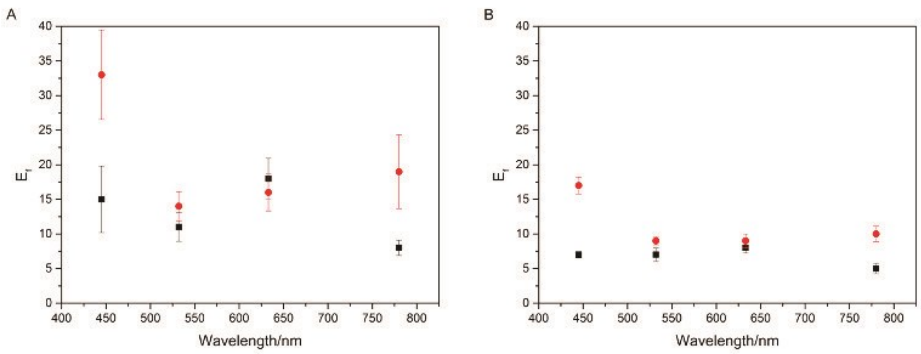


**Figure 10.** Comparison of SERS enhancement factors of the G mode (A) and of the 2D mode (B) of SLG in the glass/AgNPs/SLG hybrid system plotted as a function of excitation wavelength for two sample geometries: the straight one - black squares, the inverted one - red circles.

optical fields (hot spots) localized between the NPs in these dimers and/or trimers.[39,40,42] However, the dimers and trimers are less abundant than the single NPs (Figure 7 B and D). Therefore, at the 780 nm excitation, a smaller contact area between SLG and the optical near fields excited in Ag NPs dimers and trimers appears to be compensated by the larger optical fields strength. The additional enhancement by a factor of approximately 2 in the inverted sample geometry is thus observed at both the 445 and 780 nm excitations (Figure 10 and Table 2).

Furthermore, standard deviations of the SERS Efs experienced by the G and the 2D mode of SLG in both sample geometries and at all excitations have been determined for each of these 16 spectral measurements from five spectral maps, and they are depicted as error bars in Figure 10A,B. Their values are fairly low for the 2D mode at all excitations and in both sample geometries (Figure 10 B). For the G mode, low values of the error bars have been obtained at 532 and 633 nm excitations in both sample geometries and at 780 nm excitation in the straight sample geometry, while relatively large error bars have been determined at 445 nm excitation in both sample geometries and at 780 nm excitation in the straight geometry (Figure 10A). The large standard deviations at 445 nm excitation have their origin in fluctuations of the spectral background in the 1500−1650 $cm^{-1}$ region encountered at this particular excitation. At 780 nm excitation, the large signal fluctuations in the same spectral region have been observed only in the inverted sample geometry (i.e., for the measurement "through glass", Figure 9A), and they are attributed to fluorescence from the glass slide.[43] In summation, these results indicate that the glass/AgNPs/SLG hybrid sample is fairly homogenoues on the large scale of the SERS spectral mapping, since the large standard deviations are limited to 3 of 16 spectral mapping measurements, and they have been explained by extrinsic spectral effects unrelated to the sample morphology.

## ■ CONCLUSIONS

Two approaches to coassembling of SLG and 2D-arrays of ethanethiol (ET) modified Ag NPs were adopted, and each of them resulted into a different hybrid SERS active system: (i) with and (ii) without ET chemisorbed to Ag NPs, i.e., with and without the molecular spacer between the Ag NPs surface and SLG. Comparison of their morphological, structural and optical characteristics enabled us to address the specific advantages of the spacer presence and/or removal.

The system with the ET spacer resulted from overlaying SLG on a glass slide by ET-modified, hydrophobic Ag NPs, which assembled on the hydrophobic SLG surface into a 2-D array. The efficiency of the ET molecular spacer was proved by observation of the SERS spectral bands of the G and 2D mode of SLG unaffected by doping and/or strain. Preservation of the native structure of SLG, the consistence of the excitation wavelength dependence of the SERS enhancement of the G and 2D mode of SLG at excitations in the 445−780 nm range with the SPE of the AgNPs-ET array as well as the manifestations of the second part of the EM SERS enhancement experienced by the G and the 2D modes of SLG, respectively, have provided evidence of the EM mechanism origin of the SERS enhancement of the SLG modes in this hybrid system. Overlaying of SLG by the ET-modified Ag NPs can thus be viewed as a prospective pathway to SERS spectral probing of "real life" SLG samples deposited on various substrates and exposed to various conditions that induce doping and/or strain.

Furthermore, the excitation wavelength selective additional enhancement of SERS of the Ag-ET modes observed at 633 and 532 nm excitations (falling into the region of the largest SPE of the hybrid) by a factor of 4 has been tentatively attributed to the increased reflectance of SLG in the near field resonantly excited in the Ag NPs-ET array. This explanation is in accord with the earlier observations that optical properties of SLG can be modified by the near field of Ag NPs array even in the case when SLG is distanced from the AgNPs surface by a spacer.

Preparation of the second hybrid system by deposition of the components in the reverse order, i.e., by overdeposition of the Ag NPs-ET array on glass by SLG, resulted in the removal of the chemisorbed ET and annealing of Ag NPs, i.e., into formation of the glass/AgNPs/SLG hybrid. The direct contact between the Ag NPs and SLG manifests itself in the SERS spectra of SLG by the wavenumber positions of the G mode and the 2D mode consistent with a weak n-doping of SLG by Ag NPs. Annealing of the Ag NPs causes their merging into larger monomers with a broad distribution of sizes as well as into dimers and trimers of fused NPs, and results in a very broad SPE curve of the hybrid, which extends over the overall visible spectral region.

Exploration of the effect of localization of the same plasmonic enhancer (namely of the array of the annealed Ag NPs) on the top and/or underneath SLG by SERS spectral mapping of the glass/Ag NPs/SLG in two different sample orientations with respect to the exciting laser beam, i.e., in the straight and in the inverted sample geometry, respectively, (at four excitations in the 445−780 nm range) revealed that for



DOI: 10.1021/acs.langmuir.7b03462
*Langmuir* 2017, 33, 14414−14424

both SLG modes, the Efs are the same at 532 and 633 nm excitations, and by a factor of 2 higher in the inverted sample geometry than in the straight one at 445 and 780 nm. These excitation wavelength dependent differences have been tentatively explained by the interplay of two factors: absorption of both the incident and the scattered light by the Ag NPs, and increased absorption and reflectance of SLG in the optical near field resonantly excited in Ag NPs, in relation to our hybrid system preparation (SLG on the top of Ag NPs array) and the actual morphology of the Ag NPs array in the hybrid. We propose that, owing to its morphological characteristics and optical properties, this particular glass/annealed-AgNPs-array/SLG hybrid system could provide a suitable platform for GERS/SERS of aromatic molecules. In more general terms, we have found that localization of the same plasmonic enhancer underneath or above SLG can affect the optical properties of the hybrid system; however, the magnitude and the excitation wavelength dependence of this effect will depend on the actual morphology of the plasmonic enhancer.

## ■ ASSOCIATED CONTENT

### Supporting Information

The Supporting Information is available free of charge on the ACS Publications website at DOI: 10.1021/acs.langmuir.7b03462.

Figures S1−S6: TEM image and PSD of parent Ag NP hydrosol, photographic depiction of Ag NPs-ET film preparation and transfer, SERS spectrum of glass/Ag NPs-ET system, Raman spectrum of glass/SLG system, SPE spectrum of glass/SLG/AgNPs-ET system in relation to its SERS spectrum at 633 nm, TEM image of Ag NPs/SLG system; Tables S1−S3: assignment of ET and Ag-ET spectral bands, SERS enhancement factors of Ag-ET spectral bands in glass/AgNPs-ET and glass/SLG/AgNPs-ET hybrids (PDF)

## ■ AUTHOR INFORMATION


### Corresponding Author

*E-mail: vlc@natur.cuni.cz.

### ORCID

Veronika Sutrová: 0000-0001-8320-2078
Ivana Šloufová: 0000-0002-4757-6029
Martin Kalbáč: 0000-0001-9574-4368
Blanka Vlčková: 0000-0003-0553-3722


### Notes

The authors declare no competing financial interest.

## ■ ACKNOWLEDGMENTS

Financial support by the 15-01953S grant awarded by the Czech Science Foundation is gratefully acknowledged. We also acknowledge assistance provided by the Research Infrastructure NanoEnviCz, supported by the Ministry of Education, Youth and Sports of the Czech Republic under Project No. LM2015073 and Project No. CZ.02.1.01/0.0/0.0/16_013/0001821. V.S. acknowledges financial support by the 892217 students grant awarded by Grant Agency of Charles University.

## ■ REFERENCES


(1) Le Ru, E. C.; Etchegoin, P. G. *Principles of Surface-enhanced Raman Spectroscopy and Related Plasmonic Effects*; Elsevier: Amsterdam, 2009.

(2) Maier, S. A. *Plasmonics, Fundamentals and Applications*; Springer Science+Business Media LLC: New York, 2007.

(3) Procházka, M. *Surface-Enhanced Raman Spectroscopy-Bioanalytical, Biomolecular and Medical Applications*; Springer International Publishing: Cham, Switzerland, 2016.

(4) Bonaccorso, F.; Sun, Z.; Hasan, T.; Ferrari, A. C. Graphene photonics and optoelectronics. *Nat. Photonics* **2010**, *4*, 611−622.

(5) Liu, Y.; Cheng, R.; Zhou, H.; Bai, J.; Liu, G.; Liu, L.; Huang, Y.; Duan, X. Plasmon resonance enhanced multicolour photodetection by graphene. *Nat. Commun.* **2011**, *2*, 579.

(6) Niu, J.; Shin, J. Y.; Son, J.; Lee, Y.; Ahn, J. H.; Yang, H. Shifting of surface plasmon resonance dute to electromagnetic coupling between graphene and Au nanoparticles. *Opt. Express* **2012**, *20*, 19690.

(7) Zhu, J.; Liu, Q. H.; Lin, T. Manipulating light absorption of graphene using plasmonic nanoparticles. *Nanoscale* **2013**, *5*, 7785−7789.

(8) Du, Y.; Zhao, Y.; Qu, Y.; Chen, Ch.-H.; Chen, Ch.-M.; Chuang, Ch.-H.; Zhu, Y. Enhanced light-matter interaction of graphene-gold nanoparticle hybrid films for high-performance SERS detection. *J. Mater. Chem. C* **2014**, *2*, 4683−4691.

(9) Lee, S.; Kim, J. Desing of optical metamaterial mirror with metallic nanoparticles for floating-gate graphene optoelectronic devices. *Opt. Express* **2015**, *23*, 21809.

(10) Mat Teridi, M. A.; Sookhakian, M.; Basirun, W. J.; Zakaria, R.; Schneider, F. K.; da Silva, W. J.; Kim, J.; Lee, S. J.; Kim, H. P.; Mohd Yusoff, A. R.; Jang, J. Plasmon enhanced organic devices utilizing highly ordered nanoimprinted gold nanodisk and nitrogen doped graphene. *Nanoscale* **2015**, *7*, 7091−7100.

(11) Schedin, F.; Lidorikis, E.; Lombardo, A.; Kravets, V.G.; Geim, A. K.; Grigorenko, A. N.; Novoselov, S. K.; Ferrari, C. A. Surface-enhanced Raman Spectroscopy of Graphene. *ACS Nano* **2010**, *4*, 5617−5626.

(12) Fu, X.; Bei, F.; Wang, X.; O'Brien, S.; Lombardi, R. J. Excitation profile of surface-enhanced Raman scattering in graphene-metal nanoparticle based derivatives. *Nanoscale* **2010**, *2*, 1461−1466.

(13) Heeg, S.; Fernandez-Garcia, R.; Oikonomou, A.; Schedin, F.; Narula, R.; Maier, A. S.; Vijayaraghavan, A.; Reich, S. Polarized Plasmonic Enhancement by Au Nanostructures Probed through Raman Scattering of Suspended Graphene. *Nano Lett.* **2013**, *13*, 301−308.

(14) Kravets, V. G.; Schedin, F.; Jalil, R.; Britnell, L.; Novoselov, K. S.; Grigorenko, A. N. Surface Hydrogenation and Optics of a Graphene Sheet Transferred onto a Plasmonic Nanoarray. *J. Phys. Chem. C* **2012**, *116*, 3882−3887.

(15) Xu, W. G.; Mao, N. N.; Zhang, J. Graphene: A Platform for Surface-Enhanced Raman Spectroscopy. *Small* **2013**, *9*, 1206−1224.

(16) Kalbáč, M.; Valeš, V.; Vejpravová, J. The Effect of a Thin Gold Layer on Graphene: A Raman Spectroscopy Study. *RSC Adv.* **2014**, *4*, 60929−60935.

(17) Zhao, Y.; Zhu, Y. W. Graphene-Based Hybrid Films for Plasmonic Sensing. *Nanoscale* **2015**, *7*, 14561−14576.

(18) Ek Weiss, J.; Costa, S.; Frank, O.; Fridrichová, M.; Vlčková, B.; Vejpravová, J.; Kalbac, M. SERS of Isotopicallly Labeled 12C/13C Graphene Bilayer−Gold Nanostructured Film Hybrids: Graphene Layer as Spacer and SERS Probe. *J. Phys. Chem. C* **2017**, *121*, 11680−11686.

(19) Gong, T.; Zhang, J.; Zhu, Y.; Wang, W.; Zhang, X.; Zhang, J. Optical properties and surface-enhanced Raman scattering of hybrid structures with Ag nanoparticles and graphene. *Carbon* **2016**, *102*, 245−254.

(20) Jorio, A.; Saito, R.; Dresselhaus, G.; Dresselhaus, M. S. *Raman Spectroscopy in Graphene Related Systems*; Wiley-VCH Verlag GmbH & Co. KGaA: Weinheim, Germany, 2011.

(21) Ferrari, A. C.; Basko, D. M. Raman spectroscopy as a versatile tool for studying the properties of graphene. *Nat. Nanotechnol.* **2013**, *8*, 235−245.

(22) Zaretski, A. V.; Marin, B. C.; Moetazedi, H.; Dill, T. J.; Jibril, L.; Kong, C.; Tao, A. R.; Lipomi, D. J. Using the Thickness of Graphene




DOI: 10.1021/acs.langmuir.7b03462
*Langmuir* 2017, 33, 14414−14424

to Template Lateral Subnanometer Gaps between Gold Nanostructures. *Nano Lett.* **2015**, *15*, 635−640.
(23) Xu, S.; Jiang, S.; Wang, J.; Wei, J.; Yue, W.; Ma, Y. Graphene isolated Au nanoparticle arrays with high reproducibility for high-performance surface-enhanced Raman scattering. *Sens. Actuators, B* **2016**, *222*, 1175−1183.
(24) Xu, S.; Man, B.; Jiang, S.; Wang, J.; Wei, J.; Xu, S.; Liu, H.; Gao, S.; Liu, H.; Li, Z.; Li, H.; Qiu, H. Graphene/Cu Nanoparticle Hybrids Fabricated by Chemical Vapor Deposition As Surface-Enhanced Raman Scattering Substrate for Label-Free Detection of Adenosine. *ACS Appl. Mater. Interfaces* **2015**, *7*, 10977−10987.
(25) Dai, Z.; Xiao, X.; Wu, W.; Zhang, Y.; Liao, L.; Guo, S.; Ying, J.; Shan, Ch.; Sun, M.; Jiang, Ch Plasmon-driven reaction controlled by the number of graphene layers and localized surface plasmon distribution during optical excitation. *Light: Sci. Appl.* **2015**, *4*, e342.
(26) Zhang, X.; Dai, Z.; Si, S.; Zhang, X.; Wu, W.; Deng, H.; Wang, F.; Xiao, X.; Jiang, C. Ultrasensitive SERS substrate integrated with uniform subnanometer scale "hot spots" created by a graphene spacer for the detection of mercury ions. *Small* **2017**, *13*, 1603347.
(27) Vlčková, B.; Matějka, P.; Šimonová, J.; Pančoška, P.; Čermáková, K.; Baumruk, V. Surface Enhanced (Resonance) Raman Spectra of Free Base 5,10,15,20−Tetrakis (4-carboxyphenyl)-Porphyrin and Its Silver Complex In Systems With Silver Colloid: Direct Adsorption versus Adsorption via Molecular Spacer. *J. Phys. Chem.* **1993**, *97*, 9719−9729.
(28) Michl, M.; Vlčková, B.; Mojzeš, P. Ag Colloid-1-alkanethiol Films: Spacer-modified Substrates for SERRS Spectroscopy of Chromophoric Molecules. *Vib. Spectrosc.* **1999**, *19*, 239−242.
(29) Vlčková, B.; Šmejkal, P.; Michl, M.; Procházka, M.; Mojzeš, P.; Lednický, F.; Pfleger, J. Surface-enhanced Resonance Raman Spectroscopy of Porphyrin and Metalloporphyrin Species in Systems with Ag Nanoparticles and Their Assemblies. *J. Inorg. Biochem.* **2000**, *79*, 295−300.
(30) Corra, S.; Lewandowska, U.; Benetti, E. M.; Wennemers, H. Size-Controlled Formation of Noble-Metal Nanoparticles in Aqueous Solution with a Thiol-Free Tripeptide. *Angew. Chem., Int. Ed.* **2016**, *55*, 8542−8245.
(31) Kalbáč, M.; Frank, O.; Kavan, L. The control of graphene double-layer formation in copper-catalyzed chemical vapor deposition. *Carbon* **2012**, *50*, 3682−3687.
(32) Hallam, T.; Berner, N. C.; Yim, C.; Duesberg, G. S. Strain, Bubbles, Dirt, and Folds: A Study of Graphene Polymer-Assisted Transfer. *Adv. Mater. Interfaces* **2014**, *1*, 1400115.
(33) Bohren, C. F.; Huffman, D. R. *Absorption and Scattering of Light by Small Particles*; WILEY-VCH Verlag GmbH & Co. KGaA: Weinheim, Germany, 2004.
(34) Cialla, D.; Petschulat, J.; Hübner, U.; Schneidewind, H.; Zeisberger, M.; Mattheis, R.; Pertsch, T.; Schmitt, M.; Möller, R.; Popp, J. Investigation on the Second Part of the electromagnetic SERS Enhancement and Resulting Fabrication Strategies of Anisotropic Plasmonic Arrays. *ChemPhysChem* **2010**, *11*, 1918−1924.
(35) Ling, X.; Xie, L.; Fang, Y.; Xu, H.; Zhang, H.; Kong, J.; Dresselhaus, M. S.; Zhang, J.; Liu, Z. Can graphene be used as a Substrate for Raman Enhancement? *Nano Lett.* **2010**, *10*, 553−561.
(36) Ling, X.; Huang, S.; Mao, N.; Kong, J.; Dresselhaus, M. S.; Zhang, J. Lighting Up the Raman Signal of Molecules in the Vicinity of Graphene Related Materials. *Acc. Chem. Res.* **2015**, *48*, 1862−1870.
(37) Huang, S.; Ling, X.; Liang, L.; Song, Y.; Fang, W.; Zhang, J.; Kong, J.; Meunier, V.; Dresselhaus, M. S. Molecular Selectivity of Graphene-Enhanced Raman Scattering. *Nano Lett.* **2015**, *15*, 2892−2901.
(38) Hao, Q.; Wang, B.; Bossard, J. A.; Kiraly, B.; Zeng, Y.; Chiang, I.-K.; Jensen, L.; W erner, D. H.; Huang, T. J. Surface-Enhanced Raman Scattering Study on Graphene-Coated Metallic Nanostructure Substrates. *J. Phys. Chem. C* **2012**, *116*, 7249−7254.
(39) Gunnarsson, L.; Rindzevicius, T.; Prikulis, J.; Kasemo, B.; Käll, M.; Zou, S.; Schatz, G. C. Confined Plasmon in Nanofabricated Single Silver Particle Pairs: Experimental Observation of Strong Interparticle Interactions. *J. Phys. Chem. B* **2005**, *109*, 1079−1087.
(40) Feng, X.; Ruan, F.; Hong, R.; Ye, J.; Hu, J.; Hu, G.; Yang, Z. Synthetically Directed Self-Assembly and Enhanced Surface-Enhanced Raman Scattering Property of Twinned Crystalline Ag/Ag Homojunction Nanoparticles. *Langmuir* **2011**, *27*, 2204−2210.
(41) Giovannetti, G.; Khomyakov, P. A.; Karpan, V. M.; van den Brink, J.; Kelly, P. J. Doping graphene with metal contacts. *Phys. Rev. Lett.* **2008**, *101*, 026803.
(42) Tamaru, H.; Kuwata, H.; Miyazaki, H. T.; Miyano, K. Resonant light scattering from individual Ag nanoparticles and particle pairs. *Appl. Phys. Lett.* **2002**, *80*, 1826−1828.
(43) Tuschel, D. Selecting an Excitation Wavelength for Raman Spectroscopy. *Spectroscopy* **2016**, *31*, 14−23.



DOI: 10.1021/acs.langmuir.7b03462
*Langmuir* 2017, 33, 14414−14424

Supporting information

# Effect of ethanethiolate spacer on morphology and optical responses of Ag nanoparticle array - single layer graphene hybrid systems

Veronika Sutrová[a,c], Ivana Šloufová[a], Zuzana Melniková[b], Martin Kalbáč[b], Ewa Pavlova[c], Blanka Vlčková[a]*

[a] Charles University, Faculty of Science, Department of Physical and Macromolecular Chemistry, Hlavova 8, Prague 2, 128 40, Czech Republic, vlc@natur.cuni.cz

[b] J. Heyrovsky Institute of Physical Chemistry of the ASCR, v.v.i, Dolejškova 3, 182 21 Prague 8, Czech Republic

[c] Institute of Macromolecular Chemistry AS CR, Heyrovsky Sq. 2, 162 06 Prague 6, Czech Republic

* Corresponding author E-mail: vlc@natur.cuni.cz

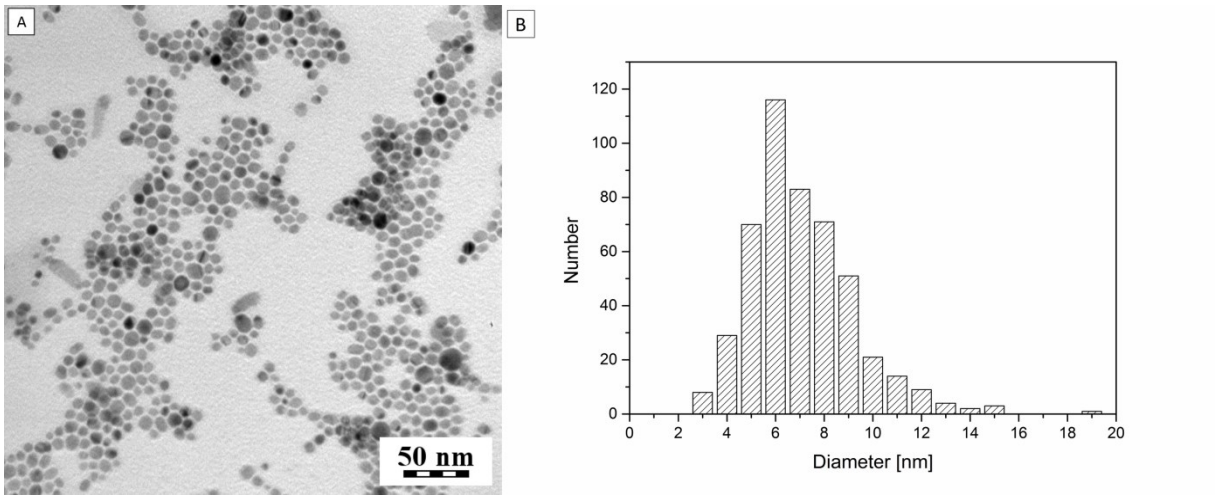


Fig S1: Left: TEM image of a dried drop of parent Ag NP hydrosol prepared according to the ref. S1 (identical with the ref. 23 in the main paper). Right: Particle size distribution determined from the TEM image of the depositd Ag NPs hydrosol.

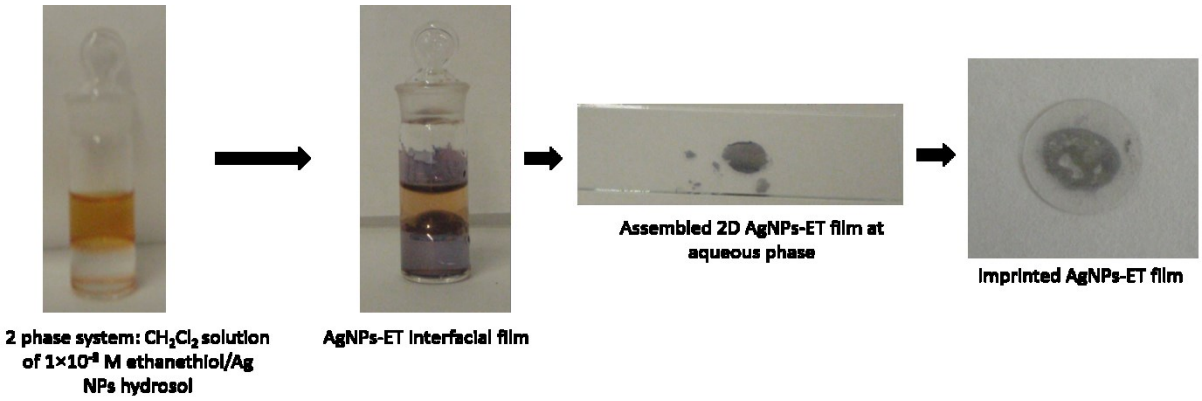


Fig S2: Photographic depiction of the Ag NPs-ET interfacial nanoparticulate film preparation and of its transfer on a glass slide by imprinting.

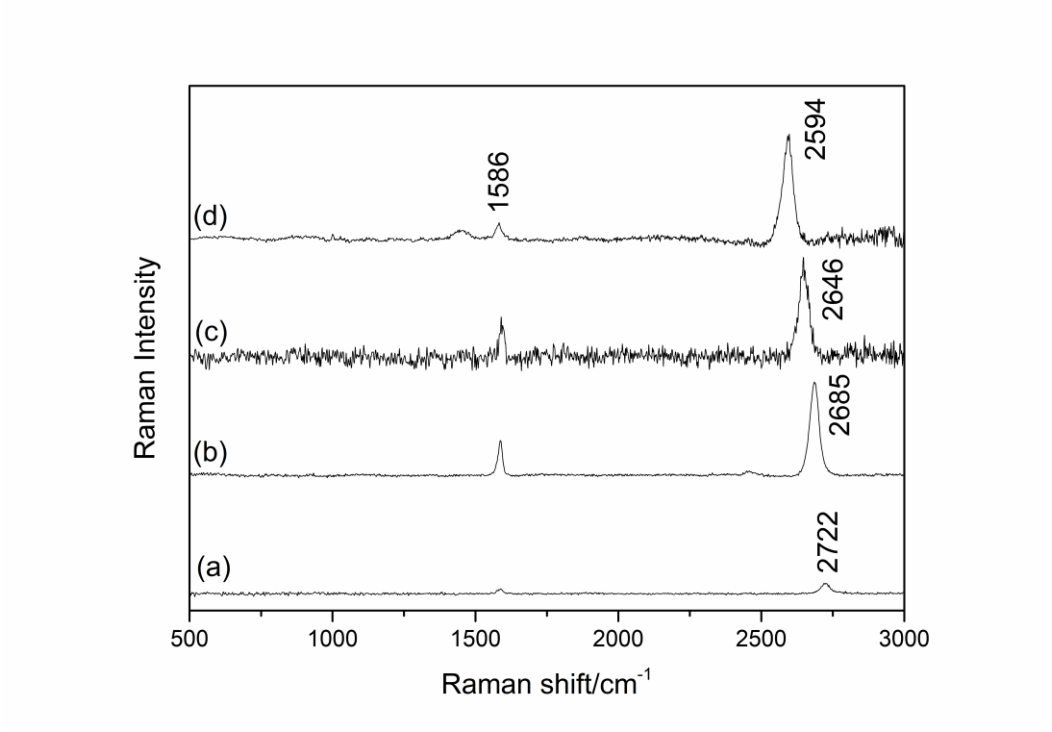


Fig S3: SERS spectra of SLG obtained from glass/SLG reference system at (a) 445 nm (b) 532 nm (c) 633 nm (d) 780 nm excitations.

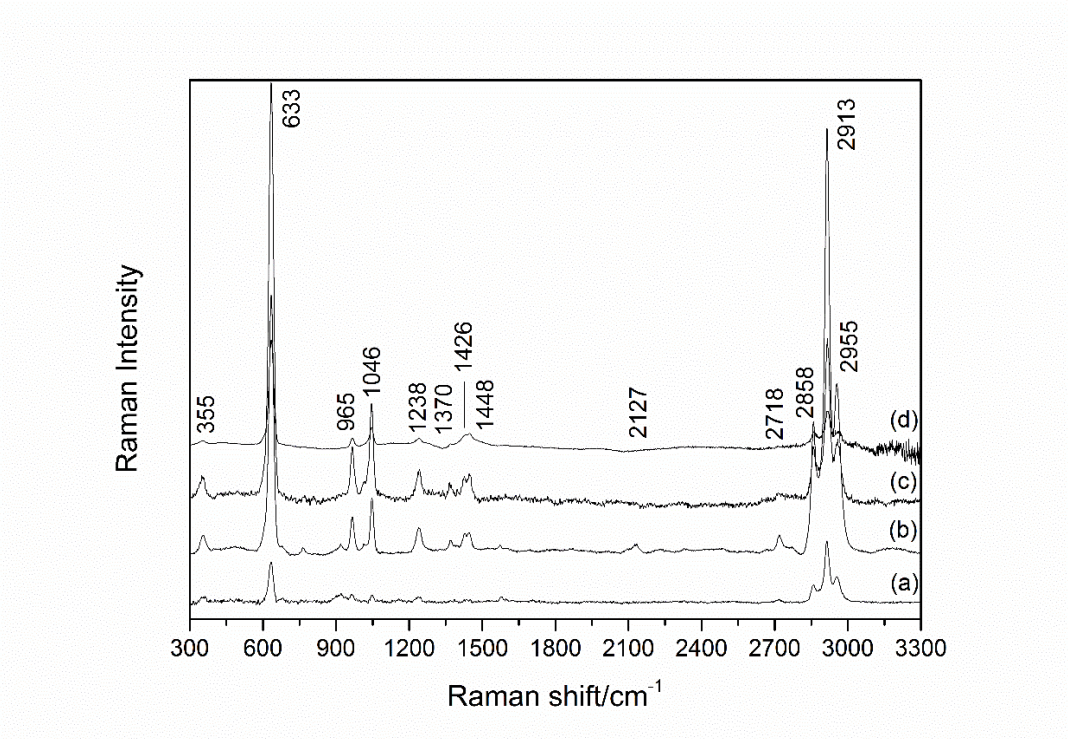


Fig S4: SERS spectra of Ag-ethanethiolate species obtained from the glass/AgNPs-ET array reference system at (a) 445 nm (b) 532 nm (c) 633 nm (d) 780 nm excitations.

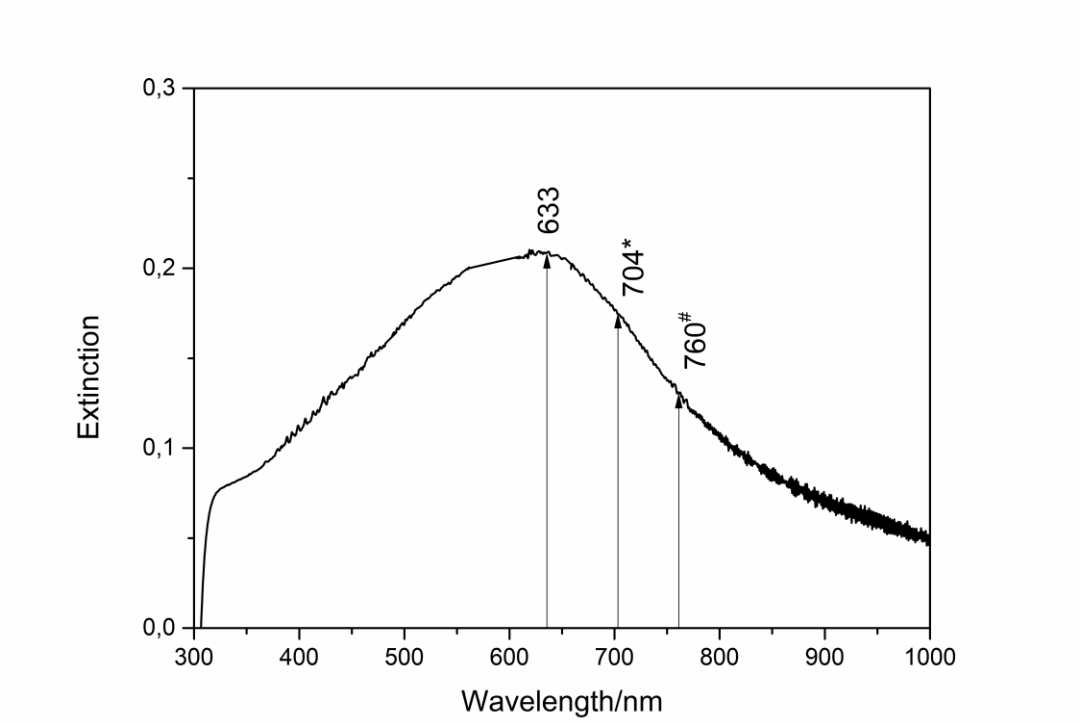


Fig S5: Surface plasmon extinction (SPE) spectrum of glass/SLG/AgNPs-ET hybrid system in relation to (i) the 633 nm excitation wavelength (unlabelled arrow), (ii) the wavelength of photons scattered by the G mode of SLG (1585 $cm^{-1}$) at 633 excitation ($^{*}$-labelled arrow) and (iii) wavelength of photons scattered by the 2D mode of SLG (2648 $cm^{-1}$) at 633 excitation ($^{\#}$-labelled arrow).

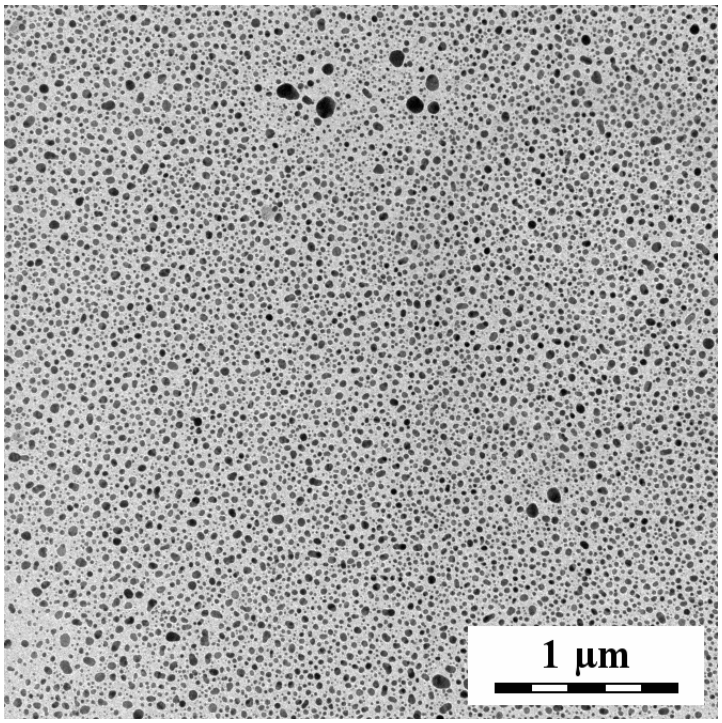


Fig S6: TEM image of the glass/annealed AgNPs array/SLG at low magnification

Table S1: Assignment of Raman spectral bands of ethanethiol and SERS spectral bands of Ag-ET species in Ag NPs-ET array based on refs S1-S4.

| **Average wavenumbers/cm$^{-1}$** | | **Wavenumber range** | **Type of vibration** |
|---|---|---|---|
| Ethanethiol | AgNPs-ET array | | |
| – | 350 | 600 – 700 | -AgS |
| 659 | 632 | 580 – 1000 | C – S stretching |
| – | 964 | 850 – 1000 | -$CH_3$ rocking |
| 1090 | 1045 | 1000 – 1150 | C – C stretching |
| 1272 | 1238 | 1200 – 1400 | $CH_2$ rocking |
| – | 1368 | 1330 – 1385 | -$CH_3$ symmetric deformation (bending) |
| – | 1426 | 1385 – 1445 | $CH_2$ scissoring deformation (bending) |
| 1448 | 1446 | 1400 – 1480 | $CH_3$ antisymmetric deformation (bending) |
| 2570 | – | 2520 – 2600 | -SH |
| 2737 | 2716 | – | Overtone of 1368 cm$^{-1}$ |
| – | 2858 | 2840 – 2870 | Symmetric -$CH_2$ stretching |
| 2870 | – | 2885 – 2865 | Symmetric -$CH_3$ stretching |
| 2927 | 2913 | 2915 – 2940 | Antisymmetric -$CH_2$ stretching |
| 2960 | 2964 | 2950 – 2975 | Antisymmetric -$CH_3$ stretching |

Table S2: The average SERS enhancement factors of the modes of the Ag-ET surface species in glass/ AgNPs-ET reference system

| $\lambda_{exc}$/nm | $E_f$ |
|---|---|
| 445 | $5\times10^5$ |
| 532 | $5\times10^6$ |
| 633 | $2\times10^6$ |
| 780 | $1\times10^6$ |

Table S3: Enhancement factors of ethanethiol bands in glass/SLG/Ag-NPs-ethanethihol film in comparison to glass/Ag-NPs-ethanethiol film

| **$\lambda_{exc}$ = 445 nm** | | | | **$\lambda_{exc}$ = 532 nm** | | | |
|---|---|---|---|---|---|---|---|
| Position | Intensity _ | Intensity _ with | Ef | Position | Intensity _ | Intensity _ with | Ef |
| 633 | 354 | 275 | $\lambda_{exc}$ = 532 | 633 | 11046 | 40230 | 3 |
| 965 | 80 | 42 | 1 | 965 | 1518 | 5490 | 4 |
| 1047 | 34 | 34 | 1 | 1047 | 1813 | 7360 | 3 |
| 1238 | 34 | 37 | 1 | 1238 | 1576 | 6160 | 3 |
| 1426 | 4 | 4 | 1 | 1426 | 489 | 2110 | 4 |
| 1448 | 7 | 14 | 2 | 1448 | 579 | 1930 | 4 |
| 2859 | 187 | 199 | 1 | 2859 | 8173 | 27000 | 4 |
| 2914 | 799 | 864 | 1 | 2914 | 17627 | 97720 | 4 |
| 2957 | 251 | 257 | 1 | 2957 | 8991 | 30500 | 4 |
| **$\lambda_{exc}$ = 633 nm** | | | | **$\lambda_{exc}$ = 780 nm** | | | |
| Position | Intensity | Intensity with | Ef | Position | Intensity | Intensity with | Ef |
| 633 | 12525 | 54052 | 4 | 633 | 17238 | 19001 | 1 |
| 965 | 1219 | 4936 | 4 | 965 | 1233 | 1374 | 1 |

| | | | | | | | |
|---|---|---|---|---|---|---|---|
| 1047 | 2898 | 8630 | 4 | 1047 | 2728 | 3137 | 1 |
| 1238 | 1021 | 3647 | 3 | 1238 | 788 | 864 | 1 |
| 1426 | 462 | 1398 | 3 | 1426 | 948 | 964 | 1 |
| 1448 | 695 | 2360 | 4 | 1448 | 1478 | 1524 | 1 |
| 2859 | 2022 | 8817 | 3 | 2859 | 3958 | 4296 | 1 |
| 2914 | 7050 | 29747 | 4 | 2914 | 7699 | 8661 | 1 |
| 2957 | 1994 | 8528 | 4 | 2957 | 1975 | 2026 | 1 |

**References to Supporting Info:**

[S1] Michl, M.; Vlčková, B.; Mojzeš, P. Ag Colloid-1-alkanethiol Films: Spacer-modified Substrates for SERRS Spectroscopy of Chromophoric Molecules.*Vibrational Spectrosc.* **1999,** *19,* 239-242.

[S2] Bensebaa, F.; Zhou, Y.; Brolo, A.G.; Irish, D.E.; Deslandes, Y.; Kruus, E.; Ellis, T.H. Raman characterization of metal-alkanethiolates, *Spectrochim. Acta A*, **1999**, *55*, 1229-1236.

[S3] Kudelski, A. Characterization of thiolate-based mono- and bilayers by vibrational spectroscopy: A review. *Vibrational Spectrosc* **2005**, *39,* 200-213.

[S4] Socrates, G. *Infrared and Raman Characteristic Group Frequencies*, John Wiley & Sons, LTD, England, 2001.

## 8.3. Publication III: Excitation wavelength dependence of combined surface- and graphene-enhanced Raman scattering experienced by free-base phthalocyanine localized on single layer graphene-covered Ag nanoparticle array

Veronika Sutrová[a,d] Ivana Šloufová[a] Peter Mojzeš[b], Zuzana Melniková[c] Martin Kalbáč[c], Blanka Vlčková[a*]

[a] Charles University, Faculty of Science, Department of Physical and Macromolecular Chemistry, Hlavova 8, Prague 2, 128 40, Czech Republic, vlc@natur.cuni.cz

[b] Charles University, Faculty of Mathematics and Physics, Institute of Physics, Ke Karlovu 5, Prague 2, 121 16, Czech Republic

[c] J. Heyrovsky Institute of Physical Chemistry of the ASCR, v.v.i, Dolejškova 3, 182 21 Prague 8, Czech Republic

[d] Institute of Macromolecular Chemistry AS CR, Heyrovsky Sq. 2, 162 06 Prague 6, Czech Republic

My contribution:

All experimental work: i.e. samples preparations, SERS, GERS and SERS + GERS spectral testing, TEM imaging, except of SLG sample preparation, data evaluation, construction of excitation profiles, calculation of enhancement factors and principal participation in MS preparation.

THE JOURNAL OF PHYSICAL CHEMISTRY C

Article

Cite This: J. Phys. Chem. C 2018, 122, 20850−20860

pubs.acs.org/JPCC

# Excitation Wavelength Dependence of Combined Surface- and Graphene-Enhanced Raman Scattering Experienced by Free-Base Phthalocyanine Localized on Single-Layer Graphene-Covered Ag Nanoparticle Arrays

Veronika Sutrová,[†,∥] Ivana Šloufová,[†] Peter Mojzeš,[‡] Zuzana Melníková,[§] Martin Kalbáč,[§] and Blanka Vlčková*[,†]

[†]Faculty of Science, Department of Physical and Macromolecular Chemistry, Charles University, Hlavova 8, Prague 2 128 40, Czech Republic

[‡]Faculty of Mathematics and Physics, Institute of Physics, Charles University, Ke Karlovu 5, Prague 2 121 16, Czech Republic

[§]J. Heyrovsky Institute of Physical Chemistry of the ASCR, v.v.i, Dolejškova 3, 182 21 Prague 8, Czech Republic

[∥]Institute of Macromolecular Chemistry AS CR, Heyrovsky Sq. 2, 162 06 Prague 6, Czech Republic

Supporting Information

**ABSTRACT:** Hybrid systems constituted by plasmonic nanostructures and single-layer graphene (SLG) as well as their employment as platforms for surface-enhanced Raman scattering (SERS) of the molecular species have recently become a subject of interest. By contrast, only a few studies were targeted specifically on the combination of SERS with graphene-enhanced Raman scattering (GERS) of aromatic molecules. In this paper, we have investigated the mechanisms of combined SERS + GERS by micro-Raman spectral mapping of the hybrid system constituted by annealed Ag nanoparticles (NPs) on the glass substrate overdeposited first by SLG and, subsequently, by a monolayer (ML) of free-base phthalocyanine ($H_2Pc$) molecules, as well as of glass/SLG/$H_2Pc$(ML) and of graphite/$H_2Pc$(ML) reference systems. Raman mapping was performed at multiple excitation wavelengths spanning the 532−830 nm range and was complemented by surface plasmon extinction and transmission electron microscopy images of the Ag NP platform. Observation of SERS + GERS in the aforementioned hybrid system was established by the determination of GERS, SERS, and SERS + GERS enhancement factors. By construction and the mutual comparison of GERS + SERS and GERS excitation profiles of $H_2Pc$ vibrational modes, operation of two mechanisms of GERS additively with the electromagnetic SERS enhancement in SERS + GERS of $H_2Pc$ in the glass/Ag NPs/SLG/$H_2Pc$(ML) hybrid system has been ascertained. Finally, achievement of the same level of the weak negative doping of SLG by Ag NPs in the probed hybrid system and by glass in the reference system has been established as a necessary condition for the proper evaluation of mechanisms of combined SERS and GERS, and evidence for the fulfillment of this condition in the hybrid systems reported here was provided.

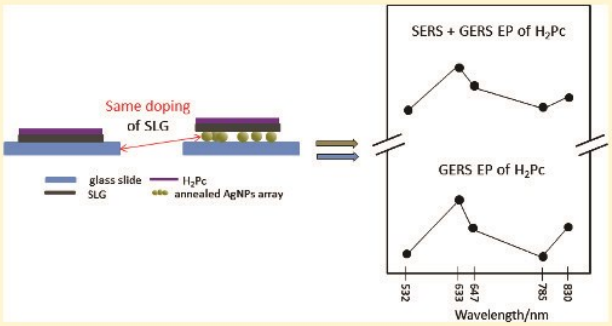


## 1. INTRODUCTION

One of the primary as well as persistent stimuli for design, preparation, and applications of hybrid systems constituted by plasmonic metal nanostructures (NSs) and chromophoric molecules is a possibility to combine the molecular resonance enhancement of Raman scattering of the chromophores with the enhancement of both the incident and the Raman scattered radiation by the resonance excitation of surface plasmons localized on the NSs, followed by the resulting dipole emission, that is, with the electromagnetic (EM) mechanism of surface-enhanced Raman scattering (SERS), giving rise to surface-enhanced resonance Raman scattering (SERRS).[1−7] The design of such hybrid systems has been targeted on the most efficient coupling of the two enhancement mechanisms upon preservation of the native structure of the chromophores, which, in some cases, can be perturbed by the direct chromophore−metal NS interaction.[5,7] It has been demonstrated that separation of the chromophore from the metal NS by insertion of a thin molecular spacer into the hybrid system can lead to the fulfillment of both goals: preservation of the native structure of the chromophore without a loss in the overall SERRS enhancement by a molecular resonance damping.[3−7]

Received: June 29, 2018
Revised: August 15, 2018
Published: August 16, 2018





DOI: 10.1021/acs.jpcc.8b06218
J. Phys. Chem. C 2018, 122, 20850−20860

Single-layer graphene (SLG), an ultrathin (0.3 nm) array of hexagonally packed carbon atoms, was proposed as a prospective alternative to molecular spacers.[8−19] In particular, it has been demonstrated that the EM mechanism enhancement experienced by the second layer of isotopically labeled SLG deposited over the first layer of SLG (mimicking thus localization of planar aromatic molecules on a SLG spacer) is lower only by a factor of 0.7 than that in the first SLG layer.[14] In addition to that, the SLG spacer was shown to induce, under appropriate resonance conditions, an additional enhancement of Raman scattering of planar aromatic molecules, denoted as graphene-enhanced Raman scattering (GERS).[20] Four mechanisms of GERS have been theoretically predicted,[21] and the factors affecting the observation of GERS and the magnitude of GERS enhancement factors (EFs) were reviewed and summarized.[22,23] Recently, we have reported on the evidence for the operation of two mechanisms of GERS in the spectra of the glass/SLG/$H_2Pc$ monolayer (ML) hybrid system ($H_2Pc$ = free-base phthalocyanine) measured at excitations in the 532−830 nm range: (i) broadening of the $Q_y(0-0)$ absorption band of $H_2Pc$ accompanied by a modification of localization of this resonant electronic transition within the $H_2Pc$ molecule induced by the SLG−$H_2Pc$ interaction and (ii) a charge transfer (CT) from the Fermi level of SLG to the lowest unoccupied molecular orbital (LUMO) of $H_2Pc$.[24]

The idea of combining the GERS and the EM SERS enhancement of Raman or RRS of a particular molecular species leads to design, preparation, and probing of several types of hybrid systems constituted by plasmonic NSs, SLG, and planar aromatic molecules.[15−19] In particular, regular Au NSs constituted by Au nanoparticles (NPs) and/or nanohole arrays were employed for a comparison of SERS + GERS spectra of methylene blue (MB) dye obtained from the Au NS/SLG/MB hybrid system with its SERS spectra from the Au NS/MB hybrid at 647 nm excitation.[15] A threefold and/or ninefold additional average GERS enhancement of MB vibrational modes was established in the former system with the nanoholes and the NPs, respectively.[15]

In this work, we employ a strategy alternative to that employed previously in ref 15 and more elaborated owing to the employment of multiple excitation wavelengths covering the 532−830 nm range for comparison of the GERS and the EM SERS + GERS spectra of a particular molecular species. Our first goal has been obtaining the evidence of the GERS enhancement as well as of an additional enhancement of GERS of an aromatic molecule, namely, the free-base phthalocyanine ($H_2Pc$), by the EM mechanism of SERS induced by the localization of a plasmonic enhancer platform underneath the SLG/$H_2Pc$ hybrid system. We demonstrate that both types of enhancement have been encountered for our plasmonic enhancer/SLG/$H_2Pc$ hybrid system at all excitation wavelengths in the 532−830 nm range (vide infra), hence observation of combined SERS + GERS has been unequivocally confirmed, and employment of this term throughout this paper is fully justified. Our second goal, and in fact the most important aim, is to establish whether the mechanisms of GERS and the resonance conditions of their operation remain preserved upon combination of GERS with SERS for this particular aromatic molecule. In addition to that, we attempt to ascertain whether the EM SERS and the GERS enhancements experienced by $H_2Pc$ in the above-mentioned hybrid system are simply additive, that is, whether their combined EFs are simply multiplicative.

For fulfillment of these goals, we have designed, prepared, and probed spectrally the appropriate testing as well as reference hybrid systems. In particular, we considered that the selected plasmonic enhancer in the plasmonic enhancer/SLG/molecule hybrid system has to provide the EM SERS enhancement throughout the overall range of excitation wavelengths, that is, 532−830 nm. The array of Ag NPs annealed upon SLG deposition and recently reported by us[25] was expected and found to be suitable for the fulfillment of this condition. Furthermore, the selection of $H_2Pc$ as the appropriate molecular species was motivated by the results of our aforementioned study of GERS of $H_2Pc$,[24] as well as by the interesting electronic structure of this molecule,[26−32] leading to its prospective applications in molecular photonics and optoelectronics,[30] in gas sensor development,[31] and as a sensitizer in the photodynamic therapy of cancer.[32] In particular, $H_2Pc$ is a chromophoric aromatic molecule of $D_{2h}$ symmetry, showing the $Q_x$ and the $Q_y$ electronic absorption bands in the visible spectral region, namely, in the 620−720 nm range. The actual positions of these bands' maxima were found to be strongly dependent on the molecular environment (e.g., a solvent and/or inert matrix element employed for the isolation matrix preparation).[26−29] As an example, the electronic absorption spectrum of a saturated solution of $H_2Pc$ in toluene is provided in Figure S1 of the Supporting Information. In the case of the SLG/$H_2Pc$ hybrid system, the positions of the $Q_x$ and the $Q_y$ electronic absorption bands depend on the bilayer and/or ML coverage of SLG by $H_2Pc$ molecules, as revealed by GERS excitation profiles (EPs).[24]

In addition to that, on the basis of the previously reported dependence of the GERS mechanism operation on the actual position of the Fermi level of SLG,[33,34] we have speculated that the difference in doping of SLG by Ag in the Ag NPs/SLG/$H_2Pc$ hybrid system and by a substrate in the substrate/SLG/$H_2Pc$ reference hybrid system could actually induce differences in the operation of GERS in each of the two hybrids, which would not be related specifically to the SERS + GERS combination. We address this issue in the first part (section 3.1) of Results and Discussion, and we have used these results for selection of the appropriate glass substrate (denoted as glassI) for assembling the glassI/SLG/$H_2Pc$ reference system newly reported and employed in this paper. Finally, as tools for achievement of our goals, we employ the determination of GERS, SERS, and SERS + GERS EFs of selected Raman active modes of $H_2Pc$ (section 3.2) as well as the construction of SERS + GERS and GERS EPs of Raman spectral bands of $H_2Pc$ from the excitation wavelength-dependent spectra of the tested and the reference hybrid systems, respectively (section 3.3). Finally, we specify the two mechanisms of GERS, which operate in the SERS + GERS of the glassI/Ag NPs/SLG/$H_2Pc$ hybrid system and their resonance conditions (section 3.4).

## 2. EXPERIMENTAL SECTION

**2.1. Materials.** 29,31*H*-Phthalocyanine, $H_2Pc$ (*β*-form, 98%), 1-ethanethiol (97%), and cellulose nitrate were purchased from Sigma-Aldrich. Analytical grade $AgNO_3$ and sodium borohydride as well as spectral grade dichloromethane and toluene (UVASOL) were purchased from Merck. Distilled deionized water was also used as a solvent where appropriate. Special glass slides different from those employed in ref 24, namely, the microscope glass cover slides (Glaswarenfabrik Karl Hecht GmbH & Co KG), were employed as substrates, and they are denoted as glassI throughout this paper.



DOI: 10.1021/acs.jpcc.8b06218
J. Phys. Chem. C 2018, 122, 20850−20860

**2.2. Preparation Procedures.** *2.2.1. Ag NP Hydrosol.* Ag NP hydrosol was prepared by reduction of $AgNO_3$ by sodium borohydride according to the previously published procedure.[35]

*2.2.2. GlassI/AgNPs/SLG and GlassI/SLG Systems.* First, the arrays of Ag NPs modified by chemisorbed ethanethiol (Ag-ET NPs) were prepared according to the procedure reported by Michl et al.[35] Briefly, a two-phase system constituted by 2 mL of Ag NP hydrosol and 2 mL of a $1 \times 10^{-3}$ M solution of ethanethiol in dichloromethane was vigorously shaken until a lustrous nanoparticulate film appeared at the interface between the aqueous and the organic phase. The interfacial film was then transferred by a pipette into the central part of a special glass slide for optical microscopy and was let to dry in air. Both the central part of the slide containing the array of the Ag-ET NPs and the exteriors of the Ag NPs-free glass slide were then over-deposited by SLG prepared by using the chemical vapor deposition procedure,[36] in particular, the nitrocellulose (NC) method[37] of the as-prepared SLG transfer. The majority of the NC layer from the resulting glassI/Ag NPs-ET/SLG/NC hybrid was removed by methanol drops at room temperature. The sample was then annealed at 160 °C for 30 min in order to remove the NC residuals from the SLG surface. SERS spectral evidence of removal of not only the NC residuals but also of the adsorbed ET from the Ag NP surfaces has been provided, and morphological characterization of the sample showed annealing of Ag NPs.[25]

*2.2.3. GlassI/Ag NPs/SLG/$H_2$Pc(ML) and GlassI/SLG/$H_2$Pc-(ML) Hybrid Systems.* The hybrid systems were prepared by adapting the procedure employed for the preparation of the glass/SLG/$H_2$Pc(ML-*X*) systems.[24] The adapted procedure is graphically depicted in Figure S2 in the Supporting Information. Briefly, the parent glassI/Ag NPs/SLG hybrid system (in which the areas not covered by Ag NPs were distinguished by optical microscopy) was overlaid by a thin layer of a saturated ($<5 \times 10^{-5}$ M) solution of $H_2$Pc in toluene (which was filtered by the 1 $\mu$m filter prior to use), and it was kept in the toluene-saturated atmosphere in a sealed weighing bottle for 24 h to accomplish the adsorption of $H_2$Pc onto the SLG surface. The sample was then extracted from the weighing bottle, and the solution layer was removed by soaking into a slip of filter paper. In the second step, the excess $H_2$Pc molecules were removed by overlaying the as-prepared sample by a thin layer of pure toluene and by keeping it in the same setup as described above for 10 min. The solvent layer was then removed by the filter paper, and the overall second step procedure was repeated 10 times.

*2.2.4. Graphite/$H_2$Pc(ML) Reference System.* The graphite/$H_2$Pc(ML) reference system was prepared by the procedure analogous to that described above for the hybrid systems. The graphite substrate preparation and the specifically developed strategy of Raman spectral mapping of the graphite/$H_2$Pc-(ML) system were adopted from ref 24.

**2.3. Instrumentation.** Raman (RRS, GERS, and GERS + SERS) spectra as well as optical images of all hybrid samples and reference hybrid samples were obtained using a WITec alpha300 Raman micro-spectrometer. An objective (Zeiss) with 100× magnification was used for all the above-mentioned Raman spectral measurements performed at 532, 633, 647, 785, and 830 nm excitations. For measurements on WITec alpha300, two spectrographs equipped with charge-coupled device detectors optimized for the blue-green and the red-NIR (near-infrared) spectral ranges have been used, the first one for the collection of spectra at 532 nm excitation and the second one for the other four excitation wavelengths, that is, 633, 647, 785, and 830 nm. The following lasers, excitation wavelengths, and laser power values (at the sample) were employed: SHG Nd:$YVO_4$, 532 nm (2.3 mW); He−Ne, 633 nm (2.5 mW); $Kr^+$ ion, 647 nm (5.0 mW), diode, 785 nm (50.0 mW), diode, 830 nm (11.0 mW). Raman spectral mapping was performed by using the 25 $\mu$m × 25 $\mu$m area scans with 50 × 50 points. Two types of the areas were selected for the Raman spectral mapping of the combined glassI/AgNPs/SLG/$H_2$Pc(ML) and glassI/SLG/$H_2$Pc(ML) samples: (i) the areas of the sample showing the presence of both SLG and Ag NPs on the optical images corresponding to the glassI/AgNPs/SLG/$H_2$Pc(ML) hybrids probed for GERS + SERS and (ii) the areas with SLG, but without Ag NPs, representing the glassI/SLG/$H_2$Pc(ML) reference system (probed for GERS). The graphite/$H_2$Pc(ML) hybrid was employed as the second reference system for Raman and resonance Raman spectral probing of a ML of $H_2$Pc. Surface plasmon extinction (SPE) (UV/vis) spectra were measured on a Shimadzu UV-2401 spectrometer. Transmission electron microscopy (TEM) images were obtained with a Tecnai G2 (FEI) transmission electron microscope with an acceleration voltage of 120 keV.

**2.4. GERS, SERS, and SERS + GERS EFs.** GERS EFs of selected $H_2$Pc modes were determined as the intensity ratios of the corresponding Raman bands in the average spectra of the glassI/SLG/$H_2$Pc(ML) area of the hybrid sample and in those of the graphite/$H_2$Pc(ML) reference sample. SERS EFs of GERS of $H_2$Pc were ascertained as the intensity ratios of the corresponding Raman bands in the average spectra of the glassI/AgNPs/SLG/$H_2$Pc(ML) area of the hybrid sample and in those of the glassI/SLG/$H_2$Pc(ML) area of the reference sample. SERS + GERS EFs represent the intensity ratios of the corresponding Raman bands in the average spectra of the glassI/AgNPs/SLG/$H_2$Pc(ML) area of the hybrid sample and in those of the graphite/$H_2$Pc(ML) reference sample. While the SERS enhancement of GERS of $H_2$Pc has been evaluated at all five excitation wavelengths, the GERS and the SERS + GERS EFs could be exactly determined only at 633 and 647 nm excitations, at which the resonance Raman spectra of $H_2$Pc have been obtained from the graphite/$H_2$Pc(ML) reference sample. All the intensity ratios were determined in terms of the integrated band areas, and all spectra were baseline-corrected. The procedure of determination of the standard deviations of the EFs is described in Text S1 in the Supporting Information.

**2.5. SERS + GERS and GERS EPs.** EPs of the $H_2$Pc bands in the SERS + GERS spectra obtained from the glassI/AgNPs/SLG/$H_2$Pc hybrid samples at 532, 633, 647, 785, and 830 nm excitations as well as GERS EPs of $H_2$Pc bands in the glassI/SLG/$H_2$Pc(ML) reference system were constructed as plots of their normalized band intensities as a function of the excitation wavelength. Raman spectra of polystyrene acquired under the very same experimental conditions as those of the samples were employed as the external intensity standards. At each excitation wavelength, the intensities of the $H_2$Pc Raman bands (in terms of the integrated band areas) in the spectrum of the hybrid and/or the reference sample were normalized to the intensity of the 1004 $cm^{-1}$ Raman band of polystyrene. The procedure of determination of the standard deviations of the normalized band intensities is described in Text S1 in the Supporting Information. The same procedures of the wave-



DOI: 10.1021/acs.jpcc.8b06218
J. Phys. Chem. C 2018, 122, 20850−20860

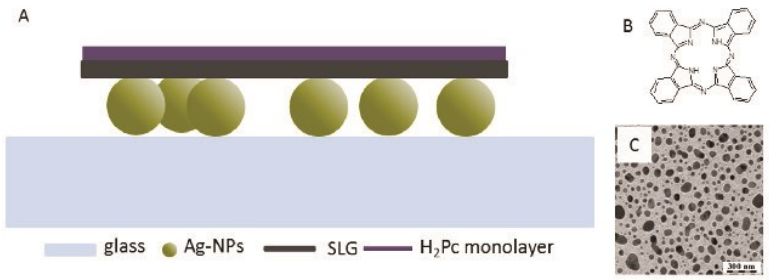


**Figure 1.** (A) Schematic depiction of the glassI/AgNPs/SLG/$H_2Pc$(ML) hybrid system used for micro-Raman measurements of SERS + GERS of the $H_2Pc$ (B) molecular structure of $H_2Pc$; (C) TEM image of the array of annealed Ag NPs employed as the plasmonic enhancer in the glassI/Ag NPs/SLG/$H_2Pc$ hybrid system.

number and intensity calibration of the Raman microspectrometer as those described in ref 24 have been employed.

## 3. RESULTS AND DISCUSSION

**3.1. Characterization and Spectral Probing of the Glass(I)/AgNPs/SLG/$H_2Pc$(ML) Hybrid System and of the Reference System.** The glassI/AgNPs/SLG/$H_2Pc$(ML) hybrid system used for SERS + GERS micro-Raman spectral probing is schematically depicted in Figure 1A. The molecular structure of $H_2Pc$ is shown in Figure 1B, and the TEM image of the annealed Ag NPs employed as the plasmonic enhancer in the hybrid system (Figure 1A) is presented in Figure 1C. A closer inspection of the TEM image in Figure 1C reveals the presence of monomers as well as dimers and trimers of annealed Ag NPs. The rather broad range of Ag NP shapes and sizes is expected (in accord with ref 25) to cause extension of the SPE of this plasmonic enhancer over the visible and the onset of the NIR spectral region.

The SPE spectra of the glassI/AgNPs/SLG system before and after deposition of $H_2Pc$ are compared in Figure 2. The

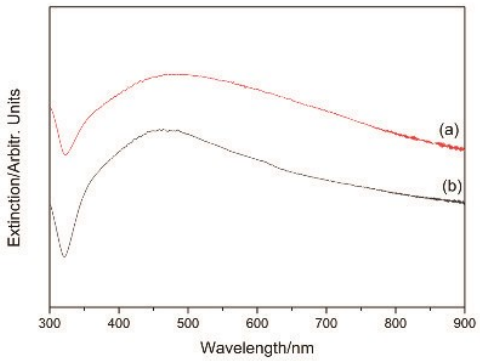


**Figure 2.** SPE spectra of the glass/Ag NPs/SLG hybrid system: before (a) and after (b) deposition of the $H_2Pc$ ML.

major feature, that is, the extension of SPE over the visible and NIR spectral region, remains preserved upon the $H_2Pc$ deposition, and the differences between the two SPE curves (Figure 2, spectra a and b) are evaluated as minor.

An optical image showing (i) the glassI/AgNPs/SLG/$H_2Pc$(ML) and (ii) the glassI/SLG/$H_2Pc$(ML) parts of the same sample and the boundary between these two parts is presented in Figure 3A. The SERS + GERS and the GERS parts of the spectral map of the 683 $cm^{-1}$ mode of $H_2Pc$ measured at 785 nm excitation and spanning the same sample area as that in Figure 3A are shown in Figure 3B. The spectral

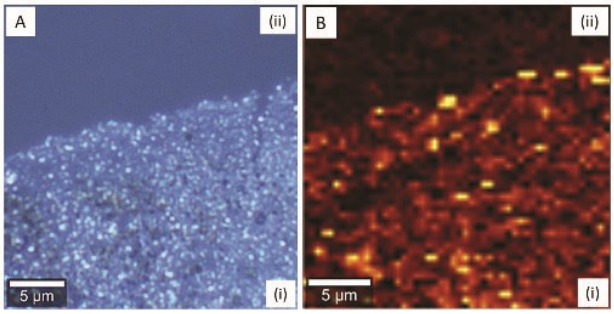


**Figure 3.** (A) Optical image of the hybrid sample employed for GERS and SERS + GERS spectral measurements (mapping) of $H_2Pc$ with the clearly distinguished boundary between the (i) glass/AgNPs/SLG/$H_2Pc$ part of the sample used for SERS + GERS measurements and (ii) glass/SLG/$H_2Pc$ part of the sample utilized for GERS measurements. (B) Spectral map of the 683 $cm^{-1}$ band of $H_2Pc$ acquired at 785 nm excitation from the same area of the sample as the optical image (A). The spectral map (B) shows the markedly higher intensity of the Raman signal from the (i) glass/AgNPs/SLG/$H_2Pc$ part of the sample (SERS + GERS) than from the (ii) glass/SLG/$H_2Pc$ part of the sample (GERS).

map (Figure 3B) shows the markedly higher intensity of the Raman signal of the 683 $cm^{-1}$ mode of $H_2Pc$ from the (i) glassI/AgNPs/SLG/$H_2Pc$(ML) part of the sample than from the (ii) glassI/SLG/$H_2Pc$ part of the sample, which, in turn, provides a qualitative evidence of observation of SERS + GERS of $H_2Pc$ in the former case and of GERS of $H_2Pc$ in the latter one.

For the actual spectral mapping by which the average spectra were acquired at all five excitation wavelengths, the maps spanning entirely the glassI/AgNPs/SLG/$H_2Pc$(ML) area of the sample (fully covered by a single layer of Ag NPs) were used for the SERS + GERS measurements, and those spanning the glassI/SLG/$H_2Pc$(ML) area were employed for GERS. As an example, an optical image of the glassI/AgNPs/SLG/$H_2Pc$(ML) area of the sample and the SERS spectral maps of the G mode (1590 $cm^{-1}$) and 2D (2595 $cm^{-1}$) mode of SLG as well as the SERS + GERS spectral maps of the 683 and 1540 $cm^{-1}$ modes of $H_2Pc$ acquired from this area at 785 nm excitation are shown in Figure S3A–E, respectively, in the Supporting Information.

SERS spectra of SLG and SERS + GERS spectra of $H_2Pc$ obtained from the glassI/Ag NPs/SLG/$H_2Pc$(ML) hybrid system at 532, 633, 647, 785, and 830 nm excitations are shown in Figure 4A (full range spectra) and Figure 4B (details in the 400–1800 $cm^{-1}$ range). The average wavenumber of the G mode band in the spectra of the glassI/AgNPs/SLG/$H_2Pc$ is



DOI: 10.1021/acs.jpcc.8b06218
J. Phys. Chem. C 2018, 122, 20850–20860

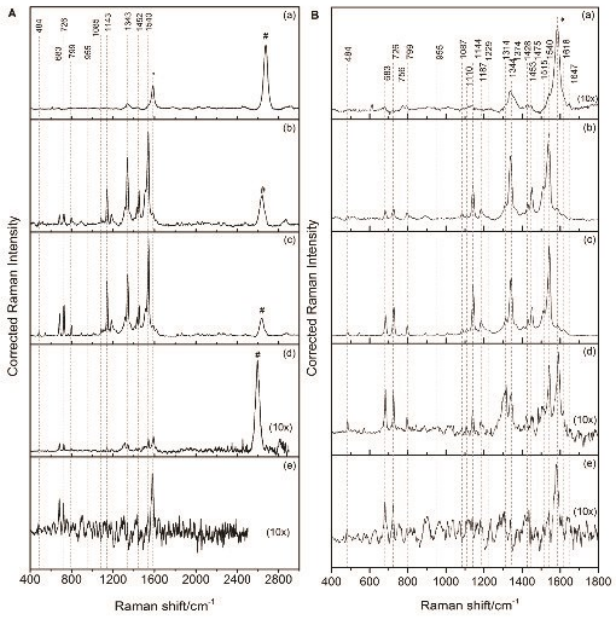


**Figure 4.** (A) Full range (400−3000 $cm^{-1}$) and (B) detailed (400−1800 $cm^{-1}$) SERS + GERS spectra of $H_2Pc$ measured from the glassI/AgNPs/SLG/$H_2Pc$(ML) hybrid system at (a) 532, (b) 633, (c) 647, (d) 785, and (e) 830 nm excitations. The SERS spectral band of the G mode is marked by *, and the SERS spectral bands of the dispersive 2D mode are marked by #.

1590 $cm^{-1}$, that is, exactly the same as reported for the glass/Ag NPs/SLG system.[25] This result indicates that deposition of a ML of $H_2Pc$ molecules onto the glassI/Ag NPs/SLG platform has not caused any additional doping of SLG by $H_2Pc$ molecules. The 1590 $cm^{-1}$ position of the G band is 5 $cm^{-1}$ higher than in the pristine SLG[39,40] and, in accord with refs 25 and 38, indicates a weak n-doping of SLG by Ag.

Furthermore, the G band in the Raman spectra of the glassI/SLG/$H_2Pc$(ML) reference system is located at 1592 $cm^{-1}$, and its position is thus comparable (within the experimental error) with that in the glassI/AgNPs/SLG/$H_2Pc$(ML) system. This comparison indicates that the magnitude of the weak n-doping of SLG by glass in the former system is analogous to the weak n-doping of SLG by Ag in the latter system. Consequently, the positions of the Fermi level of SLG are nearly identical in both systems, and they were estimated to be ca. −4.4 eV (i.e., upshifted by ca. 0.2 eV from the Fermi level of pristine SLG at −4.6 eV[20]) on the basis of the graph in Figure 8.5 in ref 39. Therefore, the fundamental conditions of operation of the mechanisms of GERS are virtually identical in the glassI/AgNPs/SLG/$H_2Pc$(ML) hybrid system employed for SERS + GERS spectral probing and in the glassI/SLG/$H_2Pc$(ML) system used as the reference system for GERS in this paper.

Furthermore, we have noticed that the position of the G band of SLG in our glassI/SLG/$H_2Pc$(ML) reference system (1592 $cm^{-1}$) is lower by 7 $cm^{-1}$ than that reported for the glass/SLG/$H_2Pc$(ML) system in ref 24 (1599 $cm^{-1}$). This comparison indicates that the n-doping by glass (in particular, by surface groups and/or water entrapped between glass and SLG) is markedly weaker than that by the glass slides used in ref 24. Such differences in n-doping by glass have been reported previously, and they have been attributed to a different content of Na in the particular sample of glass.[41] The comparison of the positions of the Fermi level of SLG (i) at −4.4. eV in the glassI/SLG/$H_2Pc$(ML) reference system and (ii) at −4.3 eV in the GERS sample in ref 24 (further referred to as the glassII/SLG/$H_2Pc$(ML) system in this paper) demonstrates the importance of doping of SLG by the substrates. On the other hand, once this important factor is properly evaluated, it can be employed for adjusting the Fermi level position of SLG.

The average wavenumbers of the $H_2Pc$ bands in SERS + GERS spectra of the glassI/AgNPs/SLG/$H_2Pc$(ML) hybrid system as well as in the GERS spectra of the glassI/SLG/$H_2Pc$(ML) reference system, together with their assignment based on refs 27 and 42, are listed in Table 1. The wavenumbers of SERS + GERS and the GERS spectral bands show a reasonably good mutual agreement (within 3 $cm^{-1}$).

**Table 1. Average Wavenumbers of the $H_2Pc$ Bands in SERS + GERS Spectra of the GlassI/AgNPs/SLG/$H_2Pc$(ML) Hybrid System and in GERS Spectra of the GlassI/SLG/$H_2Pc$(ML) Reference System Complemented by Their Assignment Based on Refs 24, 27, 42**

| GERS of $H_2Pc$ | GERS + SERS of $H_2Pc$ | mode symmetry | mode description |
|---|---|---|---|
| 486 | 484 | $B_{1g}$ | benzene ring rocking & central ring deformation |
| 683 | 683 | $A_g$ | bridging C−N−C sym. def. and benzene ring deformation |
| 728 | 726 | $A_g$ | pyrrole deformation and C−N−C rocking |
| 800 | 799 | $A_g$ | pyrrole and benzene ring C−C str. |
| 952 | 955 | IR act | C−H out-of-plane deformation |
| 1086 | 1085 | $B_{1g}$ | N−H in-plane deformation |
| 1143 | 1143 | $A_g$ | benzene ring C−C str. and C−H deformation |
| 1343 | 1343 | $A_g$ | benzene ring C−C str. and pyrrole C−C stretch |
| 1453 | 1452 | $A_g$ | C−H def. |
| 1543 | 1540 | $A_g$ | bridging $C_\alpha$−$N_m$−$C_\alpha$ asym. str. and $C_\alpha$−$N_H$−$C_\alpha$ sym. str. |

**3.2. GERS, SERS, and SERS + GERS EFs of Selected Spectral Bands of $H_2Pc$ Localized in the GlassI/SLG/$H_2Pc$ Reference Hybrid System and in the GlassI/AgNPs/SLG/$H_2Pc$ Hybrid System, Respectively.** Raman spectra of $H_2Pc$ were obtained from the glassI/AgNPs/SLG/$H_2Pc$(ML) probed hybrid system (Figure 4) as well as from the glassI/SLG/$H_2Pc$(ML) reference system at all five excitation wavelengths. By contrast, the graphite/$H_2Pc$ second reference system yielded Raman spectra of $H_2Pc$ only upon resonance with the $Q_y(0-0)$ electronic transition, that is, at 633 and 647 nm excitations, in accord with ref 24. Therefore, the EFs evaluating the SERS enhancement of GERS of $H_2Pc$ in the probed hybrid system (denoted as SERS + GERS/GERS EFs and abbreviated as SERS EFs) could be determined at all five excitation wavelengths (details in section 2.4 of the Experimental Section), and their average values as a function of excitation wavelength are listed in Table 2. The average EFs are of comparable values in the 633−830 nm range. The slightly larger EFs at 633 and 830 nm are attributed to plasmon resonances with the more abundant large spherical or slightly ellipsoidal Ag NPs and with less abundant dimers or trimers of Ag NPs upon generation of strong optical fields, respectively.

On the other hand, GERS EFs (details in section 2.4) could be numerically evaluated only at 633 and 647 nm excitations



DOI: 10.1021/acs.jpcc.8b06218
J. Phys. Chem. C 2018, 122, 20850−20860

**Table 2. Average SERS EFs of the Vibrational Modes of $H_2Pc$ at Five Excitation Wavelengths in the 532−830 nm Range[a]**

| wavelength | 532 | 633 | 647 | 785 | 830 |
|---|---|---|---|---|---|
| EFs | 5 ± 2 | 14 ± 5 | 9 ± 3 | 10 ± 3 | 13 ± 4 |

[a]The EFs were determined as the ratios of the normalized intensities of the $H_2Pc$ spectral bands in SERS + GERS spectra of the glassI/AgNPs/SLG/$H_2Pc$(ML) hybrid system and in GERS spectra of the glassI/SLG/$H_2Pc$(ML) reference system.

(Table 3); however, the aforementioned observation of the GERS signal of $H_2Pc$ from the glassI/SLG/$H_2Pc$(ML) system

**Table 3. Average Values of GERS EFs (GERS vs RRS Normalized Band Intensity Ratios), SERS EFs (SERS + GERS vs GERS Normalized Intensity Ratios), SERS + GERS EFs (SERS + GERS vs RRS Normalized Intensity Ratios) and Multiplications of SERS EFs with GERS EFs of $H_2Pc$ Vibrational Modes at 633 and 647 nm Excitations**

| | 633 nm | 647 nm |
|---|---|---|
| average GERS EFs | 3 ± 1 | 4 ± 1 |
| average SERS EFs | 14 ± 5 | 9 ± 3 |
| average SERS + GERS EFs | 43 ± 7 | 41 ± 7 |
| average SERS + GERS EFs (determined as SERS × GERS EFs) | 42 ± 9 | 36 ± 7 |

at all five excitation wavelengths, in contrast to the absence of any Raman signal of $H_2Pc$ from the graphite/$H_2Pc$(ML) second reference system at 532, 785, and 830 nm, indicates that the GERS enhancement of $H_2Pc$ modes occurs at these wavelengths as well.

These results confirm the observation of combined SERS + GERS of $H_2Pc$ from the glassI/AgNPs/SLG/$H_2Pc$(ML) hybrid system and of GERS of $H_2Pc$ from the glassI/SLG/$H_2Pc$(ML) reference system. Furthermore, the average SERS + GERS EFs at 633 and 647 nm excitations (Table 3) were determined in a dual way: (i) directly from the SERS + GERS spectra (shown in Figure 4) in relation to the RRS spectra of $H_2Pc$ localized in the graphite/$H_2Pc$(ML) system (details for individual bands in Table S1 in the Supporting Information) and (ii) as products of the SERS and GERS EFs listed in the first and second row of Table 3. Their values (Table 3) are nearly identical at 633 nm excitation and mutually very close (within the experimental error) at 647 nm excitation. This comparison indicates that the SERS and GERS EFs are simply multiplicative, that is, that the two enhancement mechanisms are combined without any additional enhancement or damping. It should be noted that in our hybrid system, we can observe only the EM SERS enhancement because $H_2Pc$ is isolated from the Ag NP surface by the SLG spacer. The ordering of the components in our hybrid system is thus different from the case of CuPc molecules sandwiched between a flat Au(111) surface and SLG, for which a coupling of GERS with the chemical mechanism of SERS, namely, a CT from the Fermi level of Au to the LUMO of CuPc, has been reported.[43]

**3.3. SERS + GERS EPs of Selected Spectral Bands of $H_2Pc$ Localized in the GlassI/AgNPs/SLG/$H_2Pc$(ML) Hybrid System.** EPs of the selected spectral bands of $H_2Pc$ were constructed from the SERS + GERS spectra of the glassI/Ag NPs/SLG/$H_2Pc$(ML) hybrid system measured at 532, 633, 647, 785, and 830 nm excitations by the procedure described in section 2.5. The complete EPs are presented in Figure 5A, their details in the 750−850 nm region are depicted in Figure 5B, and the selected profiles with error bars are shown in Figure 6A. For the sake of comparison, the GERS EPs of the selected spectral bands of $H_2Pc$ determined from the GERS spectra of the glassI/SLG/$H_2Pc$(ML) reference system measured at the same five excitation wavelengths as the SERS + GERS spectra are presented in Figure 6B. Both the SERS + GERS EPs (Figures 5A and 6A) and the GERS EPs (Figure 6B) of all $H_2Pc$ spectral bands maximize at 633 nm excitation. Furthermore, the average value of the normalized intensities of the $H_2Pc$ spectral bands (depicted in Figure 5), and its average standard deviation at 633 nm excitation (EPs maximum) have been determined by the procedure described in Text S1 in the Supporting Information, yielding a value of 4 ± 0.3.

For a mutual comparison of SERS + GERS EPs and GERS EPs in Figure 6, the profiles of the 683,1143, and 1540 $cm^{-1}$ totally symmetric ($A_g$) vibrational modes of $H_2Pc$ (assigned in Table 1) have been selected from the complete set of SERS + GERS EPs in Figure 5A and complemented by error bars depicting the experimental error of the spectral mapping (Figure 6A). The GERS EPs of the same bands have been constructed from the GERS spectra of the glassI/SLG/$H_2Pc$(ML) reference system measured at the same five excitations and complemented by error bars (Figure 6B). Both the SERS + GERS EPs (Figure 6A) and the GERS EPs (Figure 6B) show a common maximum at 633 nm excitation

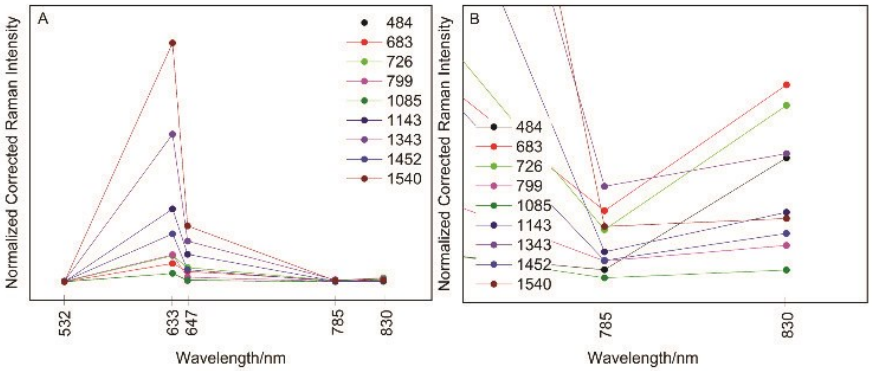


**Figure 5.** SERS + GERS EPs of spectral bands of $H_2Pc$ localized in the glassI/AgNPs/SLG/$H_2Pc$(ML) hybrid system: (A) complete EPs in the 532−830 nm range of excitation wavelengths and (B) details of the EPs in the 750−830 nm range.



DOI: 10.1021/acs.jpcc.8b06218
J. Phys. Chem. C 2018, 122, 20850−20860

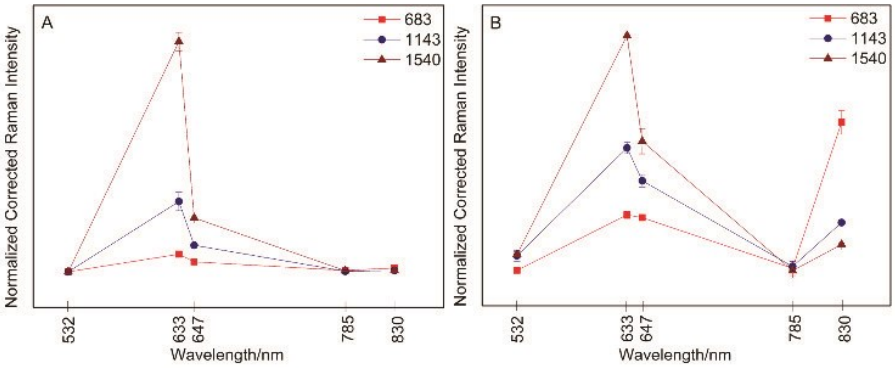


**Figure 6.** (A) SERS + GERS EPs of selected spectral bands of $H_2Pc$ measured from the glassI/AgNPs/SLG/$H_2Pc$(ML) hybrid system. (B) GERS EPs of the same bands of $H_2Pc$ as in (A) measured from the glassI/SLG/$H_2Pc$(ML) reference system. Both EPs are depicted with error bars.

and a normalized band intensity increase at 830 nm. This comparison demonstrates that the shapes of the GERS EPs of all the three spectral bands, namely, the two distinct resonance features at 633 and 830 nm, remain preserved upon the combination of SERS with GERS of $H_2Pc$.

The other common features of the selected SERS + GERS EPs in Figure 6A and the GERS EPs in Figure 6B are the sequences of the normalized band intensities of the three selected $H_2Pc$ spectral bands at 633, 647, and 830 nm excitations, in particular, the 683 > 1143 > 1540 $cm^{-1}$ sequences determined at both 633 and 647 nm excitations and the reverse 683 > 1143 > 1540 $cm^{-1}$ sequence at 830 nm excitation. This result indicates that (i) each of the two resonance features (i.e., the maximum at 633 nm and the normalized intensity increase at 830 nm) observed in both the GERS EPs (Figure 6B) and SERS + GERS EPs (Figure 6A) belongs to a different resonance electronic transition, each showing a different localization within the $H_2Pc$ molecule, and (ii) for both these resonant electronic transitions, their localization within the $H_2Pc$ molecules remains unchanged upon the combination of SERS with GERS. In summation, the only observed difference between the SERS + GERS and GERS EPs (Figure 6A,B) is the magnitude of the normalized intensity increase at 830 nm excitation, which is markedly higher in the latter case than in the former one. Such "smearing" of the SERS + GERS EP shape emerges as the only consequence of the SERS enhancement contribution to the combined SERS + GERS profiles, and it can be tentatively explained by the similar values of the EM SERS mechanism enhancement of GERS of $H_2Pc$ at 785 and 830 nm excitation (Table 2). At this point, we find appropriate to emphasize that both in the glassI/AgNPs/SLG/$H_2Pc$(ML) hybrid system used for SERS + GERS spectral measurements and construction of SERS + GERS EPs and in the glassI/SLG/$H_2Pc$(ML) reference system employed for GERS and GERS EPs construction, nearly the same level of doping of SLG by Ag NPs in the former system and by the glassI substrate in the latter one was established (section 3.1). There were thus no differences in the position of the Fermi level of SLG in the probed system and in the reference hybrid system, which could possibly hamper the comparison of SERS + GERS and GERS EPs.

**3.4. Specification of the Mechanisms of GERS and of Their Operation in GERS and SERS + GERS of $H_2Pc$ in the 532−830 nm Range.** In this section, we focus on the assignment of two resonance electronic transitions modulating the shapes of both SERS + GERS and GERS EPs presented in section 3.3, determination of their localization within the $H_2Pc$ molecule (on the basis of the sequences of the normalized band intensities of the resonantly enhanced totally symmetric $A_g$ and their localization within the $H_2Pc$ molecule mode by using the approach first reported in ref 44 for RRS) and on specification of the mechanisms of GERS operating in both SERS + GERS and GERS of $H_2Pc$ in the 532−830 nm range.

First, the electronic absorption band giving rise to the 633 nm maximum on both SERS + GERS and GERS EPs of $H_2Pc$ (Figures 5A and 6A,B) is attributed to the $Q_y(0-0)$ electronic transition of $H_2Pc$ on the basis of the previously reported electronic absorption spectra and EPs.[24,26−30] Furthermore, the same sequences of the normalized band intensities in the SERS + GERS and GERS EPs of the three selected $H_2Pc$ bands (Figure 6 and section 3.3) encountered at the 633 and 647 nm excitations indicate that the 647 nm excitation also falls into the contour of the $Q_y(0-0)$ electronic absorption band. The markedly larger normalized band intensities at 633 than at 647 nm excitation (Figures 5A and 6), together with the ∼10 nm value of the $Q_y(0-0)$ band half-width determined by detailed SERRS EPs of this electronic transition in Ag NSs/$H_2Pc$ hybrid system[26] (as the largest reported half-width of this electronic transition), indicate that the maximum of this electronic transition in both the glassI/AgNPs/SLG/$H_2Pc$-(ML) and the glassI/SLG/$H_2Pc$(ML) systems is located between the 633 and 647 nm excitations (mutually distanced by 14 nm), but closer to the 633 nm excitation, that is, within ca. 633−639 nm interval. In contrast to the normalized band intensities in GERS of $H_2Pc$, which maximize at 633 nm excitation (Figure 6A), the GERS EFs (Table 3) were determined to be larger at 647 nm (average EF = 4) than at 633 nm excitation (average EF = 3). This observation is consistent with broadening and a small blue shift (vide infra) of this electronic absorption band in both the glassI/AgNPs/SLG/$H_2Pc$(ML) hybrid system and the glassI/SLG/$H_2Pc$-(ML) reference system, in comparison to the graphite/$H_2Pc$(ML) second reference system. These changes in the position and half-width of the $Q_y(0-0)$ electronic absorption band are attributed to the SLG−$H_2Pc$(ML) interaction, and they are responsible for the GERS enhancement experienced by $H_2Pc$ spectral modes in both the probed hybrid system and the reference system at 633 and 647 nm excitations, respectively (Table 3).

Furthermore, the 1540 > 1143 > 683 $cm^{-1}$ sequence of the normalized band intensities established in both SERS + GERS



DOI: 10.1021/acs.jpcc.8b06218
J. Phys. Chem. C 2018, 122, 20850−20860

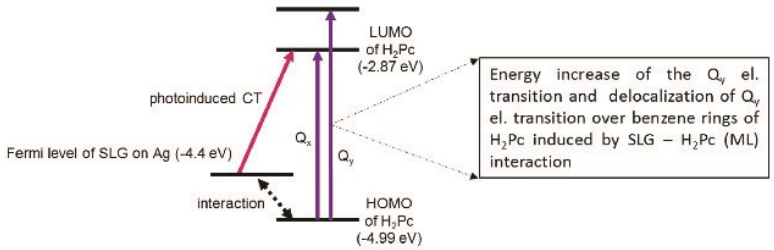


**Figure 7.** Schematic depiction of two mechanisms of GERS identified in SERS + GERS of $H_2Pc$ measured from the glassI/AgNPs/SLG/$H_2Pc$(ML) hybrid system as well as in GERS of $H_2Pc$ obtained from the glassI/SLG/$H_2Pc$(ML) system at excitations in the 532−830 nm range. The energy of the Fermi level of SLG was determined to be ca. −4.4 eV in both systems.

and GERS of $H_2Pc$ at 633 and 647 nm together with the assignment of the $H_2Pc$ vibrational modes in Table 1 and the detailed analysis of the complete GERS + SERS EPs (presented as Text S2 in the Supporting Information) indicate a preferential enhancement of the higher wavenumber modes, mainly the C−C stretching vibrations localized on benzene and pyrrole rings, the combined C−N−C stretch known as the cavity size marker,[45] and the C−H deformation modes localized on the outer benzene rings. By contrast, this electronic transition has been reported to be localized preferentially on the tetrapyrrole macrocycle for a free $H_2Pc$ molecule owing to the preferential enhancement of macrocycle breathing and deformation modes.[46] The change in localization of the $Q_y(0-0)$ resonant electronic transition within the $H_2Pc$ molecule represents another manifestation of GERS in SERS + GERS of $H_2Pc$ in the glassI/Ag NPs/SLG/$H_2Pc$(ML) system as well as in GERS of $H_2Pc$ in the glassI/SLG/$H_2Pc$(ML) reference system at 633 and 647 nm excitations, and it is also attributed to the SLG−$H_2Pc$(ML) interaction (Figure 7).

The second resonance which manifests itself by the relative intensity increase at 830 nm excitation has no analogue in the previously reported electronic absorption spectra of $H_2Pc$ in solutions and matrices.[26−30] On the other hand, the energy difference between the Fermi level of SLG (positioned at ca. −4.4 eV) and LUMO of $H_2Pc$ (at −2.87 eV[29]) is 1.53 eV, that is, 810 nm. This calculated value of the maximum of a CT from the Fermi level of SLG to the LUMO of $H_2Pc$ at 810 nm suggests that the 830 nm excitation is in resonance with this CT electronic transition (Figure 7). Such a CT transition has been theoretically predicted as one of the four possible mechanisms of GERS.[21]

Finally, to evaluate the importance of the same doping, that is, of the same position of Fermi level of SLG in the hybrid system probed for SERS + GERS and in the reference system providing GERS of $H_2Pc$, we have investigated the effect of the ca. 0.1 eV difference in the position of Fermi level of SLG on the operation and manifestations of the mechanisms of GERS of $H_2Pc$ by comparing GERS EFs and EPs of $H_2Pc$ vibrational modes in two glass/SLG/$H_2Pc$(ML) hybrid systems: the glassI/SLG/$H_2Pc$(ML) system reported in this work with the Fermi level of SLG at ca. −4.4. eV (further denoted as system I) and the glassII/SLG/$H_2Pc$(ML-*X*) system reported previously in ref 24 in which the Fermi level of SLG is at ca. −4.3 eV (system II). The distinct features common to both systems are manifestation of two resonances on the EPs of $H_2Pc$ vibrational modes and nearly the same localization of each of the two resonant electronic transitions within the $H_2Pc$ molecule, which, in turn, indicates that the same mechanisms of GERS operate in both systems in the 532−830 nm range. On the other hand, the following differences between the two systems were found. First, the maxima of EPs in the visible spectral region have been encountered at different excitation wavelengths, namely, at 633 nm for system I and at 647 nm for system II. Furthermore, the average GERS EFs of $H_2Pc$ vibrational modes are markedly lower for system I than for system II at both 633 and 647 nm excitations, namely, 3 and 4, respectively, for system I (this paper) and 9 and 8, respectively, for system II.[24] We have also noticed that the average GERS EF is slightly higher at 647 nm excitation for system I and at 633 nm excitation for system II. These differences are consistent with a slight blue shift of the maximum of the electronic absorption band for system I reported in this paper (but not encountered for system II[24]). This shift is tentatively attributed to a closer proximity of the Fermi level of SLG to the highest occupied molecular orbital of $H_2Pc$ (calculated as −4.99 eV[29]) in system I than in system II, which, in turn, can allow a weak interaction of these two energy levels in the former system. The second difference between the two systems is a more pronounced increase of the normalized band intensities of $H_2Pc$ vibrational modes at 830 nm excitation encountered for system I in comparison to system II. This difference is explained by a closer proximity of the 830 nm excitation wavelength to the maximum of the CT electronic transition from the Fermi level of SLG to the LUMO of $H_2Pc$ in the former case (the calculated max. at 810 nm) than in the latter one (the calculated max. at 867 nm). Although all the above-mentioned differences between systems I and II could possibly be viewed as minor, their importance largely increases in the case when they are employed as reference systems for combined SERS + GERS. For example, should the system II have been used as the reference system in this study instead of system I, these differences could be erroneously attributed to the combination of SERS with GERS of $H_2Pc$.

## 4. CONCLUSIONS

Evidence for a simultaneous operation of GERS and SERS experienced by the free-base phthalocyanine ($H_2Pc$) molecular ML localized on the top of SLG deposited over an array of annealed Ag NPs has been obtained. Preparation and characterization of the glassI/AgNPs/SLG/$H_2Pc$(ML) hybrid systems together with the glassI/SLG/$H_2Pc$(ML) and graphite/$H_2Pc$(ML) reference systems and their micro-Raman spectral mapping at five excitations in the 532−830 nm range, followed by the determination of SERS, GERS, and SERS + GERS EFs and construction of SERS + GERS and GERS EPs of $H_2Pc$ vibrational modes, have emerged as an appropriate strategy for a detailed elucidation of the combined mechanism of SERS + GERS. Importantly, the same positions



DOI: 10.1021/acs.jpcc.8b06218
J. Phys. Chem. C 2018, 122, 20850−20860

of Fermi level of SLG (at −4.4 eV) were obtained in the glassI/Ag NPs/SLG/$H_2$Pc(ML) hybrid system probed for SERS + GERS and in the glassI/SLG/$H_2$Pc(ML) reference system probed for GERS. This was achieved by employment of the appropriate glass substrate, which induces a small negative doping of SLG comparable to the doping of SLG by Ag.

GERS, SERS, and GERS + SERS EF values have provided evidence that the combined SERS + GERS of $H_2$Pc is observed at all excitations in the 532−830 nm range. This observation is attributed to a proper selection of the array of annealed Ag NPs as the plasmonic enhancer operating in the broad wavelength range. In addition to that, the mechanisms of SERS and GERS in combined SERS + GERS were found to operate additively (i.e., their EFs are simply multiplicative) at 633 and 647 nm excitations. Furthermore, the comparison of SERS + GERS and GERS EPs of $H_2$Pc vibrational modes has revealed that the two distinct resonance features, that is, the maximum at 633 nm and the normalized intensity increase from 785 to 830 nm excitation encountered in GERS EPs, remain preserved in the SERS + GERS EPs as well. In this respect, the SERS + GERS EPs resemble the SERRS EPs, the shapes of which are modulated by RRS of chromophoric molecules.

The particular mechanisms of GERS operating in both SERS + GERS and GERS of $H_2$Pc in our probed and reference hybrid systems, respectively, at different excitation wavelengths have been identified and found to be consistent with two of the four theoretically predicted mechanisms of GERS.[21] In particular, modification of localization of the resonant $Q_y(0-0)$ electronic transition (with maximum at ca. 633−639 nm) within the $H_2$Pc molecule together with broadening and a small blue shift of its spectral band has been ascertained and ascribed to the SLG−$H_2$Pc(ML) interaction. The resonance observed at 830 nm excitation is attributed to the CT electronic transition from the Fermi level of SLG to the LUMO of $H_2$Pc with the calculated maximum at ca. 810 nm. A slightly less pronounced (but still clearly detectable) manifestation of this CT transition in the SERS + GERS EPs in comparison to GERS EPs is the only difference between the SERS + GERS and GERS EPs of $H_2$Pc encountered under the conditions of our experiment, that is, upon the same position of Fermi level of SLG in the probed and reference systems, respectively.

The importance of the last mentioned experimental condition was further demonstrated by the comparison of GERS EPs and EFs of two glass/SLG/$H_2$Pc hybrid systems (system I in this work and system II in ref 24), for which the mutual difference in the position of Fermi level was established to be ∼0.1 eV. Distinct differences in the GERS EP shapes and GERS EF values were found between the two systems. Therefore, provided that system II would have been taken as the reference system instead of system I, these differences could be incorrectly ascribed to the mutual coupling of SERS with GERS.

In summation, observation of the combined SERS + GERS in a plasmonic NS/SLG/aromatic molecules hybrid system is conditioned by the overlap between the wavelength range of the plasmon resonance of the particular plasmonic NS and the range of wavelengths in which one of the mechanisms of GERS operates for a particular molecule. Another important aspect of SERS + GERS combination stems from the (now well established) fact that the GERS mechanism operation is, for any molecule, strongly dependent on the actual position of the Fermi level of SLG, which, in turn, is set to a particular value by doping of SLG by the plasmonic metal in the plasmonic NS/SLG/molecules hybrid system. This aspect has to be taken into account upon designing and probing hybrid systems for SERS + GERS of aromatic molecules as well as upon selection of an appropriate substrate/SLG/molecule reference system for the evaluation of the GERS mechanism contribution to combined SERS + GERS.

## ■ ASSOCIATED CONTENT

### Supporting Information

The Supporting Information is available free of charge on the ACS Publications website at DOI: 10.1021/acs.jpcc.8b06218.

Electronic absorption spectrum of $H_2$Pc, preparation scheme of $H_2$Pc(ML) deposition, additional optical images and SERS + GERS spectral maps of the glassI/AgNPs/SLG/$H_2$Pc(ML) hybrid system, SERS + GERS EFs of individual $H_2$Pc spectral bands, and complete sequences of normalized band intensities in SERS + GERS EPs (PDF)

## ■ AUTHOR INFORMATION


### Corresponding Author

*E-mail: vlc@natur.cuni.cz.

### ORCID

Veronika Sutrová: 0000-0001-8320-2078
Ivana Šloufová: 0000-0002-4757-6029
Peter Mojzeš: 0000-0002-9952-6939
Zuzana Melníková: 0000-0001-5582-9236
Martin Kalbáč: 0000-0001-9574-4368
Blanka Vlčková: 0000-0003-0553-3722


### Notes

The authors declare no competing financial interest.

## ■ ACKNOWLEDGMENTS

I.S., P.M., and B.V. thank the Czech Science Foundation for the financial support by the 17-05007S grant. V.S. acknowledges the financial support by the 892217 students grant awarded by the Grant Agency of Charles University. M.K. and Z.M. acknowledge the support from MSMT project ERC-CZ (LL1301). The authors also acknowledge the assistance provided by the Research Infrastructure NanoEnviCz, supported by the Ministry of Education, Youth and Sports of the Czech Republic under project no. LM2015073 and project no. CZ.02.1.01/0.0/0.0/16_013/0001821. The authors also thank Jana Vejpravova (Charles University) for helpful discussions.

## ■ REFERENCES


(1) Procházka, M. *Surface-Enhanced Raman Spectroscopy-Bioanalytical, Biomolecular and Medical Applications*; Springer International Publishing: Switzerland, 2016.

(2) Aroca, R. *Surface-Enhanced Vibrational Spectroscopy*; John Wiley and Sons, Ltd.: Chichester, U.K., 2006.

(3) Cotton, T. M. Applications of SERS to Biomolecular Systems. In *Spectroscopy of Surfaces*; Clark, R. J. H., Hester, R. E., Eds.; Wiley: New York, 1988; pp 91−153.

(4) Matějka, P.; Vlčková, B.; Bednárová, L.; Maloň, P. Advances and Challenges in Optical Molecular Spectroscopy Including Surface Plasmon Resonance-Based Methods for Bioanalysis. In *Natural Products Analysis: Instrumentation, Methods and Applications*; Havlíček, V., Spížek, J., Eds.; John Wiley and Sons: Hoboken, N.J., USA, 2014; pp 163−238.




DOI: 10.1021/acs.jpcc.8b06218
J. Phys. Chem. C 2018, 122, 20850−20860

(5) Vlčková, B.; Matějka, P.; Šimonová, J.; Čermaková, K.; Pančoška, P.; Baumruk, V. Surface-enhanced resonance Raman spectra of free base 5,10,15,20-tetrakis(4-carboxyphenyl)porphyrin and its silver complex in systems with silver colloid: direct adsorption in comparison to adsorption via molecular spacer. *J. Phys. Chem.* **1993**, *97*, 9719−9729.
(6) Weitz, D. A.; Garoff, S.; Gersten, J. I.; Nitzan, A. The Enhancement of Raman Scattering, Resonance Raman Scattering, and Fluorescence from Molecules Adsorbed on a Rough Silver Surface. *J. Chem. Phys.* **1983**, *78*, 5324−5338.
(7) Kokošková, M.; Procházka, M.; Šloufová, I.; Vlčková, B. SERRS Spectra and Excitation Profiles of Ru(II) Polypyridine Complexes Attached to Ag Nanoparticle Aggregates: Structural, Electronic, and Resonance Damping Effects of Chemisorption. *J. Phys. Chem. C* **2013**, *117*, 1044−1052.
(8) Xu, W.; Ling, X.; Xiao, J.; Dresselhaus, M. S.; Kong, J.; Xu, H.; Liu, Z.; Zhang, J. Surface Enhanced Raman Spectroscopy on a Flat Graphene Surface. *Proc. Natl. Acad. Sci. U.S.A.* **2012**, *109*, 9281−9286.
(9) Xu, W.; Mao, N.; Zhang, J. Graphene: A Platform for Surface-Enhanced Raman Spectroscopy. *Small* **2013**, *9*, 1206−1224.
(10) Zaretski, A. V.; Marin, B. C.; Moetazedi, H.; Dill, T. J.; Jibril, L.; Kong, C.; Tao, A. R.; Lipomi, D. J. Using the Thickness of Graphene to Template Lateral Subnanometer Gaps between Gold Nanostructures. *Nano Lett.* **2015**, *15*, 635−640.
(11) Zhang, N.; Tong, L.; Zhang, J. Graphene-Based Enhanced Raman Scattering toward Analytical Applications. *Chem. Mater.* **2016**, *28*, 6426−6435.
(12) Dai, Z.-g.; Xiao, X.-h.; Wu, W.; Zhang, Y.-p.; Liao, L.; Guo, S.-s.; Ying, J.-j.; Shan, C.-x.; Sun, M.-t.; Jiang, C.-z. Plasmon-Driven Reaction Controlled by the Number of Graphene Layers and Localized Surface Plasmon Distribution During Optical Excitation. *Light: Sci. Appl.* **2015**, *4*, No. e342.
(13) Zhang, X.; Dai, Z.; Si, S.; Zhang, X.; Wu, W.; Deng, H.; Wang, F.; Xiao, X.; Jiang, C. Ultrasensitive SERS Substrate Integrated with Uniform Subnanometer Scale "Hot Spots" Created by a Graphene Spacer for the Detection of Mercury Ions. *Small* **2017**, *13*, 1603347.
(14) Weiss, J. E.; Costa, S.; Frank, O.; Fridrichová, M.; Vlčková, B.; Vejpravová, J.; Kalbáč, M. SERS of Isotopically Labeled 12C/13C Graphene Bilayer−Gold Nanostructured Film Hybrids: Graphene Layer as Spacer and SERS Probe. *J. Phys. Chem. C* **2017**, *121*, 11680−11686.
(15) Hao, Q.; Wang, B.; Bossard, J. A.; Kiraly, B.; Zeng, Y.; Chiang, I.-K.; Jensen, L.; Werner, D. H.; Huang, T. J. Surface-Enhanced Raman Scattering Study on Graphene-Coated Metallic Nanostructure Substrates. *J. Phys. Chem. C* **2012**, *116*, 7249−7254.
(16) Kang, L.; Chu, J.; Zhao, H.; Xu, P.; Sun, M. Recent Progress in the Applications of Graphene in Surface-Enhanced Raman Scattering and Plasmon-Induced Catalytic Reactions. *J. Mater. Chem. C* **2015**, *3*, 9024−9037.
(17) Xu, S.; Man, B.; Jiang, S.; Wang, J.; Wei, J.; Xu, S.; Liu, H.; Gao, S.; Liu, H.; Li, Z.; Li, H.; Qiu, H. Graphene/Cu Nanoparticle Hybrids Fabricated by Chemical Vapor Deposition as Surface-Enhanced Raman Scattering Substrate for Label-Free Detection of Adenosine. *ACS Appl. Mater. Interfaces* **2015**, *7*, 10977−10987.
(18) Gopal, J.; Abdelhamid, H. N.; Huang, J.-H.; Wu, H.-F. Nondestructive detection of the freshness of fruits and vegetables using gold and silver nanoparticle mediated graphene enhanced Raman spectroscopy. *Sens. Actuators, B* **2016**, *224*, 413−424.
(19) Xu, S.; Jiang, S.; Wang, J.; Wei, J.; Yue, W.; Ma, Y. Graphene Isolated Au Nanoparticle Arrays with High Reproducibility for High-Performance Surface-Enhanced Raman Scattering. *Sens. Actuators, B* **2016**, *222*, 1175−1183.
(20) Ling, X.; Xie, L.; Fang, Y.; Xu, H.; Zhang, H.; Kong, J.; Dresselhaus, M. S.; Zhang, J.; Liu, Z. Can Graphene Be Used as a Substrate for Raman Enhancement? *Nano Lett.* **2010**, *10*, 553−561.
(21) Barros, E. B.; Dresselhaus, M. S. Theory of Raman Enhancement by Two-Dimensional materials: Applications for Graphene-Enhanced Raman Spectroscopy. *Phys. Rev. B: Condens. Matter Mater. Phys.* **2014**, *90*, 035443.
(22) Ling, X.; Huang, S.; Deng, S.; Mao, N.; Kong, J.; Dresselhaus, M. S.; Zhang, J. Lighting Up the Raman Signal of Molecules in the Vicinity of Graphene Related Materials. *Acc. Chem. Res.* **2015**, *48*, 1862−1870.
(23) Huang, S.; Ling, X.; Liang, L.; Song, Y.; Fang, W.; Zhang, J.; Kong, J.; Meunier, V.; Dresselhaus, M. S. Molecular Selectivity of Graphene-Enhanced Raman Scattering. *Nano Lett.* **2015**, *15*, 2892−2901.
(24) Uhlířová, T.; Mojzeš, P.; Melníková, Z.; Kalbáč, M.; Sutrová, V.; Šloufová, I.; Vlčková, B. Raman Excitation Profiles of Hybrid Systems Constituted by Single-Layer Graphene and Free Base Phthalocyanine: Manifestations of Two Mechanisms of Graphene-Enhanced Raman Scattering. *J. Raman Spectrosc.* **2017**, *48*, 1270−1281.
(25) Sutrová, V.; Šloufová, I.; Melníková, Z.; Kalbáč, M.; Pavlova, E.; Vlčková, B. Effect of Ethanethiolate Spacer on Morphology and Optical Responses of Ag Nanoparticle Array-Single Layer Graphene Hybrid Systems. *Langmuir* **2017**, *33*, 14414−14424.
(26) Brotman, A.; Burstein, E. Raman Scattering-Excitation Profiles of Molecules Adsorbed on Metal Surfaces: Free-Base Phthalocyanine on Silver. *Phys. Scr.* **1985**, *32*, 385−390.
(27) Murray, C.; Dozova, N.; McCaffrey, J. G.; Shafizadeh, N.; Chin, W.; Broquier, M.; Crépin, C. Visible Luminescence Spectroscopy of Free-Base and Zinc Phthalocyanines Isolated in Cryogenic Matrices. *Phys. Chem. Chem. Phys.* **2011**, *13*, 17543−17554.
(28) Cook, M.; Chambrier, I. *The Porphyrin Handbook: Phthalocyanines: Properties and Materials*; Kadish, K., Guilard, R., Smith, K. M., Eds.; Academic Press, 2003; Chapter Phthalocyanine Thin Films: Deposition and Structural Studies; Vol. *17*, pp 37−128.
(29) Nilson, K.; Åhlund, J.; Brena, B.; Göthelid, E.; Schiessling, J.; Mårtensson, N.; Puglia, C. Scanning tunneling microscopy study of metal-free phthalocyanine monolayer structures on graphite. *J. Chem. Phys.* **2007**, *127*, 114702.
(30) Menaa, B.; Takahashi, M.; Tokuda, Y.; Yoko, T. Dispersion and Photoluminescence of Free-Metal Phtalocyanine Doped in Sol-Gel Polyphenylsiloxane Glass Film. *J. Photochem. Photobiol., A* **2008**, *194*, 362−366.
(31) Kaya, E. N.; Basova, T.; Polyakov, M.; Durmuş, M.; Kadem, B.; Hassan, A. Hybrid Materials of Pyrene Substituted Phthalocyanines with Single-Walled Carbon Nanotubes: Structure and Sensing properties. *RSC Adv.* **2015**, *5*, 91855−91862.
(32) Ochsner, M. Photophysical and Photobiological Processes in the Photodynamic Therapy of Tumors. *J. Photochem. Photobiol., B* **1997**, *39*, 1−18.
(33) Xu, H.; Xie, L.; Zhang, H.; Zhang, J. Effect of Graphene Fermi Level on the Raman Scattering Intensity of Molecules on Graphene. *ACS Nano* **2011**, *5*, 5338−5344.
(34) Joo, Y.; Kim, M.; Kanimozhi, C.; Huang, P.; Wong, B. M.; Roy, S. S.; Arnold, M. S.; Gopalan, P. Effect of Dipolar Molecule Structure on the Mechanism of Graphene-Enhanced Raman Scattering. *J. Phys. Chem. C* **2016**, *120*, 13815−13824.
(35) Michl, M.; Vlčková, B.; Mojzeš, P. Ag colloid-ethanethiol films: spacer-modified substrates for surface-enhanced resonance Raman scattering spectroscopy of chromophoric molecules. *Vib. Spectrosc.* **1999**, *19*, 239−242.
(36) Kalbáč, M.; Frank, O.; Kavan, L. The Control of Graphene Double-Layer Formation in Copper-Catalyzed Chemical Vapor Deposition. *Carbon* **2012**, *50*, 3682−3687.
(37) Hallam, T.; Berner, N. C.; Yim, C.; Duesberg, G. S. Strain, Bubbles, Dirt, and Folds: A Study of Graphene Polymer-Assisted Transfer. *Adv. Mater. Interfaces* **2014**, *1*, 1400115.
(38) Giovannetti, G.; Khomyakov, P. A.; Brocks, G.; Karpan, V. M.; van den Brink, J.; Kelly, P. J. Doping Graphene with Metal Contacts. *Phys. Rev. Lett.* **2008**, *101*, 026803.
(39) Jorio, A.; Saito, R.; Dresselhaus, G.; Dresselhaus, M. S. *Raman Spectroscopy in Graphene Related Systems*; Wiley-VCH Verlag GmbH & Co. KGaA: Weinheim, Germany, 2011.


DOI: 10.1021/acs.jpcc.8b06218
*J. Phys. Chem. C* 2018, 122, 20850−20860

(40) Ferrari, A. C.; Basko, D. M. Raman Spectroscopy as a Versatile Tool for Studying the Properties of Graphene. *Nat. Nanotechnol.* **2013**, *8*, 235−246.
(41) Dissanayake, D. M. N. M.; Ashraf, A.; Dwyer, D.; Kisslinger, K.; Zhang, L.; Pang, Y.; Efstathiadis, H.; Eisman, M. D. Spontaneous and Strong Multilayer Graphene n-Doping on Soda-Lime Glass and its Applications in Graphene-Semiconductor Junctions. *Sci. Rep.* **2016**, *6*, 21070.
(42) Murray, C.; Dozova, N.; McCaffrey, J. G.; FitzGerald, S.; Shafizadeh, N.; Crépin, C. Infra-red and Raman Spectroscopy of Free-Base and Zinc Phthalocyanines Isolated in Matrices. *Phys. Chem. Chem. Phys.* **2010**, *12*, 10406−10422.
(43) Lin, W.-I.; Gholami, M. F.; Beyer, P.; Severin, N.; Shao, F.; Zenobi, R.; Rabe, J. P. Strongly Enhanced Raman Scattering of Cu-Phthalocyanine Sandwiched between Graphene and Au(111). *Chem. Commun.* **2017**, *53*, 724−727.
(44) Clark, R. J. H.; Dines, T. J. Resonance Raman Spectroscopy, and Its Application to Inorganic Chemistry. New Analytical Methods (27). *Angew. Chem., Int. Ed. Engl.* **1986**, *25*, 131−158.
(45) Tackley, D. R.; Dent, G.; Smith, W. E. Phthalocyanines: Structure and Vibrations. *Phys. Chem. Chem. Phys.* **2001**, *3*, 1419−1426.
(46) Heutz, S.; Salvan, G.; Silaghi, S. D.; Jones, T. S.; Zahn, D. R. T. Raman Scattering as a Probe of Crystallinity in PTCDA and H2Pc Single-Layer and Double-Layer Thin Film Heterostructures. *J. Phys. Chem. B* **2003**, *107*, 3782−3788.



DOI: 10.1021/acs.jpcc.8b06218
*J. Phys. Chem. C* 2018, 122, 20850−20860

# SUPPORTING INFORMATION

# Excitation Wavelength Dependence of Combined Surface- and Graphene-Enhanced Raman Scattering Experienced by Free-base Phthalocyanine Localized on Single Layer Graphene-Covered Ag Nanoparticle Array

Veronika Sutrová[a,d] Ivana Šloufová[a] Peter Mojzeš[b], Zuzana Melniková[c] Martin Kalbáč[c], Blanka Vlčková[a*]

[*] Correspondence to: Blanka Vlčková, Charles University, Faculty of Science, Department of Physical and Macromolecular Chemistry, Hlavova 8, Prague 2, 128 40, Czech Republic, vlc@natur.cuni.cz

[a] Charles University, Faculty of Science, Department of Physical and Macromolecular Chemistry, Hlavova 8, Prague 2, 128 40, Czech Republic

[b] Charles University, Faculty of Mathematics and Physics, Institute of Physics, Ke Karlovu 5, Prague 2, 121 16, Czech Republic

[c] J. Heyrovsky Institute of Physical Chemistry of the ASCR, v.v.i, Dolejškova 3, 182 21 Prague 8, Czech Republic

[d] Institute of Macromolecular Chemistry AS CR, Heyrovsky Sq. 2, 162 06 Prague 6, Czech Republic

**CONTENT:**

**Table S1 – page S4**

**Text S2 – page S5 - S6**

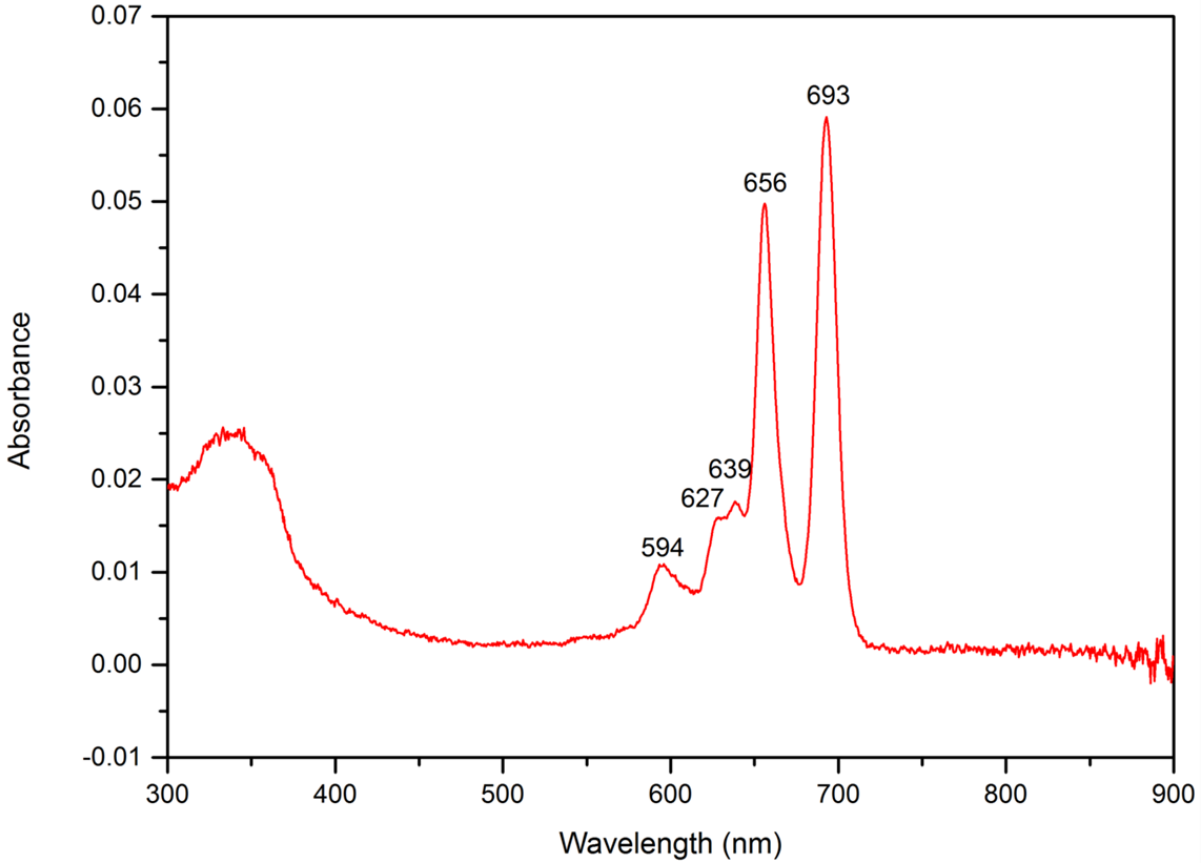


**Figure S1** Electronic absorption spectrum of a filtered saturated (<5x10$^{-5}$ M) solution of $H_2Pc$ in toluene.

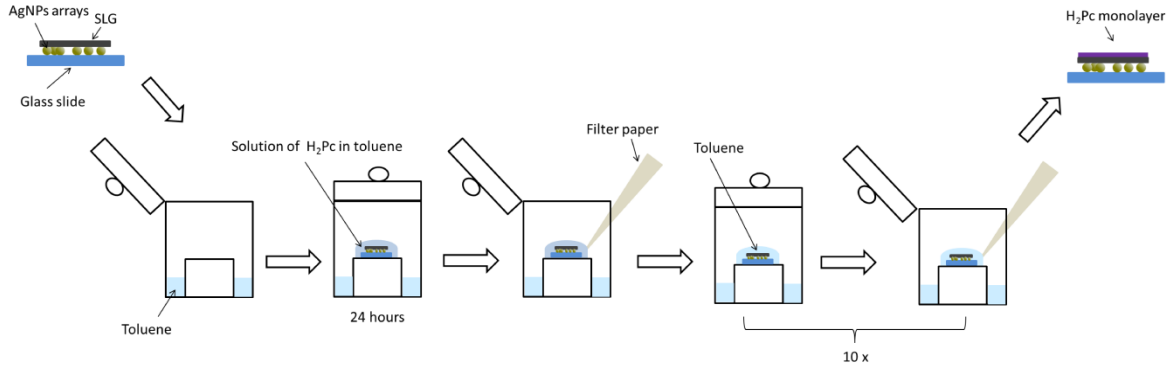

**Figure S2** Schematic depiction of the final step of the glassI/AgNPs/SLG/$H_2$Pc(ML) hybrid system preparation: overdeposition of the glassI/AgNPs/SLG hybrid system by a monolayer (ML) of $H_2$Pc molecules.

**Text S1**

A generally known formula for calculation of the standard deviation for a function *u* of two variables *(x,y)*, each of which suffers from random errors:

$$u = u(x, y)$$

$$s_{\bar{u}} = \sqrt{\left(\frac{\partial u}{\partial x}\right)^2 s_{\bar{x}}^2 + \left(\frac{\partial u}{\partial y}\right)^2 s_{\bar{y}}^2}$$

has been adapted for calculations of the average standard deviations of the average values of enhancement factors (EFs) and of the normalized band intensities. As an example, the formula for calculation of the average standard deviations of the average values of SERS EFs is provided:

$$s_{E_F} = E_F \sqrt{\left(\frac{s_{I_{SERS}}}{I_{SERS}}\right)^2 + \left(\frac{s_{I_{RRS}}}{I_{RRS}}\right)^2}$$

where

$s_{EF}$ = average standard deviation of the average value of SERS EF

$E_F$ = average value of SERS EF

$I_{SERS}$ = average value of SERS spectral bands intensity

$I_{RRS}$ = average value of RRS spectral bands intensity

$s_{I_{SERS}}$ = average standard deviation of the average SERS spectral bands intensity

$s_{I_{RRS}}$ = average standard deviation of the average RRS spectral bands intensity

The average spectral band intensity was calculated as an average of spectral band intensities at each of the 50 x 50 points of a 25 μm x 25 μm microRaman spectral map, and the average standard deviations were calculated as the average values of differences between the particular spectral band intensity at each point of the map and the average spectral band intensity. The

values of the average standard deviations thus reflect the degree of heterogeneity of the microRaman spectral maps on μm scale.

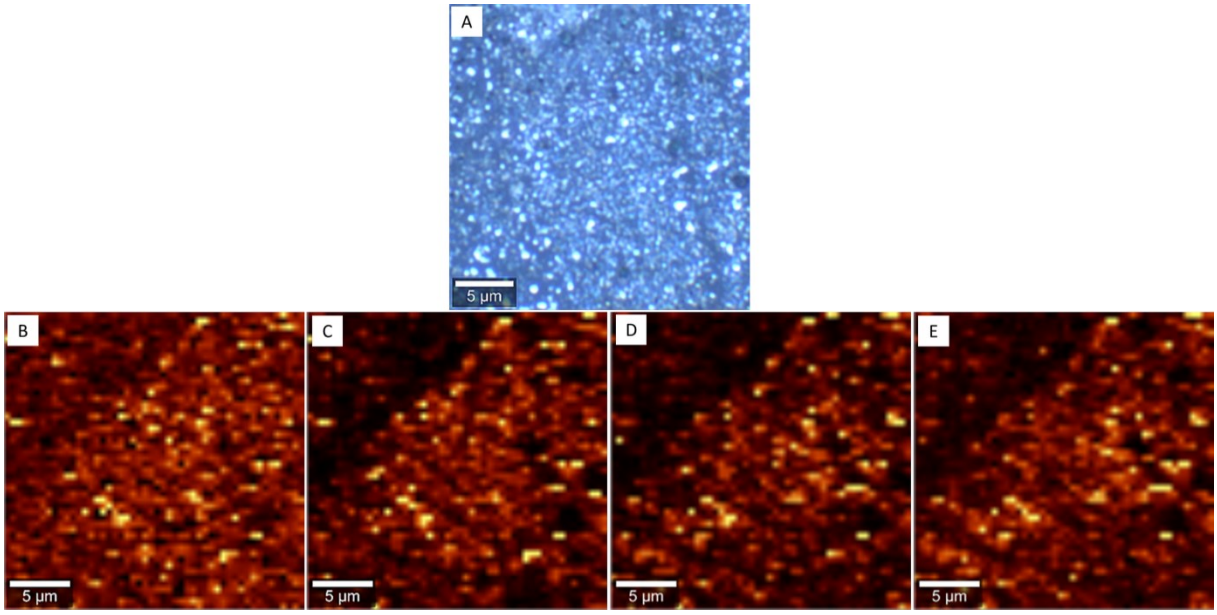


**Figure S3 (A) -** an optical image of the glassI/AgNPs/SLG/$H_2$Pc(ML) area of the sample; **(B)** and **(C) -** SERS spectral maps of the G mode (1590 $cm^{-1}$) and 2D (2595 $cm^{-1}$) mode of SLG; **(D)** and **(E) -** SERS+GERS spectral maps of the 683 $cm^{-1}$ and 1540 $cm^{-1}$ modes of $H_2$Pc. The spectral maps **(B)-(D)** were acquired from the same area as the optical image **(A)** at 785 nm excitation.

**Table S1** SERS+GERS enhancement factors experienced by Raman modes of the $H_2$Pc molecule localized in the glassI/AgNPs/SLG/$H_2$Pc(ML) hybrid system.

| **Peak position [$cm^{-1}$]** | **EFs GERS + SERS vs RR** | |
|---|---|---|
| | **633 nm** | **647 nm** |
| 484 | 26 ± 6 | 25 ± 4 |
| 683 | 34 ± 7 | 25 ± 6 |
| 726 | 14 ± 5 | 20 ± 3 |
| 798 | 22 ± 5 | 28 ± 5 |
| 1085 | 32± 8 | 27± 5 |
| 1143 | 46 ± 7 | 53 ± 12 |
| 1343 | 39 ± 5 | 33 ± 8 |

| | | |
|---|---|---|
| 1452 | 67 ± 6 | 72 ± 9 |
| 1540 | 107 ± 15 | 88 ± 13 |

**Text S2**

**Detailed analysis of the sequences of normalized band intensities in SERS+GERS EPs of the spectral bands of $H_2Pc$ localized in glassI/AgNPs/SLG/$H_2Pc$(ML) hybrid systems**

The sequences of the normalized band intensities in SERS+GERS excitation profiles (EPs) of the spectral bands of $H_2Pc$ localized in glassI/AgNPs/SLG/$H_2Pc$(ML) were determined at 633 and 647 nm excitations from the complete EPs presented in Figure 5A and at 830 nm excitation from the detailed EPs depicted in Figure 5B. The sequences of the normalized band intensities were analyzed in terms of the symmetry of the corresponding vibrations and their localization within the $H_2Pc$ molecule. For the totally symmetric normal vibrations ($A_g$), their normalized relative band intensities are proportional to the magnitude of changes of their normal coordinates upon the resonant electronic transition. Their evaluation thus allows for determination of the localization of the resonant electronic transitions within a molecule. [24,44] The sequence of the most intense bands (maxima in $cm^{-1}$) in EM SERS+GERS of $H_2Pc$ at 633 nm excitation was determined as follows: 1540 ($A_g$) > 1343 ($A_g$) > 1143 ($A_g$) > 1452 ($A_g$) > 799 ($A_g$) ~ 726 ($A_g$) > 683 ($A_g$) > 1085 ($B_{1g}$) ~ 484 ($B_{1g}$). At 647 nm excitation, the sequence of the most intense bands was found to be: 1540 ($A_g$)> 1343 ($A_g$) > 1143 ($A_g$) > 726 ($A_g$) ~1452 ($A_g$) ~ 683 ($A_g$) ~ 799 ($A_g$) > 1085 ($B_{1g}$) > 484 ($B_{1g}$). The common feature of both sequences of the spectral bands is a preferential enhancement of the totally symmetric $A_g$ modes over the $B_{1g}$ modes, and a preferential enhancement of higher wavenumber $A_g$ modes of localized on the pyrrole and on the benzene rings over the low wavenumber $A_g$ macrocycle modes (the latter aspect being more pronounced at 633 than at 647 nm excitation). Importantly, the sequences of the most enhanced bands are similar to those reported for GERS of $H_2Pc$ in ref.[24] and they indicate that both the 633 and the 647 nm excitations fall into the electronic absorption band of the $Q_y$ 0-0 electronic transition within the $H_2Pc$ molecules assembled into a monolayer on the surface of SLG, i.e. upon the conditions of the SLG-$H_2Pc$ (ML) interaction.

The sequence of the most intense bands at 830 nm excitation was established as: 683 ($A_g$) > 726 ($A_g$) > 1343 ($A_g$) ~484 ($B_{1g}$) > 1143 ($A_g$) ~ 1540 ($A_g$) > 1452 ($A_g$) > 799 ($A_g$) > 1086 ($B_{1g}$). In contrast to the previously established sequences of the most enhanced bands at 633 and 647

nm excitation, the low wavenumber bands of the $H_2Pc$ macrocycle are among the most enhanced bands in SERS-GERS of $H_2Pc$. This effect is analogous to that observed for GERS of $H_2Pc$ in ref.[24], however, the preferential enhancement of the low wavenumber bands of the $H_2Pc$ macrocycle is even more pronounced in the SERS-GERS EPs presented in this paper (Figure 5B) than in the GERS ones [24], since the low wavenumber 684 and 726 $cm^{-1}$ bands show the largest normalized band intensities of all bands at 830 nm excitation. This observation thus provides a clearcut evidence that the LUMO of $H_2Pc$ is populated by a different electronic transitions at 830 nm excitation than at 633 and 647 nm excitations (as depicted in Figure 7). The former electronic transition is attributed to the charge transfer (CT) electronic transition from the Fermi level of SLG to LUMO of $H_2Pc$ (first reported in ref.[24] for GERS of $H_2Pc$).

References [24,44] are the same as those listed in the MS text, in particular:

(24) Uhlířová, T. Mojzeš, P. Melniková, Z.; Kalbáč, M.; Šloufová, I.; Vlčková, B. Raman Excitation Profiles of Hybrid Systems Constituted by Single-layer Graphene and Free Base Phthalocyanine: Manifestations of Two Mechanisms of Graphene-enhanced Raman Scattering. *J. Raman Spectrosc.* **2017**,*48*, 1270-1281.

(44) Clark, R. J. H.; Dines, T. J. Resonance Raman Spectroscopy, and its Applications to Inorganic Chemistry. *Angew. Chem. Int. Ed. Engl.* **1986,** *25*, 131-158.